01 Jul 1993

Design of automotive structural components using high strength sheet steels effect of strain rate on the structural strength and crushing behavior of cold-formed steel stub columns

Chi-Ling Pan

Wei-wen Yu
Missouri University of Science and Technology, wwy4@mst.edu

Civil Engineering Study 93-1
Cold-Formed Steel Series

Nineteenth Progress Report

DESIGN OF AUTOMOTIVE STRUCTURAL COMPONENTS USING HIGH STRENGTH SHEET STEELS

EFFECT OF STRAIN RATE ON THE STRUCTURAL STRENGTH AND CRUSHING BEHAVIOR OF COLD-FORMED STEEL STUB COLUMNS

by

Chi-Ling Pan
Post-Doctoral Fellow

Wei-Wen Yu
Project Director

A Research Project Sponsored by the American Iron and Steel Institute

July 1993

Department of Civil Engineering
University of Missouri-Rolla
Rolla, Missouri

TABLE OF CONTENTS

TABLE OF CONTENTS (cont.)

LIST OF TABLES

LIST OF TABLES (cont.)

LIST OF TABLES (cont.)

LIST OF TABLES (cont.)

LIST OF FIGURES

LIST OF FIGURES (cont.)

LIST OF FIGURES (cont.)

LIST OF FIGURES (cont.)

I. INTRODUCTION

In the past, a considerable amount of theoretical and experimental research has been undertaken to study material properties and the behavior of structures under dynamic loads and impact loads. For the purpose of investigating the structural behavior and strength of cold-formed steel members under dynamic loads, a research project was conducted at the University of Missouri-Rolla from January 1988 through December 1991 to study the effect of strain rate on mechanical properties of sheet steels and the structural behavior and strength of cold-formed steel members. The test results of material properties, stub columns, and beams with evaluations were summarized in the Eighteenth Progress Report[1].

Because the previous studies were limited only to the structural members which were assembled with the same material in a given section, the research work reported herein under the sponsorship of the American Iron and Steel Institute (AISI) was concentrated on a study of the structural strength of hybrid automotive structural components using different sheet steels. In the first phase of the project, two selected sheet steels (25AK and 50SK) have been tested for establishing the mechanical properties in tension and compression under different strain rates. The nominal yield strengths of these two sheet steels are equal to approximately 25 and 50 ksi and the range of strain rates used in the test varied from 10^{-4} to 1.0 in./in./sec.. Details of the tension and compression coupon tests were presented in the Seventeenth Progress Report[2]

Due to the lack of drop tower test equipment at the University of Missouri-Rolla, a total of fifty-two (52) drop tower tests of stub columns were conducted at General Motors Corporation during the Summer of 1992.

The impact velocities used in the drop tower tests were 28.5 and 43.2 km/hr. The research findings are presented in Reference 3.

At the University of Missouri-Rolla, the study of stub columns including hybrid sections fabricated from 25AK and 50SK sheet steels subjected to dynamic loads was initiated in January 1993. Ninty-six (96) box-shaped stub columns and forty-eight (48) hat-shaped stub columns were tested under the strain rates varied from 10^{-4} to 10^{-1} in./in./sec.. The test results of a total of 144 test specimens were reported herein. Among these specimens, 80 specimens were hybrid sections.

In Chapter II of this report, the literature review is related to the structural strength of steel members under dynamic loading conditions. The experimental investigation of the structural behavior of stub columns subjected to static and dynamic loads are discussed in Chapter III. The test data of specimens fabricated from two types of sheet steels are evaluated in Chapter IV. Finally, the results of stub column tests are summarized in Chapter V.

II. REVIEW OF LITERATURE

A. GENERAL

Two current trends in automobile design have increased the complexity of material selection for automobiles. On the one hand, there has been the steady drive to develop designs that increase the safety of occupants during auto collisions. At the same time, in the interests of fuel and material economy, the steel industry has been developed high-strength steels for use by the automotive industry in designing lighter-weight steel components[4].

Because material properties are influenced by impact loading, a large number of research projects were conducted for a variety of structures under specified loading conditions in the past three decades. Recent research has been directed to analytical procedures which take into account more precise constitutive relationships including strain rate sensitivity, strain harding, and geometric change arising from overloads.

In view of the fact that in the current AISI Automotive Steel Design Manual[5], the design criteria for effective design width are based on the test results under static loading condition, this study involved the investigation of the validity of these effective design width formulas for the design of cold-formed steel structural members fabricated from either the same material or two different materials subjected to dynamic loads. Another primary objective for this investigation is to study the crushing behavior of these members. Therefore, a review of the structural behavior of compression elements under static loads and the strengths of axially loaded members subjected to dynamic or impact loads are necessary.

B. STRUCTURAL BEHAVIOR OF COMPRESSION ELEMENTS UNDER STATIC LOADS

1. Elastic Local Buckling of Flat Compression Elements. The compression flat elements may buckle locally in the elastic or inelastic range depending on the width-to-thickness ratio of the compression elements. The elastic local buckling stress, $(f_{cr})_E$, of compression elements subjected to a uniform compression can be determined by the following equation:

$$(f_{cr})_E = \frac{k\pi^2 E}{12(1-\mu^2)(w/t)^2} \qquad (2.1)$$

where E = modulus of elasticity

k = buckling coefficient

t = thickness of element

w = width of element

μ = poisson's ratio = 0.3 for steel

The value of k depends upon the magnitude of the aspect ratio of the plate and the boundry conditions. It is noted that the k value is equal to four for a square plate and for any plate with an aspect ratio equal to an interger. It is also noted that the value approaches to four for a long plate with an aspect ratio larger than four. Therefore, a minimum value of k equal to four for the stiffened compression elements is conservatively used in practical design without considering the rotational restraint along the unloaded edges.

2. Inelastic Buckling of Flat Compression Elements. The preceding discussion on elastic local buckling is valid as long as the computed critical buckling stress is below the proportional limit of the material. When a plate buckles at a stress level beyond the proportional limit, this

type of buckling is referred to as inelastic buckling. The analytical study of local buckling in the inelastic range is rather complicated because of the anisotropic nature of the compression element. However, analytical studies of the plates buckled in the inelastic range have been performed by numerous researchers.[6-10]

In the late ninteenth century, the tangent modulus theory and the reduced modulus theory were proposed by Engesser. In 1924, Bleich[6] extended the theory of flat plate stability into the inelastic range by considering the plate as an anisotropic type and by introducing a reduced modulus. He assumed that the reduced modulus is applied only to a plate in the direction of the compressive stress, whereas the modulus of elasticity remains the same in the perpendicular direction to the compression stress. Thus, for a simply supported plate subjected to uniformly compressive stresses in one direction, the following equation can be used for determining the inelastic buckling stress:

$$(f_{cr})_I = \eta(f_{cr})_E = \frac{\eta k \pi^2 E}{12(1-\mu^2)(w/t)^2} \qquad (2.2)$$

where $\eta = \sqrt{\tau} = \sqrt{E_t/E}$

E_t = tangent modulus of steel

It is noted that the inelastic buckling stress ($(f_{cr})_I$) is in terms of the elastic buckling stress ($(f_{cr})_E$) and the plasticity reduction factor (η).

3. Postbuckling Behavior of Flat Compression Elements. The compression elements of thin-walled structural members with relatively large w/t ratios can continue to carry additional loads after the attainment of

elastic local buckling. The stresses in the compression elements will redistribute until the stresses along supported edges reach the yield stress of steel. Then, the maximum load-carrying capacity of the member will be reached.

A grid model shown in Figure 2.1[11] can be used for the deflected shape of a stiffened compression element in the postbuckling range. The transverse bars, which are anchored at the sides of grid, act as tie rods to support the deflection of the longitudinal struts. This meams that the tension membrane stress developed in the transverse direction restrains the lateral displacement caused by the longitudinal load. As a result, additional load can be carried by the plate after the elastic buckling load is reached because of the transverse membrane stress and the redistribution of longitudinal stress. As shown in Figure 2.2(a)[11], the stress distribution is uniform prior to its buckling. After buckling, the stress distribution is nonuniform as shown in Figure 2.2(b)[11]. It is assumed that the maximum load is reached when the stress at the supported edges reaches the yield stress of the steel as shown in Figure 2.2(c)[11].

Because the membrane stresses are developed in the transverse direction and the deflection of the plate is usually much larger than its thickness after buckling, small deflection theory of plate bending can not be applied to the postbuckling behavior. Therefore, the large deflection theory of plates was used by Von Karman[12] for the analysis of plates in the postbuckling range.

4. Development of Effective Width Formulas. A solution for the large deflection theory was difficult for use in practical design because of its complexity. Therefore, the concept of "Effective Width" has been proposed

by von Karman[13] to determine the ultimate strength of thin metal sheets in aeronautical structures in 1932. In the past, the effective width concept has been successfully used for the prediction of postbuckling strengths of stiffened and unstiffened elements.

In von Karman's[13] approach, it was assumed that the entire load is carried by two effective strips with a uniformly distributed stress equal to the edge stress, f_{max}, as shown in Figure 2.3[11], instead of using the full width of the compression element with actual, nonuniform stress distribution. The effective width can be considered as a particular width of the plate which just buckles when the compression stress reaches the yield strength of steel. The effective width (b) of the stiffened element derived by von Karman is shown in Equation 2.3.

$$b = Ct\sqrt{\frac{E}{F_y}} = 1.9t\sqrt{\frac{E}{F_y}} \qquad (2.3)$$

where $C = \pi/\sqrt{3(1-\mu^2)} = 1.9$

The following equation can be derived from Equation 2.1 for a stiffened compression element with k = 4.0:

$$w = Ct\sqrt{\frac{E}{f_{cr}}} \qquad (2.4)$$

From Equations 2.3 and 2.4, the following relationship of b and w can be obtained:

$$\frac{b}{w} = \sqrt{\frac{f_{cr}}{F_y}} \qquad (2.5)$$

For the study of effective design width, Winter[14-16] conducted extensive tests by using cold-formed steel sections. Based on his test

results, Winter derived effective width formulas for the design of both stiffened and unstiffened compression elements under uniform compression.

Based on the accumulated design experience with a restudy of original and additional test results, the following equation was used in the AISI Specification for determination of the effective width of stiffened compression elements:

$$b = 1.9t\sqrt{\frac{E}{f_{max}}}\left[1 - 0.415\left(\frac{t}{w}\right)\sqrt{\frac{E}{f_{max}}}\right] \qquad (2.6)$$

or $$\frac{b}{w} = \sqrt{\frac{f_{cr}}{f_{max}}}\left[1 - 0.22\sqrt{\frac{f_{cr}}{f_{max}}}\right] \qquad (2.7)$$

The effective width approach was used for the design of stiffened compression elements since 1946, whereas the reduced allowable stress method was used for the design of unstiffened compression elements until the 1986 revision of AISI Specification. Based on the recent research[17], a new format of effective width formulas, which are based on Equation 2.7, has been used for the design of both stiffened and unstiffened compression elements in the AISI Specification since 1986. The effective width formulas used in the current AISI Specification and the AISI Automotive Steel Design Manual are presented in detail in the next section.

5. Current AISI Effective Width Formulas. According to the AISI Cold-Formed Steel Design Manual[18], the effective design widths of uniformly compressed stiffened and unstiffened elements can be calculated by using the following equations for load capacity determination:

$$b = w \qquad \text{when} \qquad \lambda \leq 0.673, \qquad (2.8)$$

$$b = \rho w \qquad \text{when} \qquad \lambda > 0.673, \tag{2.9}$$

where b = effective width of a compression element

w = flat width of a compression element

$$\rho = (1 - 0.22/\lambda)/\lambda \tag{2.10}$$

λ = a slenderness factor

$$\lambda = \frac{1.052}{\sqrt{k}} \left(\frac{w}{t}\right)\left(\sqrt{\frac{f}{E}}\right) \tag{2.11}$$

where f = the edge stress

E = modulus of elasticity, 29500 ksi

k = plate buckling coefficient

= 4.0 for stiffened elements supported by a web on each longitudinal edge

= 0.43 for unstiffened elements supported by a web on one longitudinal edge and free on the other

The effective width formulas for computing the load-carrying capacity of uniformly compressed elements used in the current AISI Automotive Steel Design Manual are similar to those used in AISI Cold-Formed Steel Design Manual for building construction. According to the AISI Automotive Steel Design Manual, for stiffened and unstiffened compression elements with a yield strength higher than 80 ksi, it is recommended that a reduced yield strength can be used in the calculation of Equation 2.11. The reduced yield strengths for stiffened and unstiffened compression elements are given in Reference 5.

According to the AISI Automotive Steel Design Manual, the effective design width of compression elements is used for determining the load-carrying capacity of the member when the slenderness factor λ (Equation 2.11) of compression elements exceeds a limiting value of 0.673.

When $\lambda = 0.673$, the limiting width-thickness ratio (at which full capacity is achievable) can be evaluated as

$$\left[\frac{w}{t}\right]_{lim} = 0.64\sqrt{\frac{kE}{f}} \qquad (2.12)$$

For fully stiffened compression elements under a uniform stress, k = 4, which gives a limiting w/t value as follows:

$$\left[\frac{w}{t}\right]_{lim} = S = 1.28\sqrt{\frac{E}{f}} \qquad (2.13)$$

Using a buckling coefficient of 0.43, the limiting w/t ratio for the unstiffened compression elements can be derived as follows:

$$\left[\frac{w}{t}\right]_{lim} = S = 0.42\sqrt{\frac{E}{f}} \qquad (2.14)$$

When the w/t ratio exceeds the value of S, the effective width, b, is less than the actual width w. The value of b is calculated on the basis of Equation 2.9.

C. RESPONSE OF AXIALLY LOADED MEMBERS TO DYNAMIC LOADS

The crushing behavior of thin-walled sheet metal structures such as tubes, circular cylinders, and non-circular sections under both quasi-static and dynamic axial loading conditions has been studied over the past 30

years. These structures were used to study the mechanical energy absorption in the event of a vehicle collision or accident.

The dynamic plastic collapse of energy-absorbing structures is more difficult to understand than the corresponding quasi-static collapse, on account of two effects which may be described as the "strain-rate factor" and the "inertia factor" respectively. The first of these is material property whereby the yield stress is raised, while the second can affect the collapse mode, etc[19].

In this section, some of the developments resulted from the previous research for the response of structural members subjected to dynamic loads are reviewed. Particular attention is focused on those items related to axially loaded members.

The analysis of column behavior under impact loading conditions dates back to 1933, when Koning and Taub derived equations describing the axial and transverse oscillation of pin-ended columns subjected to dynamic axial loads. They considered loads having a rectangular pulse form, of magnitude less than, equal to, or greater than the static Euler load. However, they did not recognize the possibility of dynamic overloads[20].

Macaulay and Redwood (1964) examined the behavior of rods, square tubes and small-scale models to gain insight into the effect of axial impact on railway coaches. They found important differences between the static and dynamic buckling behavior and recognized a velocity effect with two components, geometry and strain rate[21].

Some of the most significant work on the analysis of strut behavior under dynamic loading is due to Hoff[22] (1965). His analysis was directed

to study the dynamics of the buckling of elastic columns in a rapid compression test. In his study, he found that the lateral displacements of the column under rapid loading are less than those calculated from static considerations. As a consequence the load supported by the column can exceed the Euler load considerably.

Axial impact on thin-walled columns was examined theoretically by Culver and Vaidya[23] and experimentally by Logue[24], both were published in 1971. The theoretical work was applied to short duration impact loading which was defined by prescribing the time variations of the load at the end of the columns. Nonlinearity due to local buckling was accounted for by using nonlinear axial load-curvature relations derived with the aid of the effective width concept. The results of the analytical study were shown as response spectra curves which described the effect of initial deflection, pulse duration, maximum dynamic load, and the static preload on the dynamic response. It was concluded from the experimental study that maximum loads in excess of the static failure loads may be carried dynamically.

Soden, Al-Hassani, and Johnson[25] (1974) studied the crushing behavior of circular tubes under static and dynamic axial loads. The loads and deformations of tubes with various thicknesses were recorded and three failure modes were observed and studied. The majority of tube tests collapsed by progressive folding into diamond shaped lobes, while thick tubes failed by collapsing into circumferential rings. The thinnest specimens collapsed into sets of three diamonds at each level with successive sets displaced through 30 degrees to give the collapsed specimen a hexagonal formation. The initial failure loads and postbuckling loads for various modes of deformation were predicted theoretically. They found

that both the initial maximum stress and the mean post-buckling stress are seen to increase with increasing compression rate.

In 1974, Ohkubo, Akamatsu, and Shirasawa[24] examined a series of tests to study the energy absorption of closed-hat section members subjected to axial loading. In order to estimate the amount of energy absorption of the closed-hat section members subjected to dynamic axial loading, dynamic tests were performed for the same members by using pendulum type collision test equipment. By fitting experimental data, they found that the dynamic mean crushing load seems to be a linear function of the collision speed:

$$P_{md} = P_{ms}(1.0 + 0.0668V) \qquad (2.15)$$

where P_{md} = dynamic mean crushing load

P_{ms} = static mean crushing load

V = collision speed (m/s)

In 1977, Van Kuren and Scott[4] studied a series of crushing tests performed to determine the energy absorption of a range of steels at testing speeds up to 40mph and temperatures of 70 and -40 F. Open-ended square and cylindrical tubes were axially loaded to produce accordionlike deformation patterns. For four-inch-diameter cylinders at 40mph impact, Figure 2.4 shows the effect of impact velocity on energy absorbed for two test thicknesses. Based on their investigation, the conclusions are: (1) the energy absorption of steel increases with impact velocity and at low temperature; (2) tube geometry significantly influences the amount of energy absorbed. Specifically, a square tube absorbs a third less energy than a circular tube for an equal volume of material; and (3) high-strength steels

absorb energy in proportion to their strength level, the significance being that they can be used in relatively thin material to reduce vehicle weight.

Van Kuren[27] (1980) also studied the energy absorption of several automotive materials, i.e., reinforced plastics, steel, and aluminum. These curved shell specimens were crushed at impact speeds up to 25mph and temperatures of 70 and -40 F. Figure 2.5 shows the effect of impact velocity on the energy absorption of several materials. He stated that steel absorbed up to 20 times more total energy than did the reinforced plastics and over twice that absorbed by aluminum for the same thickness. Aluminum absorbed more energy per unit weight than the other materials, but steel was considerably more cost-effective.

In 1977, Wierzbicki[28] studied the dynamic crushing strength of strain-rate sensitive box columns. The main purpose of his study was to identify material and geometrical parameters in the problem of impact loading for sheet metal and to derive an expression for the strain rate correction factor. As a particular structural component, a straight retangular box column was considered to be representive of front or rear longitudinal members of an automobile body. He stated that during a vehicle collision the strain rate in the zones of localized deformation can be of the order of 10 to 100 in./in./sec.. Consequently, dynamic forces in compressed mild steel members are much greater than static ones. An approximate analysis was presented to determine dynamic strength and energy absorption of axially loaded thin-walled box columns. In this analysis, the dynamic compressive force is a product of a static crushing strength of the column and a strain-rate correction factor. The strain-rate correction factor was found to be dependent on the initial impact velocity and parameters describing the sensitivity of the material to strain rate.

In another work published in 1979, Wierzbicki and Abramowicz[29] used a simple method to calculate the dynamic correction factor for thin-walled, strain-rate sensitive structures. For the experiments run at two crushing speeds v1 and v2 with associated strain rates $\dot{\varepsilon}_1$ and $\dot{\varepsilon}_2$, the corresponding ratio of mean crushing forces P_m^1 and P_m^2 is equal to the dynamic correction factor given as follows:

$$R = \frac{P_m^1}{P_m^2} = \left(\frac{\dot{\varepsilon}_1}{\dot{\varepsilon}_2} \right)^{\frac{1}{\bar{n}}} = \left(\frac{v1}{v2} \right)^{\frac{1}{\bar{n}}} \qquad (2.16)$$

where $\bar{n}$ is the material strain-rate sensitivity calculated from the following equation:

$$\frac{\sigma}{\sigma_0} = \left(\frac{\dot{\varepsilon}}{\dot{\varepsilon}_0} \right)^{\frac{1}{\bar{n}}} \qquad (2.17)$$

It can be seen from Equation 2.16 that the dynamic correction factor does not involve any geometrical and material parameters except the constant $\bar{n}$.

In 1984, Abramowicz and Jones[30] conducted twenty-three experimental tests on 56mm-diameter steel tubes of various lengths subjected to dynamic axial loads. The columns were crushed axially on a drop hammer rig. The effective crushing distance was considered in the analysis along with the influence of material strain-rate sensitivity. The ratio of the dynamic to quasi-static mean crushing forces for identical, straight tubes of mild steel can be expressed as below:

$$\frac{P_m^d}{P_m^s} = 1 + \left(\frac{\dot{\varepsilon}}{6844}\right)^{\frac{1}{3.91}} \qquad (2.18)$$

where 3.91 and 6844 sec.$^{-1}$ are material constants.

They concluded that a modified version of Alexander's[31] theoretical analysis for axisymmetric, or concertina, deformations gives good agreements with the experimental results when the effective crushing distance is concerned and provided that the influence of material strain rate sensitivity is retained in the dynamic crushing case.

In 1981, by using semi-empirical approach, Mahmood and Paluszny[32] derived the design equations for determining the load capacity (maximum strength) and the post buckling crush resistance of thin wall, box columns subjected to static axial crush. According to Mahmood and Paluszny, the maximum load and the mean crushing load for a box-type column can be calculated by using the following equations:

$$P_u = 3418 t^{1.86} b^{0.14} (1+\alpha) \sigma_y^{0.57} \left(\frac{k_p}{\beta}\right)^{0.43} \qquad (2.19)$$

$$P_{mean} = 3420 t^{1.86} b^{0.14} (1+\alpha) \sigma_y^{0.57} \left(\frac{k_2}{\beta}\right)^{0.43} \qquad (2.20)$$

where b = width of "buckling" plate

t = thickness of plate

k_2 = plate coefficient

k_p = crippling plate coefficient

α = section aspect ratio

β = material strength coefficient

σ_y = yield strength of material

They found that the design equations correlated very closely with tests for seam welded, retangular and square box columns as well as double hat sections. They also pointed out that in determining the effective cross-sectional area, used in estimating the mean crush load, the spot welded flanges must be included. The reason being that in contrast to the maximum load case, where the contribution of flanges to the load carrying capacity is neglibible, the flanges participate in the folding process and thus contribute to the crush resistance of the section.

The crush strength characteristics and modes of collapse of thin-walled circular columns were mathematically formulated by Mahmood and Paluszny in 1984[33]. The formulation was based on the stability of shell structures subjected to axial crush, where various stages of collapse were identified and crush characteristics pertinent to column design were quantified. It was concluded that the crush characteristics of columns are functions of both column geometry (thickness to radius ratio (t/r)) and the elastic/yield properties of the material (elasticity modulus (E), poisson's ratio (ν), and yield strength (S_y)), whereas the mode of collapse (number of circumferential lobes) is governed predominantly by the geometry ratio (t/r).

Mamalis, Johnson, and Viegelahn[34] (1984) studied the uniformly thin circular cylinders and frusta (truncated circular cones) of low carbon steel subjected to axial loading at elevated strain rate. The initial axial length and the outside diameter of the cylinders and frusta (the larger top end) were kept constant while the uniform wall thickness of those specimens was varied. The load-deformation or compressive behavior of the cylinder

and frusta for the two semi-apical angles used, 5° and 10°, were recorded and the modes of collapse were observed and discussed. In this investigation, they found that with increasing slenderness ratio, thickness to initial outside diameter ratio for cylinder and thickness to initial outside mean diameter for frusta, (effectively increasing wall thickness) both the peak and mean postbuckling loads increase in a broadly parabolic manner. With increase in semi-apical angle, both the peak and postbuckling load decrease.

In 1986, Reid and Reddy[35] examined the crushing behavior of sheet metal tubes of rectangular cross-section which (1) remains constant along its length or (2) increases with a taper on one face (single-tapered) or increases with tapers on two opposite faces (double-tapered). They observed that the mean crushing loads increased under dynamic loading conditions due to material strain rate sensitivity, although there was no changes in the mode of deformation compared with that under quasi-static conditions.

Birch and Jones[21] conducted a series of axial impact and static crushing tests carried out on specimens manufactured from commercial structural mild steel tubing (seam welded) having an outside diameter D' of 64 mm, wall thickness H of 1.58 mm, a length of L of 150 mm, with stiffeners. An examination was made into the influence of stiffener depth (T), number of stiffeners (N), and the effect of placing the stiffeners externally or internally. Based on the test results, they found that the static and dynamic collapse modes are similar for plain unstiffened tubes. However, there are considerable differences between the static and dynamic collapse modes for the axially stiffened tubes which were even more pronounced in tubes with four axial stringers. The static collapse of tubes stiffened with four external stringers occurs in an unstable overall

buckling mode with peak collapse loads lower than those found in the specimens with four internal stringers. The dynamic collapse mode of the tubes stiffened with four internal stringers is generally a stable regular progressive type, while the dynamic collapse mode is an irregular progressive type, with some stability, when the tubes are stiffened with four external stiffeners.

In 1989, Kassar[36] and Pan[1] also studied the box-shaped and I-shaped stub columns subjected to dynamic loads. A total of 96 stub columns were fabricated from 35XF and 50XF sheet steels. Prior to the stub column tests, the effects of strain rate on the mechanical properties of three different sheet steels (35XF, 50XF, and 100XF) were studied experimentally. The results of the experimental study indicated that the mechanical properties of sheet steels (yield stress, proportional limit, and ultimate tensile strength) as well as the load-carrying capacity of stub columns increase with increasing strain rates.

The crush behavior of box-shaped and hat-shaped stub columns were tested under quasi-static and dynamic loads by Schell et al.[3] (1993). The hybrid stub columns were fabricated by spot welding two components using different sheet steels (25AK and 50SK) with the nominal yield stresses equal to approximately 25 ksi and 50 ksi. Comparisons were also made between single material and hybrid stub columns. The results indicate that the peak crush load, energy absorption, and mean crush load for all specimens were affected by the loading rate, composition, and cross-sectional geometry of the stub columns.

III. EXPERIMENTAL INVESTIGATION

A. GENERAL

All tests were performed in the MTS 880 Test System located in the Engineering Research Laboratory at the University of Missouri-Rolla. The materials used in this phase of study are 25AK and 50SK sheet steels with nominal yield strengths equal to approximately 25 and 50 ksi, respectively. A total of 96 box-shaped stub columns and 48 hat-shaped stub columns were tested to study the effect of strain rate on the cold-formed steel structural components including hybrid sections. These specimens were cold-fromed to shape by Rose Metal Products Inc. in Springfield, Missouri. The configurations of specimens are shown in Figures 3.1(a) and 3.1(b) for box-shaped and hat-shaped stub columns, respectively. The designation of test specimens is presented in Table 3.1. As shown in Figure 3.2, five groups of test specimens were used in this investigation: (1) Group A - box-shaped stub columns were assembled by using two hat sections fabricated from 50SK sheet steel; (2) Group B - box-shaped stub columns were assembled by using two hat sections fabricated from 25AK sheet steel; (3) Group C - box-shaped stub columns were assembled by using two hat sections fabricated from two different materials (50SK and 25AK); (4) Group D - hat-shaped stub columns were assembled by using a hat section fabricated from 50SK sheet steel and a plate of 25AK sheet steel; (5) Group E - hat-shaped stub columns were assembled by using a hat section fabricated from 25AK sheet steel and a plate of 50SK sheet steel. Groups A and B are used as control groups. Tables 3.2 through 3.6 show the specimen number, test speed, strain rate, and width-to-thickness ratio (w/t) of each individual test specimen. Four selected strain rates (10^{-4}, 10^{-3}, 10^{-2}, and 10^{-1} in./in./sec.) were used

in the tests for each case of specimens. A total of 144 stub column specimens were tested in this study. The test results are evaluated and discussed in Chapter IV of this report.

B. MATERIAL PROPERTIES

Two virgin materials, 25AK and 50SK sheet steels, were tested in tension and compression in the longitudinal and transverse directions. The tested mechanical properties were presented in the Seventeenth Progress Report[2]. Tables 3.7 and 3.8 summarize the average values of mechanical properties tested under different strain rates for 25AK and 50SK sheet steels. The thicknesses of 25AK and 50SK sheet steels are 0.078 in. and 0.074 in., respectively. To illustrate the effect of strain rate on the mechanical properties, Figures 3.3 and 3.4 show the typical stress-strain relationships for 25AK sheet steel subjected to longitudinal tension and compression with different strain rates of 10^{-4}, 10^{-2}, 10^{-1}, and 1.0 in./in./sec.. The typical stress-strain relationships for 50SK sheet steel are shown in Figures 3.5 and 3.6. The empirical equations derived on the basis of the material test results were presented in the 17th Progress Report, which were used to predict tensile and compressive yield stresses.

C. STUB COLUMN TESTS

1. Specimens. In this phase of experimental investigation, one hundred forty-four (144) stub column specimens were tested to study the effect of strain rate on the local and post-buckling strengths of compression elements. As shown in Figure 3.1(a), box-shaped stub columns were fabricated by connecting two hat sections through the unstiffened flanges. To form a hat-shaped stub column, a hat section and a plate were

assembled by attatching the plate to the unstiffened flanges of the hat section as shown in Figure 3.1(b). All test specimens were fabricated in General Motor Corporation by using spot welded connections. Six spot welds were used on each unstiffened flange of hat sections for all box-shaped stub columns in spite of the lengths of specimens. For hat-shaped stub columns, twelve spot welds were used on each flange of hat sections to assemble the specimens. To ensure a close contact between the ends of test specimens and compression platens of the test machine, all specimens were milled in the machine shop to make both ends of stub column flat and parallel.

The length of stub columns has been designed long enough (more than 3 times the largest dimension of the cross section) to develop the plate buckling wave and short enough (less than 20 times the least radius of gyration) to prevent overall buckling of the entire member as recommened in Reference 37. This criterion was also adopted in Part VII of the 1986 AISI Cold-Formed Steel Design Manual. The webs and unstiffened flanges of all hat sections were designed to be fully effective. Tables 9 through 13 give the lengths and dimensions of stub column specimens fabricated from 25AK and 50SK sheet steels. The w/t ratios of stiffened flanges ranged from 23.02 to 58.38 and from 24.14 to 61.60 for box-shaped stub columns (Groups A, B, and C) fabricated from 25AK and 50SK sheet steels, respectively. For Group D specimens, the w/t ratios of stiffened flanges ranged from 17.41 to 44.43 and the w/t ratios of plates ranged from 34.17 to 59.73. The w/t ratios of stiffened flanges and plates ranged from 9.67 to 41.98 and from 28.97 to 62.78, respectively, for Group E specimens.

2. Strain Measurements. Eight foil strain gages were used to measure strains at midheight of stub columns for specimens with small and medium w/t ratios (cases 1 and 2 of Groups A, B, C, D, and E). The location of

strain gages, numbered from 1 to 8, is shown in Figure 3.7. For the stub columns with large or extra large w/t ratios, additional four strain gages were mounted above and below the midheight of the hat sections for box-shaped stub columns (cases 3 and 4 of Groups A, B, and C) and the plates for hat-shaped stub columns (cases 3 of Groups D and E) at the location equal to one-half of the overall width. The arrangements of strain gages are shown in Figure 3.8.

The load-strain diagrams obtained from paired strain gages (No. 1-2, 5-6, and 9 through 16) were used to determine the tested local buckling load by means of the modified strain reversal method, which is discussed in Reference 38. The strain gages numbered 3, 4, 7, and 8 were used to measure the strain rate during the tests. Prior to testing, all strain gages were used to align the stub column specimens.

3. Instrumentation and Test Procedure. All tests were performed in a 110-kips 880 Material Test System (MTS) by using "stroke" (actuator displacement) as the control mode to maintain a constant actuator speed for stub column tests. This test system shown in Figure 3.9 consisted of an MTS load frame, a control console, and the CAMAC (Computer Automated Measurement and Control) data acquisition system. The data acquisition system used in this study consisted of 64 simultaneously sampling input channels at a resolution of 12 bits. The test frequency or sampling rate depended on the total test time with a maximum of 25,000 readings per second for each channel. After the data were acquired, they were downloaded to the Data General MV-10000 Mini Computer for analysis purpose.

For all tests, the maximum load range of 100 kips and the maximum stroke range of 5 inches were selected for the function generator of the test

machine. The ramp time was programmed to have a constant speed, which was calculated by the product of a selected strain rate and the overall length of the specimen. Following fabrication of the specimen and placement of strain gages, the stub column was placed in the MTS load frame. In order to obtain good test results, a small amount of preload was applied to the stub column prior to testing for the purpose of checking the alignment of specimen. If necessary, thin aluminum foils were placed at the end of the specimen in the regions of low strain until the load is uniformly distributed over the whole cross section.

4. Test Results. The failure mode of the stub column specimens varies with the width-to-thickness ratio of the stiffened compression element. Based on the readings obtained from the paired strain gages attached back to back along the centerline of the stiffened elements, no local buckling occurred in the specimens with small w/t ratios (case 1 of Groups A through E) as shown in Figure 3.10. For specimens with medium w/t ratios (case 2 of Groups A through C and case 2 of Group E), the specimens normally buckled in the inelastic range as shown in Figure 3.11. The local buckling occured in the elastic range for the specimens having large w/t ratios (cases 3 and 4 of Groups A and C, case 4 of Group B, and case 3 of Groups D and E). When local buckling occurred in the test specimens, the stresses in the compression flanges redistributed over the cross section until the edge stress reached to the maximum value. Typical load-strain relationship for the specimen with large w/t ratios is shown in Figure 3.12.

The location of local buckling for the box-shaped stub columns as well as hat-shaped stub columns with small or medium w/t ratios was found to be at the end for most cases. Figure 3.13 illustrates a specimen with small w/t ratio at the beginning of buckling, and Figure 3.14 shows the final

folding pattern for the same specimen. However, the specimens with large w/t ratios failed locally at or near the midheight of specimens regardless of the strain rate for most cases. Figure 3.15 is an example of test specimen with large w/t ratio.

For all tests, the maximum displacement of 5.0 inches was applied to the specimens in order to study the crushing behavior of stub columns. For most box-shaped stub columns (Groups A, B, and C), regular folding was developed in the stub columns with smaller w/t ratios and irregular folding was observed in those with larger w/t ratios during the test. In addition to folding, other failure modes such as bending, twisting, lateral buckling, and openning were also observed in some stub columns. As shown in Figure 3.16, the specimens bent about X-X axis and Y-Y axis were defined as bending and lateral buckling, respectively. For the purpose of differentiating the failure modes, Figures 3.17 through 3.21 illustrate these failure types. For most specimens in case 3 of Groups A, B, and C, due to the use of smaller L/r ratios, the stub columns buckled after attaining one or two folds in the specimens. Consistent failure type of folding was noted in most hat-shaped stub columns (Groups D and E). Figures 3.22 through 3.33 show typical load-displacement diagrams for box-shaped stub columns (Groups A, B, and C) tested under different strain rates. Similarly, Figures 3.34 through 3.39 show typical load-displacement diagrams for hat-shaped stub columns (Groups D and E). Although a constant speed was applied to the test specimen during the test, however, the strain rate could not be retained constant after the ultimate load was reached in the specimen. Therefore, the value of strain rate was defined as the slope of the strain-time relationship before the attainment of the ultimate loads. A typical

strain-time diagram for the strain rate of 0.01 in./in./sec. is shown in Figure 3.40.

IV. EVALUATION OF EXPERIMENTAL DATA

A. GENERAL

In the previous UMR research, two types of stub column specimens fabricated from two sheet steels (35XF and 50XF) were tested under different strain rates to study the behavior of stiffened and unstiffened compression elements. It was concluded that the predicted ultimate loads of stub columns can be improved by using the dynamic yield stresses[1]. Because the previous studies were limited only to the structural members which were assembled with the same material in a given section, this research was concentrated on a study of the structural strength of hybrid automotive structural components using different sheet steels. In addition, some stub column specimens fabricated from the same material were also tested.

Two sheet steels (25AK and 50SK) which were used to fabricate the stub column specimens were tested and presented in the Seventeenth Progress Report[2]. Because the material properties and stress-strain relationships are influenced by strain rate, comparisons are made between the experimental results and the predicted failure loads which were calculated according to the current AISI Automotive Steel Design Manual by using static and dynamic material properties. The crushing behavior of these stub columns are also discussed in this chapter.

B. CRITICAL LOCAL BUCKLING LOADS

All stub column specimens were tested under an axial compressive load. The compression element of stub columns may buckle in the elastic or inelastic range, depending on the w/t ratio of the compression element.

The elastic critical local buckling stress, $(f_{cr})_E$, of a stiffened element under uniform compression can be calculated by using Equation 2.1.

$$(f_{cr})_E = \frac{k\pi^2 E}{12(1-\mu^2)(w/t)^2} \qquad (2.1)$$

The buckling coefficient used in Equation 2.1 is equal to 4.0 for stiffened compression elements supported along both longitudinal edges. When the elastic critical buckling stress exceeds the proportional limit, the compression element buckles in the inelastic range. The inelastic buckling stress, $(f_{cr})_I$, can be computed by using the following equation, which is based on the tangent modulus concept[39].

$$(f_{cr})_I = F_y - \frac{F_{pr}(F_y - F_{pr})}{(f_{cr})_E} \qquad (4.1)$$

where F_y = compressive yield stress of steel

F_{pr} = proportional limit of steel

$(f_{cr})_E$ = elastic critical local buckling stress

Once the critical local buckling stress ($(f_{cr})_E$ or $(f_{cr})_I$) was calculated, the computed critical local buckling load of a stub column corresponding to the initiation of local buckling of its controlling compression element can be calculated as follows:

$$P_{cr} = A_g f_{cr} \qquad (4.2)$$

where A_g = gross cross-sectional area of the stub column

f_{cr} = critical local buckling stress

Based on the dimensions of compression elements and the mechanical properties of sheet steel, the critical local buckling loads of box-shaped

stub columns fabricated from the same material (Groups A and B) can be obtained according to Equation 4.2. However, the critical local buckling loads for the stub columns fabricated from two different sheet steels (Groups C, D, and E) could not be determined easily because the governing critical local buckling stress is not known. Therefore, the stress-strain relationships of both sheet steels must be investigated for determining the governing critical local buckling stress in the hybrid sections. Comparing the strains obtained from the critical local buckling stresses for both components, the smaller strain will be used to calculate the stresses for each components. Then, the critical local buckling loads can be calculated by adding the loads from two different components. The following empirical equations were derived from material tests and used to compute the stresses and strains for 25AK and 50SK sheet steels under different strain rates:

For 25AK sheet Steel $$Y = A + B/X + C/X^2 \qquad (4.3)$$

For 50SK sheet Steel $$Y = D + E \times X + F \times X^2 \qquad (4.4)$$

where Y = compressive stress

X = compressive strain

when strain rate = 10^{-4} in./in./sec.:

A = 23.45 B = -0.525 C = -0.008

D = 1.403 E = 334.7 F = -454.7

when strain rate = 10^{-2} in./in./sec.:

A = 27.32 B = -0.475 C = -0.035

D = 1.350 E = 328.6 F = -407.6

when strain rate = 10^{-1} in./in./sec.:

A = 31.19 B = -0.426 C = -0.062

$$D = 1.192 \quad E = 310.0 \quad F = -266.1$$

The strains used for determining the above equations were selected from the proportional limit to the yield point of steel. The predicted and tested critical local buckling loads are presented in Tables 4.1 through 4.3 for box-shaped stub columns, and Tables 4.4 and 4.5 for hat-shaped stub columns. The critical local buckling stresses of hybrid sections (Groups C, D, and E) listed in column (1) of Tables 4.3 through 4.5 are calculated based on Equations 4.3 and 4.4. On the basis of dynamic material properties, the predicted critical local buckling loads are shown in column (2) of Tables 4.1 through 4.5. The tested critical local buckling loads listed in column (3) of these tables were determined from load-strain relationships by using the modified strain reversal method. It can be seen that the tested critical local buckling load increases with increasing strain rate for most stub column tests, except for the box-shaped stub columns fabricated from 50SK sheet steel (Group A). Comparisons of the computed and tested critical local buckling loads are listed in column (4) of these tables. The mean values of $(P_{cr})_{test}/(P_{cr})_{comp}$ ratios for Groups A and B specimens seem to indicate that a good agreement can be achieved between the tested and computed critical local buckling loads for specimens fabricated from 50SK sheet steel but the computed critical local buckling loads are underestimated for specimens fabricated from 25AK sheet steel. Similar results can also be found for Groups D and E specimens, for which the predicted critical local buckling stresses were calculated for 25AK and 50SK sheet steels, respectively.

C. ULTIMATE AXIAL LOADS

For the stub columns fabricated from the same material, it is assumed that the stub column reaches its ultimate load when the maximum edge stress in the stiffened elements reaches the yield stress of steel. Therefore, the ultimate load of the stub column can be calculated by mutiplying the effective cross-sectional area by the yield stress of steel as expressed in Equation 4.5.

$$(P_u)_{comp} = A_e F_y \qquad (4.5)$$

where A_e = effective cross-sectional area of the stub column

F_y = yield stress of steel.

The AISI effective width formulas (Equations 2.8 and 2.9) can be used to compute the effective cross-sectional area.

It should be noted that the previous equation is valid only for the stub columns fabricated from one material such as Groups A and B. For the stub columns fabricated from two different sheet steels, even though one of two components reaches its yield point of steel, the stub column may continuously carry additional load until another component reaches its yield point of steel. Therefore, the ultimate strength of such a stub column fabricated from two different materials such as Groups C, D, and E can be calculated by using the following equation:

$$(P_u)_{comp} = (A_e)_1 (F_y)_1 + (A_e)_2 (F_y)_2 \qquad (4.6)$$

The subscripts of "1" and "2" used in Equation 4.6 represent the components in the stub column fabricated from two different sheet steels. The effective design widths to be used for determining the effective

cross-sectional areas, $(A_e)_1$ and $(A_e)_2$, were computed on the basis of $(F_y)_1$ and $(F_y)_2$, respectively. It should be noted that the yield strengths and the cross-sectional areas of two components in a hybrid section are different. Therefore, Equation 4.6 can be used to compute the ultimate load only if the length of column is short enough without overall buckling and both ends of the column are flat and parallel.

The predicted and tested ultimate loads are presented in Tables 4.6 through 4.8 for box-shaped stub columns and Tables 4.9 and 4.10 for hat-shaped stub columns. The computed ultimate loads listed in column (3) of these tables are based on the static compressive yield stress, while the values listed in column (4) of these tables are based on the dynamic yield stress corresponding to the strain rate used in the test. The dynamic compressive yield stresses were determined by using equations listed in Figures 3.5 and 3.7 of 17th Progress Report[2] for 25AK and 50SK sheet steels, respectively. The tested ultimate loads are listed in columns (5) of these tables. It is noted from Tables 4.6 through 4.10 that the tested ultimate load increases with increasing strain rate for specimens having the similar w/t ratios. Comparisons of the computed and tested ultimate loads are listed in columns (6) and (7). From the comparisons of the mean values and standard deviations of $(P_u)_{test}/(P_u)_{comp}$ ratios listed in columns (6) and (7) of these tables, it can be seen that the computed ultimate loads using dynamic yield stresses are somewhat better than the computed ultimate loads using static yield stress. Similar to the results of critical local buckling loads, the computed ultimate loads are underestimated for box-shaped stub columns fabricated from 25AK sheet steel (Group B) and a good agreement can be achieved between the tested ultimate loads and computed values calculated based on dynamic yield stresses for specimens

fabricated from 50SK sheet steel (Group A). As expected, the ultimate loads of Group C specimens are close to the average values of the ultimate loads of Groups A and B specimens having the similar dimensions.

It is well known that cold-forming operation increases the yield stress and tensile strength of the steel particularly in the corners of cross sections. In order to consider the effect of cold-work on the axial strength of stub columns, comparisons between the tested ultimate loads and the predicted ultimate loads based on the applicable tensile yield stresses are discussed in the following paragraphs.

According to the AISI Cold-Formed Steel Design Specification, the load-carrying capacity of a compact section (i.e. $\rho = 1$) including the cold work of forming can be determined by substituting F_{ya} for F_y, where F_{ya} is the average yield stress of the full section, and can be computed as follows:

$$F_{ya} = C(F_y)_c + (1-C)F_{yf} \tag{4.7}$$

where

F_{ya} = average tensile yield stress of steel.

C = ratio of the total corner cross-sectional area to the total cross-sectional area of the full section.

F_{yf} = weighted average tensile yield stress of flat portions.

$(F_y)_c = B_c F_{yv}/(R/t)^m$, tensile yield stress of corners. (4.8)

$B_c = 3.69(F_{uv}/F_{yv}) - 0.819(F_{uv}/F_{yv})^2 - 1.79$ (4.9)

$m = 0.192(F_{uv}/F_{yv}) - 0.068$ (4.10)

R = inside bend radius.

F_{yv} = tensile yield stress of virgin steel.

F_{uv} = ultimate tensile strength of virgin steel.

The above equations are applicable when $F_{uv}/F_{yv}>1.2$, $R/t<7$, and minimum included angle$< 120°$

The predicted ultimate loads based on the applicable tensile yield stresses and the tested ultimate loads are presented in Tables 4.11 through 4.13 for box-shaped stub columns. Tables 4.14 and 4.15 present the similar data for hat-shaped stub columns. For the stub columns with small w/t ratios (first case of each group), the computed ultimate loads were calculated by considering the cold work effect and presented in these tables.

The computed ultimate loads based on the static and dynamic yield stresses are listed in columns (3) and (4) of Tables 4.11(a) through 4.15(a), respectively. Comparisons of computed and tested ultimate loads are listed in columns (6) and (7) of these tables. By comparing the mean values and standard deviations of $(P_u)_{test}/(P_u)_{comp}$ ratios listed in Tables 4.11(a) through 4.15(a). it can be seen that the computed ultimate loads using dynamic yield stresses are better than that using static yield stress. By comparing Tables 4.6 through 4.10 to Tables 4.11(a) through 4.15(a), it is noted that the ultimate loads calculated based on tensile yield stresses are better than those calculated on the basis of compressive yield stresses.

It can be seen from Table 4.12(b) that a better prediction of the ultimate loads of compact sections can be obtained by considering the cold-work effect for the box-shaped stub columns fabricated from 25AK sheet steel (Group B). However, the computed ultimate loads can not be improved by considering the cold-work effect for box-shaped stub columns fabricated from 50SK sheet steel (Group A) and hybrid sections (Groups C, D, and E).

By comparing Table 4.6 with Table 4.7 and Table 4.11 with Table 4.12, it was found that the ratios of tested to computed ultimate loads for compact

sections of box-shaped stub columns fabricated from 25AK sheet steel are larger than those fabricated from 50SK sheet steel. This fact can be explained by the load-strain diagrams shown in Figures 4.1 and 4.2. Figures 4.1 and 4.2 show the load-strain relationships of box-shaped stub column specimens 1A2A1 (50SK) and 1A2B1 (25AK), respectively. These curves were drawn from the readings of strain gages mounted on the corner of compression flanges of box-shaped stub columns. From Figure 4.1, it can be seen that the load reached its maximum value when the strain reached the yield strain for the specimen fabricated from 50SK sheet steel. However, for the specimen fabricated from 25AK sheet steel, the maximum strain under ultimate load were beyond the yield strain as shown in Figure 4.2. This is because the types of stress-strain relationship for these two sheet steels are different. The stress-strain curve for 50SK sheet steel is sharp-yielding type but it is a gradual-yielding type for 25AK sheet steel.

D. MEAN CRUSHING LOADS

The crash energy of a colliding vehicle is dissipated in the plastic deformation of structural elements. For the axial mode of energy dissipation, vehicle deceleration is controlled by the mean crush resistance of the collapsing rails while the rail deformation provides the desired crush distance to more safely decelerate the occupant. In the collapse process, the load that the column resists after the maximum compressive load has been reached is the corner crush load[3]. Generally, the load-displacement relationship of a box-shaped stub column compressed axially can be obtained as illustrated in Figure 4.3. The area under the load-displacement curve indicates the amount of energy absoption, which can

be used for determining the mean crushing load. Therefore, the mean crushing load can be defined by the following equation:

$$P_{mean} = \frac{\int_0^{\delta} P dx}{\delta} \qquad (4.11)$$

The δ value in Equation 4.11 represents the total distance of crushing. The maximum stroke range of function generator was selected to provide a 5-inch crushing distance for each test. The tested ultimate loads and the mean crushing loads of box-shaped stub columns are presented in Tables 4.16 through 4.18. Tables 4.19 and 4.20 present the similar data for hat-shaped stub columns. By comparing the ultimate and mean crushing loads, it appears that the percentage increases in mean crushing loads are lower than the percentage increases in ultimate loads for the tests conducted under similar strain rate. The spacing of connections and the type of failure mode for each individual test specimen are also presented in Tables 4.16 through 4.20. It can be seen from these tables that the failure modes of some specimens were not the regular folding type alone but also the combinations of bending, twisting, lateral buckling, or openning types.

According to Mahmood and Paluszny[32], the maximum load and the mean crushing load for a box-type column can be calculated by using Equations 2.19 and 2.20, respectively. By dividing Equation 2.19 by Equation 2.20, the ratio of the ultimate load to mean crushing load can be expressed as the following equation:

$$\frac{P_u}{P_{mean}} \cong \left(\frac{k_p}{k_2}\right)^{0.43} \qquad (4.12)$$

Figures 4.4 and 4.5 show graphically the curves of K_p and K_2, respectively. Comparisons of the tested ultiamte loads and mean crushing loads are presented in column (3) of Tables 4.16 through 4.20 for each individual test specimen. It was observed from Tables 4.16 through 4.18 that the values of P_u/P_{mean} ratio are high for cases 2 and 4 in Groups A and B. This is due to the use of larger spacing of connections as compared with cases 1 and 3. It is also due to the use of high yield stress and less thickness for the sections fabricated from 50SK sheet steel as compared with the sections fabricated from 25AK sheet steel. Therefore, the unstiffened compression flange could not provide a sufficient support to hold the sections together during the test, as can be seen in Figure 4.6. For this case, the ratio of ultiamte load to mean crushing load can be improved by reducing the spacing of connections for the sections fabricated from 50SK sheet steel.

For the box-shaped stub columns fabricated from 25AK sheet steel (Group B), the average value of P_u/P_{mean} for case 2 having an aspect ratio (depth-to-width ratio) of 1.0 is 2.61; for case 3 having an aspect ratio of 0.55 is 2.44; and for case 4 having an aspect ratio of 0.8 is 2.74. By using Equation 4.12, the ratio of ultiamte load to mean crushing load is approximately 2.88 for a square steel column having an aspect ratio equal to 1.0; 2.74 for a retangular steel column having an aspect ratio equal to 0.55; and 2.96 for a steel column having an aspect ratio equal to 0.8. The differences between the values computed by using Equation 4.12 and the values obtained from test results is about 7 to 10 percent. According to Mahmood and Paluszny[32], this is because the unstiffened flanges of hat sections participate in the folding process and thus contribute the crush resistance to the section as compared with the seam welded box-type stub

columns. For case 2 of Groups D and Group E specimens (hat-shaped stub columns) having an aspect ratio of 0.9, the difference between the predicted P_u/P_{mean} value (3.01) and the average value of P_u/P_{mean} (2.88) obtained from test results is about 4 percent. For case 3 of Groups D and E specimens having an aspect ratio of 0.53, the predicted and average tested values of P_u/P_{mean} are 2.76 and 2.87, respectively. The average tested P_u/P_{mean} value is 4 percent higher than the predicted value. Again, it colud be due to the large spacing of connections in the specimens.

Equation 4.12 seems to indicate that the ratio of ultimate load to mean crushing load is a function of depth-to-width ratio because both k_p and k_2 are depending on the aspect ratio. The following empirical equation was derived from the test results for predicting the mean crushing loads from the computed ultimate loads for box-shaped and hat-shaped stub columns failed by folding:

$$P_{mean} = [0.141(\alpha - 1.144) + 0.361]\, P_u \qquad (4.13)$$

where α = aspect ratio, d'/b'

The symbol d' represents the overall depth of cross section, while the symbol b' represents the overall width of stiffened flange of box-shaped and hat-shaped stub columns. Figure 4.7 shows the schematic definition for the symbols d' and b'. The tested mean crushing loads and the predicted values according to Equation 4.13 for box-shaped stub columns are presented in Tables 4.21 through 4.23. Tables 4.24 and 4.25 present the similar data for hat-shaped stub columns. In these tables, the tested mean crushing loads were obtained from the UMR specimens tested under the strain rates of 0.0001 and 0.1 in./in./sec. and from the GM specimens tested under the

strain rates of 25.97 and 39.37 in./in./sec.. The mean crushing loads computed according to Equation 4.13 are listed in column (2) of Tables 4.21 through 4.25. The computed ultimated loads listed in column (1) of these tables are based on Equations 4.5 and 4.6 with the dynamic tensile yield stresses corresponding to the strain rate used in the test. As discussed in the 18th Progress Report[1], the dynamic yield stresses for high strain rates can be estimated by using Equation 4.14:

$$(F_y)_{pred} = (A\, e^{(B/F_y)} + 1)(F_y)_s \qquad (4.14)$$

$$A = a_1 + b_1 \log(\dot{\varepsilon}) + c_1 \log(\dot{\varepsilon})^2 \qquad (4.15)$$

$$B = a_2 + b_2 \log(\dot{\varepsilon}) + c_2 \log(\dot{\varepsilon})^2 \qquad (4.16)$$

For tensile yield stress:

$a_{1t} = 0.023$ $\qquad$ $a_{2t} = 77.7$

$b_{1t} = 0.009$ $\qquad$ $b_{2t} = 0.069$

$c_{1t} = 0.001$ $\qquad$ $c_{2t} = -0.595$

Comparisons of the tested and predicted mean crushing loads are presented in column (4) of Tables 4.21 through 4.25. It can be seen from these tables that the predicted mean crushing loads for the strain rates of 25.97 and 39.37 in./in./sec. are conservative for box-shaped stub columns. For most specimens, the difference between the tested and predicted mean crushing loads for strain rates of 0.0001 and 0.1 in./in./sec. is within 10 percent. The predicted mean crushing loads for A4, D3, and E3 specimens are higher than the tested values. This may be due to the use of the large spacing of connections in these specimens as mentioned previously.

To examine the accuracy of Equation 4.13 for hat-shaped stub columns, comparisons of dynamic crushing load to static crushing load ratios were also made between Ohkubo's test results[26] and the values calculated on the basis of Equation 4.13. For a typical hat-shaped cross section used in Ohkubo's tests (the width of stiffened flange = 70mm; the depth of web = 60mm; the width of unstiffened flange = 18mm; the thickness of cross section = 1.2mm; the static yield strength of steel = 25 kg/mm^2; and the speed for the dynamic crushing test = 4.18 m/sec) the ratio of dynamic to static crushing loads obtained from the test is 1.30. Based on Equation 4.13, the computed ratio of dynamic to static crushing loads is also 1.30. The above simple comparison illustrates that Equation 4.13 can be used to calculate the mean crushing load for both box-shaped and hat-shaped stub column fabricated from materials other than 25AK and 50SK sheet steels.

E. GM TESTS

A total of 70 stub column tests were conducted in General Motor Corporation, among which 52 specimens were tested by using a drop silo test facility and 18 specimens were used for the quasi-static testing. Seven types of stub column specimens, including cases 1 and 3 of Groups A, B, and C and case 1 of Groups D and E specimens, were used in the GM tests. The selected speeds used in the tests were 28.5, 43.2, and 1.524×10^{-3} km/hr. The test results indicate that the loading rate, composition and cross-sectional geometry of the stub columns affect the ultimate load, energy absorption, and mean crushing load for all specimens.

Figures 4.8 and 4.9 show the comparisons of the tested mean crushing loads of the box-shaped stub columns (cases 1 and 3 of Groups A, B, and C)

for both GM and UMR tests. Figure 4.10 shows the similar data for the hat-shaped stub columns. It can be seen from these figures that the mean crushing loads were increased for the stub columns tested at high loading rates. Similar to the material tests, Figures 4.8 and 4.9 showed that the stub columns fabricated from 50SK sheet steel are less strain-rate sensitive than those fabricated from 25AK sheet steel for mean crushing loads. As can be seen in Figure 4.8, the mean crushing loads of hybrid sections (Specimen C1) under the static loading condition are close to the average values of the other two tests for both GM and UMR programs. Similar results can also be found in Figure 4.9 for both static and dynamic loading conditions.

It is noted that the mean crushing loads of both box-shaped and hat-shaped stub columns tested under static loading are different for GM and UMR tests. The main reason for causing this difference is apparently due to the fact that two plates were welded to the ends of stub columns for the GM tests. These end plates can provide some end fixity for the specimens and reduce the slenderness ratio. As can be seen from Figure 4.8, the mean crushing loads obtained from the GM tests are slightly higher than those obtained from the UMR tests. However, contrary results are shown in Figure 4.9 for case 3 specimens due to the use of large L/r ratios and large w/t ratios as compared with case 1 specimens. It should be noted that the data shown in Figures 4.8 through 4.10 for the GM tests are based on the average values of test results but for the UMR tests, the data are based on the average values of tests failed by folding. For this reason, the values shown in Figure 4.9 for the GM tests are slightly lower than those for the UMR tests. It should also be noted that, in general, slight differences are

expected for the test results obtained from two independent test labratories.

V. CONCLUSIONS

In order to investigate the effect of strain rate on the structural strength and crushing behavior of cold-formed steel hybrid sections, 96 box-shaped stub columns and 48 hat-shaped stub columns fabricated from two types of sheet steels (25AK and 50SK) were tested under different strain rates. Based on the available test results, the following conclusions can be drawn from the stub columns fabricated from 25AK and 50SK sheet steels:

1. For most cases, the ultimate load increases with increasing strain rate for specimens having the similar w/t ratios.
2. A better predictions for ultimate capacity can be achieved by using dynamic tensile yield stresses for both box-shaped and hat-shaped stub columns fabricated from 25AK and 50SK sheet steels.
3. Equation 4.6 can be used for the prediction of ultimate load for the hybrid sections fabricated from 25AK and 50SK sheet steels.
4. For the compact sections of box-shaped stub columns fabricated from 25AK sheet steel (Group B), the predicted ultimate load can be improved by considering the cold-work of forming.
5. For the compact sections of stub columns, the cold-work of forming is not the only reason to cause the discrepancies between the tested and computed ultimate loads. The tested loads are also affected by the type of stress-strain relationship.
6. The predicted ultimate loads for the stub columns fabricated from 50SK sheet steel (Group A) were found to be less conservative than the specimens fabricated from 25AK sheet steel (Group B).

7. The percentage increases in mean crushing loads are slightly less than the percentage increases in ultimate loads for the stub column specimens.
8. Similar to the material tests, the box-shaped stub columns fabricated from 50SK sheet steel are less strain-rate sensitive than those fabricated from 25AK sheet steel for the ultimate loads and mean crushing loads.
9. The ultimate loads and mean crushing loads of hybrid sections (Group C) are close to the average values of Groups A and B specimens having the similar dimensions.
10. For the design purpose, the mean crushing loads may be estimated by applying the computed ultimated loads (Equations 4.5 or 4.6) in Equation 4.13 for box-shaped and hat-shaped stub columns. The ultimate load was calculated on the basis of dynamic tensile yield stresses (Equation 4.14).

In summary, the ultimate loads and mean crushing loads of cold-formed steel stub columns increase with increasing strain rates. A better prediction for ultimate loads can be obtained by using the dynamic yield streses. The effective cross-sectional area can also be employed in the calculation of ultimate load for hybrid sections. Equation 4.13 can be used for computing the mean crushing loads of both box-shaped and hat-shaped stub columns failed by folding. It can be used only for the stub columns having the aspect ratio between 0.5 and 2.0 with sufficient connections to prevent premature failure. This equation should be verified for a large range of materials and member configurations. Future beam tests can be used to verify and improve the findings.

ACKNOWLEDGMENTS

The research work reported herein was conducted in the Department of Civil Engineering at the University of Missouri-Rolla under the sponsorship of the American Iron and Steel Institute.

The financial assistance granted by the Institute and the technical guidance provided by members of the AISI Task Force on Automotive Structural Design and the AISI Automotive Applications Committee and the AISI staff (S.J. Errera, D.C. Martin, and L.A. Rysdrop) are gratefully acknowledged. Members of the Task Force are: Messrs. J. Borchelt, C. Haddad, T. Khalil, C.M. Kim, R.W. Lautensleger, H. Mahmood, D. Malen, E.C. Oren, J.G. Schroth, T.N. Seel, M.Y. Sheh, and M.T. Vecchio.

All materials used in the experimental study were donated by Inland Steel Company and National Steel Corporation. Appreciation is expressed to General Motor Corporation and Dr. M.Y. Sheh for fabricating test specimens. Thanks are also due to Mr. B.C. Schell and Dr. M.Y. Sheh of General Motor Corporation for sharing their test information on impact and static crushing strength of hybrid sections with us.

Appreciation is also expressed to J. Bradshaw, J. McCracken, and S. Gabel, staff of the Department of Civil Engineering, for their technical support. The advice provided by Dr. J.E. Minor, Chairman of the UMR Department of Civil Engineering, is greatly appreciated.

REFERENCES

1. Pan, C.L. and W.W. Yu, "Design of Automotive Structural Components Using High Strength Sheet Steels: Influence of Strain Rate on the Mechanical Properties of Sheet Steels and Structural Performance of Cold-Formed Steel Members," Eighteenth Progress Report, Civil Engineering Study 92-3, University of Missouri-Rolla, Dec., 1992.

2. Pan, C.L. and W.W. Yu, "Design of Automotive Structural Components Using High Strength Sheet Steels: Mechanical Properties of Materials," Seventeenth Progress Report, Civil Engineering Study 92-2, University of Missouri-Rolla, May, 1992.

3. Schell, B.C., M.Y. Sheh, P.H. Tran, C.L. Pan, and W.W. Yu, "Impact and Static Crush Performance of Hybrid Hat Section Stub Columns," International Body Engineering Conference, September, 1993 (to be published).

4. Van Kuren R.C. and J.E. Scott, "Energy Absorption of High-Strength Steel Tubes under Impact Crush Conditions," Proceedings of International Automotive Engineering Congress and Exposition, Society of Automotive Engineers, 1977.

5. American Iron and Steel Institute, "Automotive Steel Design Manual," 1986 Edition, Revision 3 - February 1991.

6. Bleich, F., "Theorie und Berechnung der eisernen Brcicken," Julius Springer, Berlin, 1924.

7. Bijlaard, P.P., "Theory of Plastic Stability of Thin Plates," Pubs. International Association for Bridge and Structural Engineering, Volume VI, 1940-1941.

8. Bijlaard, P.P., "Theory of Tests on the Plastic Stability of Plates and Shells," Journal of the Aeronautical Sciences, Volume 16, 1949, pp.529-541.

9. Ilyushin, A.A., "The Elastic-Plastic Stability of Plates," Transcation in NACA Technical Memorandum 1188.

10. Stowell, E.Z., "A Unified Theory of Plastic Buckling of Columns and Plates," NACA Technical Note No. 1556, April 1948.

11. Yu, W.W., Cold-Formed Steel Design, Second Edition, Wiley-Interscience, New York, 1991.

12. Von Karman, T., "Festigkeitsprobleme in Meschinenbau," Encyklpadie der Mathematischen, Volume 4, 1910, p.349.

13. Von Karman, T., E.E. Sechler, and L.H. Donnel, "The Strength of Thin Plates in Compression," Transcations, ASME, Volume 54, APM54-5, 1932.

14. Winter, G., "Strength of Thin Steel Compression Flanges," Bulletin No. 35, Part 3, Cornell University, Engineering Experiment Station, Ithaca, N.Y., 1947.

15. Winter, G., "Performance of Thin Steel Compression Flange," Preliminary Publication, 3rd Congress of the International Association for Bridge and Structural Engineering, 1948, p.137.

16. Winter, G., "Performance of Compression Plates as Parts of Structural Members," Bulletin No. 35, Cornell University, Engineering Experiment Station, Ithaca, N.Y., 1947.

17. Pekoz, T., "Development of a Unified Approach to the Design of Cold-Formed Steel Members," Report SG86-4, AISI, Washington, D.C., May 1986.

18. American Iron and Institute, Cold-Formed Steel Design Manual,, 1986 Edition with the 1989 Addendum.

19. Calladine, C.R. and R.W. English, "Strain-Rate and Inertia Effects in the Collapse of Two Types of Energy-Absorbing Structure," Int. J. Mech. Sci., Volume 26, 1984, pp.689-701.

20. Rawlings, B., "Response of Structures to Dynamic Loads," Mechanical Properties at High Rates of Strain, Institute of Physics, London, No. 21, 1974.

21. Birch, R.S. and N. Jones, "Dynamic and Static Axial Crushing of Axially Stiffened Cylindical Shells," University of Livepool, Livepool, Australia.

22. Hoff, N., "Dynamic Stability of Structures," Proceedings of an International Conference on Dynamic Stability of Structures, Northwesten University, Evanston, Illinois, October 1965.

23. Culver, C.G. and N.R. Vaidya, "Impact Loading of Thin-Walled Columns," Proceedings of the First Specialty Conference on Cold-Formed Steel Structures, University of Missouri-Rolla, August 1971.

24. Logue, J.M., "Experimental Study of Thin-Walled Columns Subjected to Impact Loading," Master Thesis, Carnegie-Mellon University, April 1971.

25. Soden, P.D., S.T.S. Al-Hassani, and W. Johnson, "The Crumpling of Polyvinylchloride Tubes under Static and Dynamic Axial Loads," Mechanical Properties at High Rates of Strain, Institute of Physics, London, No. 21, 1974.

26. Ohkubo, Y., T. Akamatsu, and K. Shirarawa, "Mean Crushing Strength of Closed Hat Section Members," SAE Paper No. 740040, February, 1974

27. Van Kuren, R.C., "Energy Absorption of Plastic, Steel, and Aluminum Shells under Impact Conditions," Proceedings of International

Automotive Engineering Congress and Exposition, Society of Automotive Engineers, 1980.

28. Wierzbicki, T., "Dynamic Crushing of Strain Rate Sensitive Box Columns," SAE Second International Conference on Vehicle Structural Mechanics, April 1977.

29. Wierzbicki, T. and W. Abramowicz, "Crushing of Thin-Walled Strain-Rate Sensitive Structures," Dynamic and Crushing Analysis of Plastic Structures, Euromech Colloquium No. 121, August 1979.

30. Abramowicz, W. and N. Jones, "Dynamic Axial Crushing of Square Tubes," Int. J. Impact Engng., Volume 2, 1984.

31. Alexander, J.M., "An Approximate Analysis of the Collapse on Thin Cylindrical Shells under Axial Loading," Quart J. Mech. Appl. Math., 1960.

32. Mahmood, H.F. and A. Paluszny, "Design of Thin Walled Columns for Crash Energy Management - Their Strength and Mode of Collapse," Fourth International Conference on Vehicle Structural, SAE 811302, Nov., 1981.

33. Mahmood, H.F. and A. Paluszny, "Axial Collapse of Thin Wall Cylindrical Columns," SAE Fifth International Conference on Vehicle Structural Mechanics, April 1984.

34. Mamalis, A.G., W. Johnson, and G.L. Viegelahn, "The Crumpling of Steel Thin-Walled Tubes and Frusta under Axial Compression at Elevated Strain-Rate: Some Experimental Results," Int. J. Mech. Sci., Volume 26, 1984, pp.537-547.

35. Reid, S.R. and T.Y. Reddy, "Static and Dynamic Crushing of Tapered Sheet Metal Tubes of Rectangular Cross-Section," Int. J. Mech. Sci., Volumn 28, No. 9, 1986, pp.623-637.

36. Kassar M. and W.W. Yu, "Design of Automotive Structural Components Using High Strength Sheet Steels: Effect of Strain Rate on the Material Properties of Sheet Steels and Structural Strengths of Cold-Formed Steel Members," Fourteenth Progress Report, Civil Engineering Study 90-2, University of Missouri-Rolla, Nov., 1990.

37. Galambos, T.V. (ed.), Guide to Stability Design Criteria for Metal Structures, 4th Edition, John Wiley & Sons Incs., New York, 1988.

38. Johnson, A.L. and G. Winter, "The Structural Performance of Austenitic Stainless Steel Members," Report No. 327, Cornell University, November 1966.

39. Bleich, F., Buckling Strength of Metal Structures, New York: Mcgraw-Hill Book Company, 1952.

Table 3.1

Designation of Stub Column Specimens Used in This Study

1st Digit	1st Letter	2nd Digit	2nd Letter	3rd Digit
Test Type	Test No.	Strain-Rate (in./in./sec.)	Section Type (Group)	w/t Ratio (case)
1: Stub-Column Test	A: 1st Test	0: 0.0001	A: Two Hat Sec. (50SK & 50SK)	1: Small
	B: 2nd Test	1: 0.001	B: Two Hat Sec. (25Ak & 25AK)	2: Medium
		2: 0.01	C: Two Hat Sec. (25AK & 50SK)	3: Large
		3: 0.1	D: Hat Sec.-50SK Plate -25AK	4: X Large
			E: Hat Sec.-25AK Plate -50SK	

Table 3.2

Number of Performed Stub Column Tests
Box-Shaped Specimens Assembled from Two Hat Sections
(50SK Sheet Steel)

Spec.	Test Speed (in./min.)	Strain Rate (in./in./sec.)	w/t	No. of Tests Performed
1A0A1	0.075	0.0001	24.30	1
1B0A1	0.075	0.0001	24.40	1
1A1A1	0.750	0.001	24.30	1
1B1A1	0.750	0.001	24.32	1
1A2A1	7.500	0.01	24.26	1
1B2A1	7.500	0.01	24.14	1
1A3A1	75.00	0.1	24.28	1
1B3A1	75.00	0.1	24.25	1
1A0A2	0.086	0.0001	44.36	1
1B0A2	0.086	0.0001	44.47	1
1A1A2	0.857	0.001	44.55	1
1B1A2	0.857	0.001	44.53	1
1A2A2	8.571	0.01	44.63	1
1B2A2	8.571	0.01	44.41	1
1A3A2	85.71	0.1	44.47	1
1B3A2	85.71	0.1	44.44	1
1A0A3	0.075	0.0001	47.79	1
1B0A3	0.075	0.0001	47.87	1
1A1A3	0.750	0.001	47.68	1
1B1A3	0.750	0.001	47.83	1
1A2A3	7.500	0.01	47.87	1
1B2A3	7.500	0.01	47.86	1
1A3A3	75.00	0.1	47.79	1
1B3A3	75.00	0.1	47.82	1
1A0A4	0.100	0.0001	61.56	1
1B0A4	0.100	0.0001	61.44	1
1A1A4	1.000	0.001	61.24	1
1B1A4	1.000	0.001	61.39	1
1A2A4	10.00	0.01	61.41	1
1B2A4	10.00	0.01	61.53	1
1A3A4	100.0	0.1	61.49	1
1B3A4	100.0	0.1	61.51	1
Subtotal				32

Table 3.3

Number of Performed Stub Column Tests
Box-Shaped Specimens Assembled from Two Hat Sections
(25AK Sheet Steel)

Spec.	Test Speed (in./min.)	Strain Rate (in./in./sec.)	w/t	No. of Tests Performed
1A0B1	0.075	0.0001	23.06	1
1B0B1	0.075	0.0001	23.03	1
1A1B1	0.750	0.001	23.13	1
1B1B1	0.750	0.001	23.08	1
1A2B1	7.500	0.01	23.17	1
1B2B1	7.500	0.01	23.16	1
1A3B1	75.00	0.1	23.17	1
1B3B1	75.00	0.1	23.02	1
1A0B2	0.086	0.0001	42.56	1
1B0B2	0.086	0.0001	42.30	1
1A1B2	0.857	0.001	42.10	1
1B1B2	0.857	0.001	42.35	1
1A2B2	8.571	0.01	42.29	1
1B2B2	8.571	0.01	42.33	1
1A3B2	85.71	0.1	42.30	1
1B3B2	85.71	0.1	42.46	1
1A0B3	0.075	0.0001	45.21	1
1B0B3	0.075	0.0001	45.29	1
1A1B3	0.750	0.001	45.35	1
1B1B3	0.750	0.001	45.24	1
1A2B3	7.500	0.01	45.35	1
1B2B3	7.500	0.01	45.37	1
1A3B3	75.00	0.1	45.42	1
1B3B3	75.00	0.1	45.29	1
1A0B4	0.100	0.0001	58.35	1
1B0B4	0.100	0.0001	58.31	1
1A1B4	1.000	0.001	58.37	1
1B1B4	1.000	0.001	58.20	1
1A2B4	10.00	0.01	58.19	1
1B2B4	10.00	0.01	58.38	1
1A3B4	100.0	0.1	58.33	1
1B3B4	100.0	0.1	58.30	1
Subtotal				32

Table 3.4

Number of Performed Stub Column Tests
Box-Shaped Specimens Assembled from Two Hat Sections
(50SK and 25AK Sheet Steels)

Spec.	Test Speed (in./min.)	Strain Rate (in./in./sec.)	w/t (50SK)	w/t (25AK)	No. of Tests Performed
1A0C1	0.075	0.0001	24.41	22.98	1
1B0C1	0.075	0.0001	24.21	23.14	1
1A1C1	0.750	0.001	24.36	23.12	1
1B1C1	0.750	0.001	24.21	23.06	1
1A2C1	7.500	0.01	24.36	23.03	1
1B2C1	7.500	0.01	24.39	23.15	1
1A3C1	75.00	0.1	24.25	23.04	1
1B3C1	75.00	0.1	24.29	23.06	1
1A0C2	0.086	0.0001	44.52	42.39	1
1B0C2	0.086	0.0001	44.66	41.96	1
1A1C2	0.857	0.001	44.64	42.20	1
1B1C2	0.857	0.001	44.68	42.43	1
1A2C2	8.571	0.01	44.68	42.26	1
1B2C2	8.571	0.01	44.53	42.33	1
1A3C2	85.71	0.1	44.24	42.12	1
1B3C2	85.71	0.1	44.41	42.44	1
1A0C3	0.075	0.0001	47.78	45.33	1
1B0C3	0.075	0.0001	47.76	45.21	1
1A1C3	0.750	0.001	47.82	45.30	1
1B1C3	0.750	0.001	47.78	45.33	1
1A2C3	7.500	0.01	47.80	45.46	1
1B2C3	7.500	0.01	47.78	45.31	1
1A3C3	75.00	0.1	47.80	45.31	1
1B3C3	75.00	0.1	47.82	45.26	1
1A0C4	0.100	0.0001	61.49	58.22	1
1B0C4	0.100	0.0001	61.39	58.28	1
1A1C4	1.000	0.001	61.53	58.28	1
1B1C4	1.000	0.001	61.40	58.26	1
1A2C4	10.00	0.01	61.42	58.29	1
1B2C4	10.00	0.01	61.60	58.16	1
1A3C4	100.0	0.1	61.57	58.07	1
1B3C4	100.0	0.1	61.41	58.22	1
Subtotal					32

Table 3.5

Number of Performed Stub Column Tests
Hat-Shaped Specimens Assembled from Hat Section
(50SK Sheet Steel) and Plate (25AK Sheet Steel)

Spec.	Test Speed (in./min.)	Strain Rate (in./in./sec.)	w/t (50SK)	w/t (25AK)	No. of Tests Performed
1A0D1	0.075	0.0001	17.51	34.26	1
1B0D1	0.075	0.0001	17.52	34.19	1
1A1D1	0.750	0.001	17.41	34.17	1
1B1D1	0.750	0.001	17.68	34.19	1
1A2D1	7.500	0.01	17.41	34.21	1
1B2D1	7.500	0.01	17.56	34.18	1
1A3D1	75.00	0.1	17.44	34.17	1
1B3D1	75.00	0.1	17.56	34.23	1
1A0D2	0.075	0.0001	23.99	40.54	1
1B0D2	0.075	0.0001	24.11	40.53	1
1A1D2	0.750	0.001	24.17	40.49	1
1B1D2	0.750	0.001	24.10	40.54	1
1A2D2	7.500	0.01	23.84	40.49	1
1B2D2	7.500	0.01	24.09	40.54	1
1A3D2	75.00	0.1	23.99	40.47	1
1B3D2	75.00	0.1	24.11	40.50	1
1A0D3	0.086	0.0001	44.33	59.63	1
1B0D3	0.086	0.0001	44.30	59.69	1
1A1D3	0.857	0.001	44.43	59.68	1
1B1D3	0.857	0.001	44.15	59.69	1
1A2D3	8.571	0.01	44.14	59.72	1
1B2D3	8.571	0.01	44.36	59.72	1
1A3D3	85.71	0.1	44.07	59.72	1
1B3D3	85.71	0.1	44.36	59.73	1
Subtotal					24

Table 3.6

Number of Performed Stub Column Tests
Hat-Shaped Specimens Assembled from Hat Section
(25AK Sheet Steel) and Plate (50SK Sheet Steel)

Spec.	Test Speed (in./min.)	Strain Rate (in./in./sec.)	w/t (50SK)	w/t (25AK)	No. of Tests Performed
1A0E1	0.075	0.0001	9.67	29.05	1
1B0E1	0.075	0.0001	10.22	29.08	1
1A1E1	0.750	0.001	10.10	29.03	1
1B1E1	0.750	0.001	10.10	28.97	1
1A2E1	7.500	0.01	9.74	29.03	1
1B2E1	7.500	0.01	9.98	29.01	1
1A3E1	75.00	0.1	10.20	29.03	1
1B3E1	75.00	0.1	10.19	28.99	1
1A0E2	0.075	0.0001	22.90	42.50	1
1B0E2	0.075	0.0001	22.93	42.53	1
1A1E2	0.750	0.001	23.20	42.64	1
1B1E2	0.750	0.001	22.92	42.55	1
1A2E2	7.500	0.01	22.96	42.50	1
1B2E2	7.500	0.01	23.06	42.51	1
1A3E2	75.00	0.1	23.01	42.51	1
1B3E2	75.00	0.1	22.89	42.49	1
1A0E3	0.086	0.0001	42.28	62.74	1
1B0E3	0.086	0.0001	41.98	62.78	1
1A1E3	0.857	0.001	42.13	62.73	1
1B1E3	0.857	0.001	42.06	62.78	1
1A2E3	8.571	0.01	42.16	62.73	1
1B2E3	8.571	0.01	42.02	62.74	1
1A3E3	85.71	0.1	42.24	62.72	1
1B3E3	85.71	0.1	42.17	62.76	1
Subtotal					24

Table 3.7

Average Mechanical Properties of 25AK Sheet Steel Used in the Experimental Study Under Different Strain Rates

Strain Rate in./in./sec.	$(F_y)_c$ (ksi)	$(F_{pr})_c$ (ksi)	$(F_y)_t$ (ksi)	$(F_u)_t$ (ksi)	Elongation (%)
0.0001	21.66	15.93	24.60	42.76	-----
0.01	24.77	19.55	27.86	44.44	49.31
0.1	29.80	22.81	31.72	47.35	50.98
1.0	38.14	*****	35.13	51.25	58.18

Table 3.8

Average Mechanical Properties of 50SK Sheet Steel Used in the Experimental Study Under Different Strain Rates

Strain Rate in./in./sec.	$(F_y)_c$ (ksi)	$(F_{pr})_c$ (ksi)	$(F_y)_t$ (ksi)	$(F_u)_t$ (ksi)	Elongation (%)
0.0001	53.35	41.98	54.97	67.07	36.09
0.01	55.91	42.46	56.83	68.98	33.34
0.1	56.96	44.36	58.06	71.04	34.45
1.0	59.41	*****	60.73	76.50	40.13

Notes:

1) $(F_y)_c$ and $(F_{pr})_c$ are based on longitudinal compression coupon tests.
2) $(F_y)_t$ and $(F_u)_t$ and Elongation are determined from longitudinal tension coupon tests.
3) Elongation was measured by using a 2-in. gage length.

Table 3.9

Dimensions of Box-Shaped Columns Assembled from Two Hat Sections
(50SK Sheet Steel)

Spec.	BF (in.)	BW (in.)	BL (in.)	Area ($in.^2$)	w/t	Length (in.)
1A0A1	2.259	1.993	0.849	1.1046	24.30	11.97
1B0A1	2.266	1.990	0.853	1.1058	24.40	11.96
1A1A1	2.259	1.990	0.847	1.1030	24.30	11.96
1B1A1	2.260	1.995	0.847	1.1046	24.32	11.97
1A2A1	2.256	1.994	0.851	1.1049	24.26	11.95
1B2A1	2.247	1.993	0.844	1.1012	24.14	11.97
1A3A1	2.257	1.993	0.847	1.1036	24.28	11.96
1B3A1	2.255	1.985	0.844	1.1000	24.25	11.95
1A0A2	3.743	1.986	0.848	1.3217	44.36	14.94
1B0A2	3.751	1.982	0.840	1.3194	44.47	14.88
1A1A2	3.757	1.988	0.847	1.3241	44.55	15.00
1B1A2	3.756	1.983	0.843	1.3213	44.53	14.99
1A2A2	3.763	1.991	0.842	1.3244	44.63	15.00
1B2A2	3.747	1.984	0.845	1.3208	44.41	15.00
1A3A2	3.751	1.983	0.845	1.3211	44.47	15.00
1B3A2	3.749	1.982	0.845	1.3205	44.44	15.00
1A0A3	3.997	1.118	0.840	1.1000	47.79	11.98
1B0A3	4.003	1.111	0.837	1.0980	47.87	11.98
1A1A3	3.989	1.115	0.840	1.0980	47.68	11.95
1B1A3	4.000	1.112	0.836	1.0975	47.83	11.96
1A2A3	4.003	1.111	0.839	1.0985	47.87	11.97
1B2A3	4.002	1.113	0.840	1.0993	47.86	11.94
1A3A3	3.997	1.111	0.840	1.0980	47.79	11.98
1B3A3	3.999	1.116	0.835	1.0983	47.82	11.94
1A0A4	5.016	1.978	0.844	1.5066	61.56	18.00
1B0A4	5.007	1.976	0.844	1.5047	61.44	17.95
1A1A4	4.992	1.983	0.850	1.5063	61.24	17.95
1B1A4	5.003	1.977	0.848	1.5055	61.39	17.97
1A2A4	5.005	1.974	0.847	1.5047	61.41	17.95
1B2A4	5.014	1.984	0.844	1.5081	61.53	17.98
1A3A4	5.011	1.986	0.846	1.5088	61.49	17.95
1B3A4	5.012	1.975	0.847	1.5060	61.51	17.94

Note : * For symbols of dimensions, see Figure 3.1(a).
* The thickness of 50SK sheet steel is 0.074 in..
* The inside bend radius (R) is 0.15625 (5/32) in. for all specimens.

Table 3.10

Dimensions of Box-Shaped Columns Assembled from Two Hat Sections
(25AK Sheet Steel)

Spec.	BF (in.)	BW (in.)	BL (in.)	Area ($in.^2$)	w/t	Length (in.)
1A0B1	2.267	1.994	0.855	1.1658	23.06	11.98
1B0B1	2.265	1.997	0.861	1.1683	23.03	11.98
1A1B1	2.273	1.993	0.854	1.1661	23.13	11.99
1B1B1	2.268	1.993	0.861	1.1675	23.07	11.96
1A2B1	2.276	1.991	0.852	1.1653	23.17	11.98
1B2B1	2.275	1.991	0.863	1.1686	23.16	11.97
1A3B1	2.276	1.999	0.855	1.1688	23.17	11.98
1B3B1	2.264	1.993	0.862	1.1672	23.02	11.97
1A0B2	3.788	1.981	0.866	1.4025	42.56	14.94
1B0B2	3.768	1.986	0.865	1.4006	42.30	14.94
1A1B2	3.752	1.994	0.867	1.4012	42.10	14.95
1B1B2	3.772	1.992	0.861	1.4018	42.35	14.93
1A2B2	3.767	1.986	0.864	1.4001	42.29	14.97
1B2B2	3.770	1.983	0.863	1.3993	42.33	14.94
1A3B2	3.768	1.981	0.860	1.3975	42.30	14.93
1B3B2	3.780	1.982	0.863	1.4006	42.46	14.97
1A0B3	3.995	1.125	0.850	1.1627	45.21	11.95
1B0B3	4.001	1.121	0.859	1.1652	45.29	11.94
1A1B3	4.006	1.123	0.845	1.1622	45.35	11.94
1B1B3	3.997	1.129	0.848	1.1636	45.24	11.97
1A2B3	4.006	1.114	0.856	1.1629	45.35	11.95
1B2B3	4.007	1.123	0.851	1.1643	45.37	11.94
1A3B3	4.011	1.115	0.850	1.1621	45.42	11.95
1B3B3	4.001	1.125	0.856	1.1655	45.29	11.95
1A0B4	5.020	1.978	0.859	1.5915	58.35	17.95
1B0B4	5.017	1.985	0.855	1.5920	58.31	17.97
1A1B4	5.021	1.983	0.853	1.5914	58.36	17.95
1B1B4	5.008	1.987	0.855	1.5912	58.20	17.94
1A2B4	5.007	1.982	0.858	1.5904	58.19	17.96
1B2B4	5.022	1.986	0.859	1.5943	58.38	17.94
1A3B4	5.018	1.980	0.855	1.5906	58.33	17.94
1B3B4	5.016	1.983	0.855	1.5912	58.30	17.92

Note : * For symbols of dimensions, see Figure 3.1(a).
* The thickness of 25AK sheet steel is 0.078 in..
* The inside bend radius (R) is 0.15625 (5/32) in. for all specimens.

Table 3.11

Dimensions of Box-Shaped Columns Assembled from Two Hat Sections
(50SK and 25AK Sheet Steels)

Spec.	Steel type	BF (in.)	BW (in.)	BL (in.)	Area ($in.^2$)	w/t	Length (in.)
1A0C1	50SK	2.267	1.990	0.847	0.5521	24.41	11.96
	25AK	2.261	1.990	0.865	0.5834	22.98	11.96
1B0C1	50SK	2.252	1.994	0.844	0.5511	24.21	11.97
	25AK	2.273	1.994	0.859	0.5840	23.13	11.97
1A1C1	50SK	2.263	1.986	0.843	0.5506	24.36	11.95
	25AK	2.272	1.986	0.857	0.5824	23.12	11.95
1B1C1	50SK	2.252	1.992	0.843	0.5507	24.21	11.96
	25AK	2.267	1.992	0.858	0.5831	23.06	11.96
1A2C1	50SK	2.263	1.991	0.845	0.5516	24.36	11.95
	25AK	2.265	1.991	0.857	0.5826	23.03	11.95
1B2C1	50SK	2.265	1.985	0.845	0.5509	24.39	11.97
	25AK	2.274	1.985	0.861	0.5830	23.15	11.97
1A3C1	50SK	2.255	1.991	0.846	0.5512	24.25	11.93
	25AK	2.266	1.991	0.858	0.5828	23.04	11.93
1B3C1	50SK	2.258	1.977	0.844	0.5491	24.29	11.95
	25AK	2.267	1.977	0.860	0.5810	23.06	11.95
1A0C2	50SK	3.755	1.981	0.846	0.6607	44.52	14.92
	25AK	3.775	1.981	0.863	0.6998	42.39	14.92
1B0C2	50SK	3.765	1.985	0.848	0.6623	44.66	14.95
	25AK	3.741	1.985	0.866	0.6982	41.96	14.95
1A1C2	50SK	3.764	1.987	0.842	0.6617	44.64	14.94
	25AK	3.760	1.987	0.864	0.6998	42.20	14.94
1B1C2	50SK	3.767	1.982	0.847	0.6619	44.68	14.93
	25AK	3.778	1.982	0.865	0.7005	42.43	14.93
1A2C2	50SK	3.767	1.979	0.843	0.6609	44.68	14.95
	25AK	3.765	1.979	0.861	0.6983	42.26	14.95
1B2C2	50SK	3.756	1.981	0.849	0.6612	44.53	14.94
	25AK	3.770	1.981	0.864	0.6995	42.33	14.94
1A3C2	50SK	3.734	1.991	0.846	0.6606	44.24	14.95
	25AK	3.754	1.991	0.862	0.6995	42.12	14.95
1B3C2	50SK	3.747	1.989	0.845	0.6612	44.41	14.93
	25AK	3.779	1.989	0.863	0.7013	42.44	14.93

Note : * For symbols of dimensions, see Figure 3.1(a).

Table 3.11 (Cont'd)

Dimensions of Box-Shaped Columns Assembled from Two Hat Sections (50SK and 25AK Sheet Steels)

Spec.	Steel type	BF (in.)	BW (in.)	BL (in.)	Area ($in.^2$)	w/t	Length (in.)
1A0C3	50SK	3.996	1.119	0.843	0.5505	47.78	11.94
	25AK	4.004	1.119	0.851	0.5812	45.33	11.94
1B0C3	50SK	3.995	1.119	0.840	0.5500	47.76	11.95
	25AK	3.995	1.119	0.851	0.5806	45.21	11.95
1A1C3	50SK	3.999	1.114	0.841	0.5497	47.82	11.95
	25AK	4.002	1.114	0.849	0.5800	45.30	11.95
1B1C3	50SK	3.996	1.113	0.839	0.5491	47.78	11.93
	25AK	4.004	1.113	0.853	0.5806	45.33	11.93
1A2C3	50SK	3.998	1.108	0.841	0.5488	47.80	11.94
	25AK	4.014	1.108	0.858	0.5814	45.46	11.94
1B2C3	50SK	3.996	1.113	0.843	0.5496	47.78	11.95
	25AK	4.003	1.113	0.851	0.5803	45.31	11.95
1A3C3	50SK	3.998	1.120	0.840	0.5504	47.80	11.94
	25AK	4.003	1.120	0.854	0.5818	45.31	11.94
1B3C3	50SK	3.999	1.118	0.842	0.5505	47.82	11.96
	25AK	3.999	1.118	0.850	0.5806	45.26	11.96
1A0C4	50SK	5.011	1.979	0.853	0.7544	61.49	17.94
	25AK	5.010	1.979	0.853	0.7942	58.22	17.94
1B0C4	50SK	5.003	1.978	0.848	0.7529	61.39	17.95
	25AK	5.014	1.978	0.848	0.7400	58.28	17.95
1A1C4	50SK	5.014	1.976	0.850	0.7537	61.53	17.93
	25AK	5.014	1.976	0.853	0.7941	58.28	17.93
1B1C4	50SK	5.004	1.981	0.847	0.7533	61.40	17.95
	25AK	5.013	1.981	0.853	0.7948	58.26	17.95
1A2C4	50SK	5.006	1.980	0.850	0.7537	61.43	17.97
	25AK	5.015	1.980	0.853	0.7948	58.29	17.97
1B2C4	50SK	5.019	1.981	0.845	0.7541	61.60	17.93
	25AK	5.005	1.981	0.854	0.7943	58.16	17.93
1A3C4	50SK	5.017	1.980	0.849	0.7544	61.57	17.94
	25AK	4.998	1.980	0.854	0.7936	58.07	17.94
1B3C4	50SK	5.005	1.988	0.844	0.7540	61.42	17.93
	25AK	5.010	1.988	0.850	0.7951	58.22	17.93

Note : * For symbols of dimensions, see Figure 3.1(a).

Table 3.12

Dimensions of Hat-Shaped Columns Assembled from Hat Section (50SK Sheet Steel) and Plate (25AK Sheet Steel)

(a) Dimensions of Hat Sections (50SK Sheet Steel)

Spec.	BF (in.)	BW (in.)	BL (in.)	Area ($in.^2$)	w/t	Length (in.)
1A0D1	1.756	1.993	0.839	0.5135	17.51	11.94
1B0D1	1.757	2.001	0.839	0.5148	17.52	11.97
1A1D1	1.749	2.003	0.839	0.5145	17.41	11.94
1B1D1	1.769	1.993	0.840	0.5146	17.68	11.94
1A2D1	1.749	1.995	0.839	0.5133	17.41	11.95
1B2D1	1.760	1.992	0.840	0.5138	17.56	11.95
1A3D1	1.751	1.999	0.844	0.5148	17.44	11.96
1B3D1	1.760	1.990	0.833	0.5125	17.56	11.98
1A0D2	2.236	2.009	0.844	0.5522	23.99	11.94
1B0D2	2.245	1.995	0.844	0.5508	24.11	11.93
1A1D2	2.249	1.998	0.848	0.5521	24.17	11.59
1B1D2	2.244	1.993	0.844	0.5504	24.10	11.94
1A2D2	2.225	2.004	0.845	0.5508	23.84	11.88
1B2D2	2.243	1.994	0.843	0.5503	24.09	11.94
1A3D2	2.236	1.994	0.847	0.5504	23.99	11.94
1B3D2	2.245	1.993	0.845	0.5506	24.11	11.94
1A0D3	3.741	1.986	0.849	0.6609	44.33	14.93
1B0D3	3.739	1.990	0.847	0.6610	44.30	14.95
1A1D3	3.748	1.993	0.850	0.6626	44.43	14.94
1B1D3	3.725	1.997	0.845	0.6608	44.15	14.94
1A2D3	3.727	1.994	0.847	0.6607	44.14	14.94
1B2D3	3.743	1.998	0.844	0.6621	44.36	14.95
1A3D3	3.722	2.002	0.847	0.6615	44.07	14.94
1B3D3	3.743	2.000	0.844	0.6623	44.36	14.93

Note : * For symbols of dimensions, see Figure 3.1(b).
* w = WF, see Figure 3.1(b).

Table 3.12 (Cont'd)

Dimensions of Hat-Shaped Columns Assembled from Hat Section (50SK Sheet Steel) and Plate (25AK Sheet Steel)

(b) Dimensions of Plates (25AK Sheet Steel)

Spec.	BP (in.)	Area ($in.^2$)	w/t	Length (in.)
1A0D1	3.511	0.2739	34.26	11.94
1B0D1	3.506	0.2735	34.19	11.97
1A1D1	3.504	0.2733	34.17	11.94
1B1D1	3.507	0.2735	34.19	11.94
1A2D1	3.507	0.2735	34.21	11.95
1B2D1	3.506	0.2735	34.18	11.95
1A3D1	3.509	0.2737	34.17	11.96
1B3D1	3.503	0.2732	34.23	11.98
1A0D2	4.006	0.3125	40.54	11.94
1B0D2	4.005	0.3124	40.53	11.93
1A1D2	4.006	0.3125	40.49	11.59
1B1D2	4.006	0.3125	40.54	11.94
1A2D2	4.003	0.3122	40.49	11.88
1B2D2	4.005	0.3124	40.54	11.94
1A3D2	4.004	0.3123	40.47	11.94
1B3D2	4.004	0.3123	40.50	11.94
1A0D3	5.500	0.4290	59.63	14.93
1B0D3	5.503	0.4292	59.69	14.95
1A1D3	5.505	0.4294	59.68	14.94
1B1D3	5.501	0.4291	59.69	14.94
1A2D3	5.505	0.4294	59.72	14.94
1B2D3	5.502	0.4292	59.72	14.95
1A3D3	5.505	0.4294	59.72	14.94
1B3D3	5.503	0.4292	59.73	14.93

Note : * For symbols of dimensions, see Figure 3.1(b).
* w = WP, see Figure 3.1(b)

Table 3.13

Dimensions of Hat-Shaped Columns Assembled from Hat Section (25AK Sheet Steel) and Plate (50SK Sheet Steel)

(a) Dimensions of Hat Sections (25AK Sheet Steel)

Spec.	BF (in.)	BW (in.)	BL (in.)	Area ($in.^2$)	w/t	Length (in.)
1A0E1	1.223	2.019	0.855	0.5054	9.67	11.94
1B0E1	1.266	1.997	0.853	0.5050	10.22	11.95
1A1E1	1.256	2.008	0.855	0.5062	10.10	11.95
1B1E1	1.256	2.000	0.858	0.5055	10.10	11.95
1A2E1	1.228	2.018	0.858	0.5061	9.74	11.96
1B2E1	1.247	2.009	0.858	0.5062	9.98	11.93
1A3E1	1.264	2.001	0.856	0.5059	10.20	11.94
1B3E1	1.263	2.003	0.858	0.5065	10.19	11.94
1A0E2	2.225	1.996	0.860	0.5831	22.90	11.95
1B0E2	2.257	2.004	0.861	0.5846	22.93	11.94
1A1E2	2.278	1.995	0.851	0.5833	23.20	11.94
1B1E2	2.256	1.994	0.860	0.5828	22.92	11.95
1A2E2	2.259	1.997	0.861	0.5837	22.96	11.95
1B2E2	2.267	1.996	0.861	0.5842	23.06	11.94
1A3E2	2.263	1.996	0.861	0.5838	23.01	11.97
1B3E2	2.254	1.997	0.865	0.5839	22.89	11.94
1A0E3	3.766	2.004	0.862	0.7025	42.28	14.94
1B0E3	3.743	2.008	0.860	0.7010	41.98	14.94
1A1E3	3.755	2.012	0.864	0.7032	42.13	14.94
1B1E3	3.749	2.010	0.859	0.7016	42.06	14.94
1A2E3	3.757	2.006	0.864	0.7024	42.16	14.94
1B2E3	3.746	1.991	0.863	0.6991	42.02	14.95
1A3E3	3.763	1.992	0.865	0.7004	42.24	14.95
1B3E3	3.758	1.992	0.860	0.6997	42.17	14.94

Note : * For symbols of dimensions, see Figure 3.1(b).
* w = WF, see Figure 3.1(b)

Table 3.13 (Cont'd)

Dimensions of Hat-Shaped Columns Assembled from Hat Section (25AK Sheet Steel) and Plate (50SK Sheet Steel)

(b) Dimensions of Plates (50SK Sheet Steel)

Spec.	BP (in.)	Area ($in.^2$)	w/t	Length (in.)
1A0E1	3.005	0.2224	29.05	11.94
1B0E1	3.005	0.2224	29.08	11.95
1A1E1	3.003	0.2222	29.03	11.95
1B1E1	3.002	0.2221	28.97	11.95
1A2E1	3.006	0.2224	29.03	11.96
1B2E1	3.005	0.2224	29.01	11.93
1A3E1	3.004	0.2223	29.03	11.94
1B3E1	3.003	0.2222	28.99	11.94
1A0E2	4.006	0.2964	42.50	11.95
1B0E2	4.008	0.2966	42.53	11.94
1A1E2	4.006	0.2964	42.64	11.94
1B1E2	4.009	0.2967	42.55	11.95
1A2E2	4.006	0.2964	42.50	11.95
1B2E2	4.007	0.2965	42.51	11.94
1A3E2	4.007	0.2965	42.51	11.97
1B3E2	4.009	0.2967	42.49	11.94
1A0E3	5.505	0.4074	62.74	14.94
1B0E3	5.506	0.4074	62.78	14.94
1A1E3	5.506	0.4074	62.73	14.94
1B1E3	5.505	0.4074	62.78	14.94
1A2E3	5.506	0.4074	62.73	14.94
1B2E3	5.506	0.4074	62.74	14.95
1A3E3	5.506	0.4074	62.72	14.95
1B3E3	5.504	0.4073	62.76	14.94

Note : * For symbols of dimensions, see Figure 3.1(b).
* w = WP, see Figure 3.1(b).

Table 4.1

Comparison of Computed and Tested Critical Local Buckling Loads
Box-Shaped Stub Columns Assembled from Two Hat Sections
(50SK Sheet Steel)

Spec.	Strain Rate (in./in./sec.)	$(f_{cr})_{comp}$ (ksi) (1)	$(P_{cr})_{comp}$ (kips) (2)	$(P_{cr})_{test}$ (kips) (3)	(3)/(2) (4)
1A0A1	0.0001	50.70	56.00	N/A	N/A
1B0A1	0.0001	50.69	56.05	N/A	N/A
1A1A1	0.001	51.52	56.83	N/A	N/A
1B1A1	0.001	51.52	56.91	N/A	N/A
1A2A1	0.01	52.76	58.29	N/A	N/A
1B2A1	0.01	52.79	58.13	N/A	N/A
1A3A1	0.1	53.87	59.45	N/A	N/A
1B3A1	0.1	53.88	59.27	N/A	N/A
1A0A2	0.0001	44.54	58.87	N/A	N/A
1B0A2	0.0001	44.50	58.71	N/A	N/A
1A1A2	0.001	44.82	59.35	N/A	N/A
1B1A2	0.001	44.83	59.23	N/A	N/A
1A2A2	0.01	45.24	59.92	N/A	N/A
1B2A2	0.01	45.35	59.90	N/A	N/A
1A3A2	0.1	46.60	61.56	N/A	N/A
1B3A2	0.1	46.61	61.55	N/A	N/A
1A0A3	0.0001	43.13	47.44	49.73	1.05
1B0A3	0.0001	43.09	47.31	47.87	1.01
1A1A3	0.001	43.43	47.68	50.81	1.08
1B1A3	0.001	43.36	47.59	47.63	1.00
1A2A3	0.01	43.64	47.94	50.46	1.05
1B2A3	0.01	43.65	47.98	48.12	1.00
1A3A3	0.1	44.99	49.40	52.32	1.06
1B3A3	0.1	44.98	49.40	49.83	1.01
1A0A4	0.0001	28.14	42.40	47.83	1.13
1B0A4	0.0001	28.25	42.51	46.46	1.09
1A1A4	0.001	28.44	42.84	47.88	1.12
1B1A4	0.001	28.30	42.61	43.58	1.02
1A2A4	0.01	28.28	42.55	47.54	1.12
1B2A4	0.01	28.17	42.48	48.31	1.14
1A3A4	0.1	28.20	42.55	45.29	1.06
1B3A4	0.1	28.19	42.46	47.53	1.12
Mean					1.066
Standard Deviation					0.050

Table 4.2

Comparison of Computed and Tested Critical Local Buckling Loads
Box-Shaped Stub Columns Assembled from Two Hat Sections
(25AK Sheet Steel)

Spec.	Strain Rate (in./in./sec.)	$(f_{cr})_{comp}$ (ksi) (1)	$(P_{cr})_{comp}$ (kips) (2)	$(P_{cr})_{test}$ (kips) (3)	(3)/(2) (4)
1A0B1	0.0001	21.20	24.72	N/A	N/A
1B0B1	0.0001	21.21	24.78	N/A	N/A
1A1B1	0.001	21.46	25.03	N/A	N/A
1B1B1	0.001	21.46	25.06	N/A	N/A
1A2B1	0.01	24.26	28.27	N/A	N/A
1B2B1	0.01	24.26	28.35	N/A	N/A
1A3B1	0.1	29.00	33.89	N/A	N/A
1B3B1	0.1	29.01	33.86	N/A	N/A
1A0B2	0.0001	20.11	28.20	N/A	N/A
1B0B2	0.0001	20.13	28.19	N/A	N/A
1A1B2	0.001	20.62	28.90	N/A	N/A
1B1B2	0.001	20.61	28.89	N/A	N/A
1A2B2	0.01	23.06	32.29	N/A	N/A
1B2B2	0.01	23.06	32.26	N/A	N/A
1A3B2	0.1	27.12	37.91	N/A	N/A
1B3B2	0.1	27.11	37.96	N/A	N/A
1A0B3	0.0001	19.91	23.15	N/A	N/A
1B0B3	0.0001	19.90	23.19	N/A	N/A
1A1B3	0.001	20.43	23.75	N/A	N/A
1B1B3	0.001	20.44	23.78	N/A	N/A
1A2B3	0.01	22.80	26.51	N/A	N/A
1B2B3	0.01	22.80	26.55	N/A	N/A
1A3B3	0.1	26.72	31.05	N/A	N/A
1B3B3	0.1	26.73	31.16	N/A	N/A
1A0B4	0.0001	18.75	29.83	37.81	1.27
1B0B4	0.0001	18.75	29.85	38.89	1.30
1A1B4	0.001	19.51	31.05	41.38	1.33
1B1B4	0.001	19.53	31.07	N/A	N/A
1A2B4	0.01	21.53	34.24	44.55	1.30
1B2B4	0.01	21.51	34.29	44.41	1.30
1A3B4	0.1	24.71	39.31	48.27	1.23
1B3B4	0.1	24.72	39.33	47.78	1.21
Mean					1.277
Standard Deviation					0.043

Table 4.3

Comparison of Computed and Tested Critical Local Buckling Loads
Box-Shaped Stub Columns Assembled from Two Hat Sections
(50SK and 25AK Sheet Steels)

Spec.	Strain Rate (in./in./sec.)	$(f_{cr})_{comp}$ (ksi) (1)	$(P_{cr})_{comp}$ (kips) (2)	$(P_{cr})_{test}$ (kips) (3)	(3)/(2) (4)
1A0C1	0.0001	50.68*	40.03	N/A	N/A
1B0C1	0.0001	50.73*	40.03	N/A	N/A
1A1C1	0.001	51.51*	40.68	N/A	N/A
1B1C1	0.001	51.54*	40.71	N/A	N/A
1A2C1	0.01	24.26**	43.20	N/A	N/A
1B2C1	0.01	24.26**	43.17	N/A	N/A
1A3C1	0.1	53.88*	45.82	N/A	N/A
1B3C1	0.1	53.87*	45.65	N/A	N/A
1A0C2	0.0001	44.48*	43.37	N/A	N/A
1B0C2	0.0001	44.43*	43.38	N/A	N/A
1A1C2	0.001	44.78*	43.93	N/A	N/A
1B1C2	0.001	44.77*	43.94	N/A	N/A
1A2C2	0.01	23.06**	44.97	N/A	N/A
1B2C2	0.01	23.06**	45.01	N/A	N/A
1A3C2	0.1	46.71*	49.47	N/A	N/A
1B3C2	0.1	46.62*	49.49	N/A	N/A
1A0C3	0.0001	43.13*	35.27	38.54	1.09
1B0C3	0.0001	43.14*	35.23	39.18	1.11
1A1C3	0.001	43.37*	35.60	40.74	1.14
1B1C3	0.001	43.39*	35.59	39.96	1.12
1A2C3	0.01	22.79**	36.57	42.26	1.16
1B2C3	0.01	22.81**	36.58	42.55	1.16
1A3C3	0.1	44.98*	40.08	42.79	1.08
1B3C3	0.1	44.98*	40.04	43.58	1.09
1A0C4	0.0001	28.20*	34.55	39.67	1.15
1B0C4	0.0001	28.30*	34.60	39.03	1.13
1A1C4	0.001	28.17*	35.03	41.91	1.20
1B1C4	0.001	28.29*	35.15	40.99	1.17
1A2C4	0.01	28.27*	36.03	42.70	1.19
1B2C4	0.01	28.27*	35.91	41.82	1.16
1A3C4	0.1	28.13*	37.02	43.72	1.18
1B3C4	0.1	28.28*	37.23	45.43	1.22
Mean					1.146
Standard Deviation					0.043

Note: The superscripts * and ** in column (1) represent the critical stresses for sections fabricated from 50SK and 25AK sheet steels, respectively.

Table 4.4

Comparison of Computed and Tested Critical Local Buckling Loads
Hat-Shaped Stub Columns Assembled from Hat Section (50SK)
and plate (25AK)

Spec.	Strain Rate (in./in./sec.)	$(f_{cr})_{comp}$ (ksi) (1)	$(P_{cr})_{comp}$ (kips) (2)	$(P_{cr})_{test}$ (kips) (3)	(3)/(2) (4)
1A0D1	0.0001	20.66**	31.73	N/A	N/A
1B0D1	0.0001	20.66**	31.78	N/A	N/A
1A1D1	0.001	21.04**	31.71	N/A	N/A
1B1D1	0.001	21.03**	31.72	N/A	N/A
1A2D1	0.01	23.65**	30.93	N/A	N/A
1B2D1	0.01	23.65**	30.95	N/A	N/A
1A3D1	0.1	55.37*	36.12	N/A	N/A
1B3D1	0.1	55.34*	35.97	N/A	N/A
1A0D2	0.0001	20.25**	32.24	N/A	N/A
1B0D2	0.0001	20.25**	32.17	N/A	N/A
1A1D2	0.001	20.71**	32.48	N/A	N/A
1B1D2	0.001	20.71**	32.40	N/A	N/A
1A2D2	0.01	23.20**	32.26	N/A	N/A
1B2D2	0.01	23.20**	32.25	N/A	N/A
1A3D2	0.1	27.35**	36.90	N/A	N/A
1B3D2	0.1	27.35**	36.91	N/A	N/A
1A0D3	0.0001	18.61**	31.87	39.81	1.25
1B0D3	0.0001	18.61**	31.88	39.86	1.25
1A1D3	0.001	19.41**	33.27	42.31	1.27
1B1D3	0.001	19.41**	33.20	41.96	1.26
1A2D3	0.01	21.36**	33.14	41.96	1.27
1B2D3	0.01	21.36**	33.19	42.70	1.29
1A3D3	0.1	24.47**	35.46	43.67	1.23
1B3D3	0.1	24.47**	35.48	44.99	1.27
Mean					1.261
Standard Deviation					0.018

Note: The superscripts * and ** in column (1) represent the critical stresses for sections fabricated from 50SK and 25AK sheet steels, respectively.

Table 4.5

Comparison of Computed and Tested Critical Local Buckling Loads
Hat-Shaped Stub Columns Assembled from Hat Section (25AK)
and plate (50SK)

Spec.	Strain Rate (in./in./sec.)	$(f_{cr})_{comp}$ (ksi) (1)	$(P_{cr})_{comp}$ (kips) (2)	$(P_{cr})_{test}$ (kips) (3)	(3)/(2) (4)
1A0E1	0.0001	49.57*	21.41	N/A	N/A
1B0E1	0.0001	49.57*	21.40	N/A	N/A
1A1E1	0.001	50.31*	21.83	N/A	N/A
1B1E1	0.001	50.33*	21.81	N/A	N/A
1A2E1	0.01	51.40*	23.65	N/A	N/A
1B2E1	0.01	51.40*	23.65	N/A	N/A
1A3E1	0.1	52.54*	25.60	N/A	N/A
1B3E1	0.1	52.56*	25.61	N/A	N/A
1A0E2	0.0001	45.27*	25.13	N/A	N/A
1B0E2	0.0001	45.26*	25.16	N/A	N/A
1A1E2	0.001	45.62*	25.50	N/A	N/A
1B1E2	0.001	45.66*	25.51	N/A	N/A
1A2E2	0.01	46.24*	27.40	N/A	N/A
1B2E2	0.01	46.23*	27.41	N/A	N/A
1A3E2	0.1	47.49*	29.71	N/A	N/A
1B3E2	0.1	47.50*	29.72	N/A	N/A
1A0E3	0.0001	27.09*	22.80	24.82	1.09
1B0E3	0.0001	27.06*	22.75	23.35	1.03
1A1E3	0.001	27.10*	23.05	24.28	1.05
1B1E3	0.001	27.06*	22.99	24.67	1.07
1A2E3	0.01	27.10*	23.67	25.82	1.09
1B2E3	0.01	27.09*	23.60	26.24	1.11
1A3E3	0.1	27.11*	24.51	25.99	1.06
1B3E3	0.1	27.08*	24.46	26.77	1.09
Mean					1.074
Standard Deviation					0.026

Note: The superscripts * and ** in column (1) represent the critical stresses for sections fabricated from 50SK and 25AK sheet steels, respectively.

Table 4.6

Comparison of Computed and Tested Ultimate Loads Based on the Effective Width Formulas in the 1991 AISI Automotive Steel Design Manual for Stub Columns Assembled from Two Hat Sections (50SK Sheet Steel)

* Based on Compressive Yield Stresses

Spec.	Strain Rate in./in./sec. (1)	w/t (2)	$(P_u)_{comp}$, kips Based on $(F_y)_s$ (3)	$(F_y)_d$ (4)	$(P_u)_{test}$ kips (5)	(5)/(3) (6)	(5)/(4) (7)
1A0A1	0.0001	24.30	58.92	58.92	59.89	1.02	1.02
1B0A1	0.0001	24.40	58.99	58.99	59.50	1.01	1.01
1A1A1	0.001	24.30	58.84	59.96	60.97	1.04	1.02
1B1A1	0.001	24.32	58.93	60.45	60.04	1.02	0.99
1A2A1	0.01	24.26	58.95	61.76	63.51	1.08	1.03
1B2A1	0.01	24.14	58.75	61.57	62.24	1.06	1.01
1A3A1	0.1	24.28	58.88	62.86	64.48	1.10	1.03
1B3A1	0.1	24.25	58.69	62.66	66.10	1.13	1.05
1A0A2	0.0001	44.36	64.93	64.93	65.02	1.00	1.00
1B0A2	0.0001	44.47	64.75	64.75	65.85	1.02	1.02
1A1A2	0.001	44.55	64.97	66.06	68.51	1.05	1.04
1B1A2	0.001	44.53	64.82	65.91	68.64	1.06	1.04
1A2A2	0.01	44.63	64.94	67.70	70.25	1.08	1.04
1B2A2	0.01	44.41	64.85	67.61	70.20	1.08	1.04
1A3A2	0.1	44.47	64.84	68.73	72.59	1.12	1.06
1B3A2	0.1	44.44	64.83	68.71	72.59	1,12	1.06
1A0A3	0.0001	47.79	51.51	51.51	53.25	1.03	1.03
1B0A3	0.0001	47.87	51.36	51.36	52.32	1.02	1.02
1A1A3	0.001	47.68	51.49	52.28	54.81	1.06	1.05
1B1A3	0.001	47.83	51.35	52.18	53.69	1.05	1.03
1A2A3	0.01	47.87	51.39	53.48	56.08	1.09	1.05
1B2A3	0.01	47.86	51.44	53.53	54.23	1.05	1.01
1A3A3	0.1	47.79	51.40	54.34	58.23	1.13	1.07
1B3A3	0.1	47.82	51.40	54.34	57.74	1.12	1.06
1A0A4	0.0001	61.56	66.35	66.35	65.22	0.98	0.98
1B0A4	0.0001	61.44	66.31	66.31	64.88	0.98	0.98
1A1A4	0.001	61.24	66.51	67.60	66.93	1.01	0.99
1B1A4	0.001	61.39	66.39	67.48	65.22	0.98	0.97
1A2A4	0.01	61.41	66.33	69.08	70.59	1.06	1.02
1B2A4	0.01	61.53	66.45	69.20	71.13	1.07	1.03
1A3A4	0.1	61.49	66.51	70.39	72.45	1.09	1.03
1B3A4	0.1	61.51	66.35	70.22	72.50	1.09	1.03
Mean						1.056	1.025
Standard Deviation						0.045	0.025

Table 4.7

Comparison of Computed and Tested Ultimate Loads Based on the Effective Width Formulas in the 1991 AISI Automotive Steel Design Manual for Stub Columns Assembled from Two Hat Sections (25AK Sheet Steel)

* Based on Compressive Yield Stresses

Spec.	Strain Rate in./in./sec. (1)	w/t (2)	$(P_u)_{comp}$, kips Based on $(F_y)_s$ (3)	$(F_y)_d$ (4)	$(P_u)_{test}$ kips (5)	(5)/(3) (6)	(5)/(4) (7)
1A0B1	0.0001	23.06	25.25	25.25	34.73	1.38	1.38
1B0B1	0.0001	23.03	25.31	25.31	34.68	1.37	1.37
1A1B1	0.001	23.13	25.26	25.45	36.83	1.46	1.45
1B1B1	0.001	23.07	25.29	25.48	36.25	1.43	1.42
1A2B1	0.01	23.17	25.24	28.87	39.42	1.56	1.37
1B2B1	0.01	23.16	25.31	28.95	38.98	1.53	1.35
1A3B1	0.1	23.17	25.32	34.83	43.04	1.70	1.24
1B3B1	0.1	23.02	25.28	34.78	43.09	1.70	1.24
1A0B2	0.0001	42.56	30.38	30.38	37.13	1.22	1.22
1B0B2	0.0001	42.30	30.34	30.34	36.44	1.20	1.20
1A1B2	0.001	42.10	30.35	30.59	39.08	1.29	1.28
1B1B2	0.001	42.35	30.36	30.60	38.74	1.28	1.27
1A2B2	0.01	42.29	30.33	34.68	42.99	1.42	1.24
1B2B2	0.01	42.33	30.31	34.66	42.50	1.40	1.23
1A3B2	0.1	42.30	30.27	41.25	48.46	1.60	1.17
1B3B2	0.1	42.46	30.34	41.31	48.17	1.59	1.17
1A0B3	0.0001	45.21	25.18	25.18	32.63	1.30	1.30
1B0B3	0.0001	45.29	25.24	25.24	32.93	1.30	1.30
1A1B3	0.001	45.35	25.17	25.37	33.61	1.34	1.32
1B1B3	0.001	45.24	25.20	25.40	33.51	1.33	1.32
1A2B3	0.01	45.35	25.19	28.62	36.59	1.45	1.28
1B2B3	0.01	45.37	25.22	28.65	36.64	1.45	1.28
1A3B3	0.1	45.42	25.17	33.57	41.08	1.63	1.22
1B3B3	0.1	45.29	25.24	33.70	40.69	1.61	1.21
1A0B4	0.0001	58.35	32.69	32.69	38.40	1.17	1.17
1B0B4	0.0001	58.31	32.71	32.71	38.89	1.19	1.19
1A1B4	0.001	58.37	32.69	32.91	41.67	1.28	1.27
1B1B4	0.001	58.20	32.17	32.94	40.84	1.27	1.24
1A2B4	0.01	58.19	32.70	36.73	44.65	1.37	1.22
1B2B4	0.01	58.38	32.75	36.78	44.75	1.37	1.22
1A3B4	0.1	58.33	32.68	43.05	48.71	1.49	1.13
1B3B4	0.1	58.30	32.70	43.07	48.56	1.49	1.13
Mean						1.412	1.263
Standard Deviation						0.148	0.080

Table 4.8

Comparison of Computed and Tested Ultimate Loads Based on the Effective Width Formulas in the 1991 AISI Automotive Steel Design Manual for Stub Columns Assembled from Two Hat Sections (50SK and 25AK Sheet Steels)

* Based on Compressive Yield Stresses

Spec.	Strain Rate in./in./sec. (1)	w/t (2)	$(P_u)_{comp}$, kips Based on $(F_y)_s$ (3)	$(F_y)_d$ (4)	$(P_u)_{test}$ kips (5)	(5)/(3) (6)	(5)/(4) (7)
1A0C1	0.0001	24.41	42.09	42.09	44.94	1.07	1.07
1B0C1	0.0001	24.21	42.05	42.05	44.94	1.07	1.07
1A1C1	0.001	24.36	41.99	42.64	48.36	1.15	1.13
1B1C1	0.001	24.21	42.01	42.66	46.70	1.11	1.09
1A2C1	0.01	24.36	42.05	45.27	50.56	1.20	1.12
1B2C1	0.01	24.39	42.02	45.24	50.12	1.19	1.11
1A3C1	0.1	24.25	42.03	48.76	51.59	1.23	1.06
1B3C1	0.1	24.29	41.88	48.59	53.98	1.29	1.11
1A0C2	0.0001	44.52	47.57	47.57	52.37	1.10	1.10
1B0C2	0.0001	44.66	47.60	47.60	51.39	1.08	1.08
1A1C2	0.001	44.64	47.60	48.26	52.91	1.11	1.10
1B1C2	0.001	44.68	47.62	48.28	52.42	1.10	1.09
1A2C2	0.01	44.68	47.52	51.06	57.16	1.20	1.12
1B2C2	0.01	44.53	47.59	51.15	56.33	1.18	1.10
1A3C2	0.1	44.24	47.63	55.09	60.04	1.26	1.09
1B3C2	0.1	44.41	47.66	55.10	57.94	1.22	1.05
1A0C3	0.0001	47.78	38.38	38.38	42.16	1.10	1.10
1B0C3	0.0001	47.76	38.34	38.34	42.45	1.11	1.11
1A1C3	0.001	47.82	38.30	38.81	43.67	1.14	1.13
1B1C3	0.001	47.78	38.28	38.79	43.38	1.13	1.12
1A2C3	0.01	47.80	38.28	41.03	46.56	1.22	1.13
1B2C3	0.01	47.78	38.31	41.07	47.00	1.23	1.14
1A3C3	0.1	47.80	38.37	44.07	48.17	1.26	1.09
1B3C3	0.1	47.82	38.35	44.03	49.63	1.29	1.13
1A0C4	0.0001	61.49	49.58	49.58	51.83	1.05	1.05
1B0C4	0.0001	61.39	49.51	49.51	51.05	1.03	1.03
1A1C4	0.001	61.53	49.52	50.18	54.62	1.10	1.09
1B1C4	0.001	61.40	49.55	50.21	53.16	1.07	1.06
1A2C4	0.01	61.42	49.57	52.74	57.40	1.16	1.09
1B2C4	0.01	61.60	49.54	52.93	55.50	1.12	1.05
1A3C4	0.1	61.57	49.56	56.68	58.43	1.18	1.03
1B3C4	0.1	61.41	49.60	56.73	60.14	1.21	1.06
Mean						1.155	1.091
Standard Deviation						0.072	0.030

Note: The values of w/t ratio shown in this table are based on the sections fabricated from 50SK sheet steel.

Table 4.9

Comparison of Computed and Tested Ultimate Loads Based on the Effective Width Formulas in the 1991 AISI Automotive Steel Design Manual for Stub Columns Assembled from Hat Section (50SK Sheet Steel) and Plate (25AK Sheet Steel)

* Based on Compressive Yield Stresses

Spec.	Strain Rate in./in./sec. (1)	w/t (2)	$(P_u)_{comp}$, kips Based on $(F_y)_s$ (3)	$(F_y)_d$ (4)	$(P_u)_{test}$ kips (5)	(5)/(3) (6)	(5)/(4) (7)
1A0D1	0.0001	34.26	33.33	33.33	34.08	1.02	1.02
1B0D1	0.0001	34.19	33.38	33.38	33.71	1.01	1.01
1A1D1	0.001	34.17	33.37	33.94	34.10	1.02	1.00
1B1D1	0.001	34.19	33.39	33.95	34.39	1.03	1.01
1A2D1	0.01	34.21	33.32	35.48	37.03	1.11	1.04
1B2D1	0.01	34.18	33.33	35.50	38.01	1.14	1.07
1A3D1	0.1	34.17	33.39	37.48	39.28	1.18	1.05
1B3D1	0.1	34.23	33.26	37.33	40.25	1.21	1.08
1A0D2	0.0001	40.54	36.23	36.23	37.27	1.03	1.03
1B0D2	0.0001	40.53	36.15	36.15	37.91	1.05	1.05
1A1D2	0.001	40.49	36.22	36.83	37.83	1.04	1.03
1B1D2	0.001	40.54	36.13	36.74	38.79	1.07	1.06
1A2D2	0.01	40.49	36.14	38.52	40.69	1.13	1.06
1B2D2	0.01	40.54	36.13	38.51	40.25	1.11	1.05
1A3D2	0.1	40.47	36.12	40.64	41.28	1.14	1.02
1B3D2	0.1	40.50	36.13	40.65	43.28	1.20	1.06
1A0D3	0.0001	59.63	40.76	40.76	41.82	1.03	1.03
1B0D3	0.0001	59.69	40.77	40.77	42.50	1.04	1.04
1A1D3	0.001	59.68	40.83	41.43	44.06	1.08	1.06
1B1D3	0.001	59.69	40.79	41.39	44.16	1.08	1.07
1A2D3	0.01	59.72	40.79	43.02	45.04	1.10	1.05
1B2D3	0.01	59.72	40.81	43.04	46.17	1.13	1.07
1A3D3	0.1	59.72	40.85	44.93	48.02	1.18	1.07
1B3D3	0.1	59.73	40.82	44.91	48.56	1.19	1.08
Mean						1.097	1.046
Standard Deviation						0.064	0.023

Note: The values of w/t ratio shown in this table are based on the sections fabricated from 25AK sheet steel.

Table 4.10

Comparison of Computed and Tested Ultimate Loads Based on the Effective Width Formulas in the 1991 AISI Automotive Steel Design Manual for Stub Columns Assembled from Hat Section (25AK Sheet Steel) and Plate (50SK Sheet Steel)

* Based on Compressive Yield Stresses

Spec.	Strain Rate in./in./sec. (1)	w/t (2)	$(P_u)_{comp}$, kips Based on $(F_y)_s$ (3)	$(F_y)_d$ (4)	$(P_u)_{test}$ kips (5)	(5)/(3) (6)	(5)/(4) (7)
1A0E1	0.0001	29.05	22.81	22.81	24.72	1.08	1.08
1B0E1	0.0001	29.08	22.80	22.80	25.50	1.12	1.12
1A1E1	0.001	29.03	22.83	23.13	26.62	1.17	1.15
1B1E1	0.001	28.97	22.80	23.11	26.09	1.14	1.13
1A2E1	0.01	29.03	22.83	24.98	27.85	1.22	1.11
1B2E1	0.01	29.01	22.82	24.97	27.80	1.22	1.11
1A3E1	0.1	29.03	22.82	27.74	30.04	1.32	1.08
1B3E1	0.1	28.99	22.83	27.75	29.51	1.29	1.06
1A0E2	0.0001	42.50	26.06	26.06	30.87	1.18	1.18
1B0E2	0.0001	42.53	26.10	26.10	30.87	1.18	1.18
1A1E2	0.001	42.64	26.04	26.32	32.14	1.23	1.22
1B1E2	0.001	42.55	26.06	26.34	31.12	1.19	1.18
1A2E2	0.01	42.50	26.08	28.37	34.49	1.32	1.22
1B2E2	0.01	42.51	26.09	28.38	33.22	1.27	1.17
1A3E2	0.1	42.51	26.09	31.50	35.96	1.38	1.14
1B3E2	0.1	42.49	26.10	31.52	35.66	1.37	1.13
1A0E3	0.0001	62.47	29.64	29.64	31.17	1.05	1.05
1B0E3	0.0001	62.78	29.59	29.59	31.02	1.05	1.05
1A1E3	0.001	62.73	29.65	29.96	32.54	1.10	1.09
1B1E3	0.001	62.78	29.61	29.91	31.56	1.07	1.06
1A2E3	0.01	62.73	29.63	32.30	35.08	1.18	1.09
1B2E3	0.01	62.74	29.56	32.21	34.39	1.16	1.07
1A3E3	0.1	62.72	29.60	35.77	36.79	1.24	1.03
1B3E3	0.1	62.76	29.56	35.73	36.93	1.25	1.03
Mean						1.199	1.114
Standard Deviation						0.095	0.057

Note: The values of w/t ratio shown in this table are based on the sections fabricated from 50SK sheet steel.

Table 4.11

Comparison of Computed and Tested Ultimate Loads Based on the Effective Width Formulas in the 1991 AISI Automotive Steel Design Manual for Stub Columns Assembled from Two Hat Sections (50SK Sheet Steel)

(a) Based on Tensile Yield Stresses (without Considering Cold-Work of Forming)

Spec.	Strain Rate in./in./sec. (1)	w/t (2)	$(P_u)_{comp}$, kips Based on $(F_y)_s$ (3)	$(F_y)_d$ (4)	$(P_u)_{test}$ kips (5)	(5)/(3) (6)	(5)/(4) (7)
1A0A1	0.0001	24.30	60.72	60.72	59.89	0.99	0.99
1B0A1	0.0001	24.40	60.79	60.79	59.50	0.98	0.98
1A1A1	0.001	24.30	60.63	61.23	60.97	1.01	1.00
1B1A1	0.001	24.32	60.72	61.32	60.04	0.99	0.98
1A2A1	0.01	24.26	60.74	62.79	63.51	1.05	1.01
1B2A1	0.01	24.14	60.53	62.58	62.24	1.03	0.99
1A3A1	0.1	24.28	60.66	64.07	64.48	1.06	1.01
1B3A1	0.1	24.25	60.47	63.87	66.10	1.09	1.03
1A0A2	0.0001	44.36	66.67	66.67	65.02	0.98	0.98
1B0A2	0.0001	44.47	66.49	66.49	65.85	0.99	0.99
1A1A2	0.001	44.55	66.71	67.30	68.51	1.03	1.02
1B1A2	0.001	44.53	66.57	67.15	68.64	1.03	1.02
1A2A2	0.01	44.63	66.69	68.69	70.25	1.05	1.02
1B2A2	0.01	44.41	66.60	68.60	70.20	1.05	1.02
1A3A2	0.1	44.47	66.59	69.90	72.59	1.09	1.04
1B3A2	0.1	44.44	66.57	69.88	72.59	1.09	1.04
1A0A3	0.0001	47.79	52.84	52.84	53.25	1.01	1.01
1B0A3	0.0001	47.87	52.68	52.68	52.32	0.99	0.99
1A1A3	0.001	47.68	52.77	53.22	54.81	1.04	1.03
1B1A3	0.001	47.83	52.69	53.12	53.69	1.02	1.01
1A2A3	0.01	47.87	52.71	54.23	56.08	1.06	1.03
1B2A3	0.01	47.86	52.76	54.28	54.23	1.03	1.00
1A3A3	0.1	47.49	52.72	55.23	58.23	1.10	1.05
1B3A3	0.1	47.82	52.73	55.24	57.74	1.10	1.05
1A0A4	0.0001	61.56	68.10	68.10	65.22	0.96	0.96
1B0A4	0.0001	61.44	68.06	68.06	64.88	0.95	0.95
1A1A4	0.001	61.24	68.25	68.83	66.93	0.98	0.97
1B1A4	0.001	61.39	68.13	68.71	65.22	0.96	0.95
1A2A4	0.01	61.41	68.07	70.06	70.59	1.04	1.01
1B2A4	0.01	61.53	68.19	70.19	71.13	1.04	1.01
1A3A4	0.1	61.49	68.25	71.57	72.45	1.06	1.01
1B3A4	0.1	61.51	68.09	71.40	72.50	1.06	1.02
Mean						1.028	1.005
Standard Deviation						0.043	0.027

Table 4.11

Comparison of Computed and Tested Ultimate Loads Based on the Effective Width Formulas in the 1991 AISI Automotive Steel Design Manual for Stub Columns Assembled from Two Hat Sections (50SK Sheet Steel)

(a) Based on Tensile Yield Stresses (without Considering Cold-Work of Forming)

Spec.	Strain Rate in./in./sec. (1)	w/t (2)	$(P_u)_{comp}$, kips Based on $(F_y)_s$ (3)	$(F_y)_d$ (4)	$(P_u)_{test}$ kips (5)	(5)/(3) (6)	(5)/(4) (7)
1A0A1	0.0001	24.30	60.72	60.72	59.89	0.99	0.99
1B0A1	0.0001	24.40	60.79	60.79	59.50	0.98	0.98
1A1A1	0.001	24.30	60.63	61.23	60.97	1.01	1.00
1B1A1	0.001	24.32	60.72	61.32	60.04	0.99	0.98
1A2A1	0.01	24.26	60.74	62.79	63.51	1.05	1.01
1B2A1	0.01	24.14	60.53	62.58	62.24	1.03	0.99
1A3A1	0.1	24.28	60.66	64.07	64.48	1.06	1.01
1B3A1	0.1	24.25	60.47	63.87	66.10	1.09	1.03
1A0A2	0.0001	44.36	66.67	66.67	65.02	0.98	0.98
1B0A2	0.0001	44.47	66.49	66.49	65.85	0.99	0.99
1A1A2	0.001	44.55	66.71	67.30	68.51	1.03	1.02
1B1A2	0.001	44.53	66.57	67.15	68.64	1.03	1.02
1A2A2	0.01	44.63	66.69	68.69	70.25	1.05	1.02
1B2A2	0.01	44.41	66.60	68.60	70.20	1.05	1.02
1A3A2	0.1	44.47	66.59	69.90	72.59	1.09	1.04
1B3A2	0.1	44.44	66.57	69.88	72.59	1.09	1.04
1A0A3	0.0001	47.79	52.84	52.84	53.25	1.01	1.01
1B0A3	0.0001	47.87	52.68	52.68	52.32	0.99	0.99
1A1A3	0.001	47.68	52.77	53.22	54.81	1.04	1.03
1B1A3	0.001	47.83	52.69	53.12	53.69	1.02	1.01
1A2A3	0.01	47.87	52.71	54.23	56.08	1.06	1.03
1B2A3	0.01	47.86	52.76	54.28	54.23	1.03	1.00
1A3A3	0.1	47.49	52.72	55.23	58.23	1.10	1.05
1B3A3	0.1	47.82	52.73	55.24	57.74	1.10	1.05
1A0A4	0.0001	61.56	68.10	68.10	65.22	0.96	0.96
1B0A4	0.0001	61.44	68.06	68.06	64.88	0.95	0.95
1A1A4	0.001	61.24	68.25	68.83	66.93	0.98	0.97
1B1A4	0.001	61.39	68.13	68.71	65.22	0.96	0.95
1A2A4	0.01	61.41	68.07	70.06	70.59	1.04	1.01
1B2A4	0.01	61.53	68.19	70.19	71.13	1.04	1.01
1A3A4	0.1	61.49	68.25	71.57	72.45	1.06	1.01
1B3A4	0.1	61.51	68.09	71.40	72.50	1.06	1.02
Mean						1.028	1.005
Standard Deviation						0.043	0.027

Table 4.11 (Cont'd)

(b) Based on Tensile Yield Stresses
(with Considering Cold-Work of Forming)

(i) Based on Static Tensile Yield Stresses

Spec.	Strain Rate (in./in./sec.)	w/t	$(F_y)_t$ (ksi)	A_e ($in.^2$)	$(P_u)_{comp}$ (kips)	$(P_u)_{test}$ (kips)	(6)/(5)
	(1)	(2)	(3)	(4)	(5)	(6)	(7)
1A0A1	0.0001	24.30	57.86	1.1046	63.90	59.89	0.94
1B0A1	0.0001	24.40	57.85	1.1058	63.97	59.50	0.93
1A1A1	0.001	24.30	57.86	1.1030	63.82	60.97	0.96
1B1A1	0.001	24.32	57.86	1.1046	63.91	60.04	0.94
1A2A1	0.01	24.26	57.85	1.1049	63.92	63.51	0.99
1B2A1	0.01	24.14	57.86	1.1012	63.72	62.24	0.98
1A3A1	0.1	24.28	57.86	1.1036	63.85	64.48	1.01
1B3A1	0.1	24.25	57.87	1.1000	63.66	66.10	1.04
Mean							0.974
Standard Deviation							0.039

(ii) Based on Dynamic Tensile Yield Stresses

Spec.	Strain Rate (in./in./sec.)	w/t	$(F_y)_t$ (ksi)	A_e ($in.^2$)	$(P_u)_{comp}$ (kips)	$(P_u)_{test}$ (kips)	(6)/(5)
	(1)	(2)	(3)	(4)	(5)	(6)	(7)
1A0A1	0.0001	24.30	57.86	1.1046	63.90	59.89	0.94
1B0A1	0.0001	24.40	57.85	1.1058	63.97	59.50	0.93
1A1A1	0.001	24.30	58.25	1.1030	64.25	60.97	0.95
1B1A1	0.001	24.32	58.24	1.1046	64.34	60.04	0.93
1A2A1	0.01	24.26	59.44	1.1049	65.68	63.51	0.97
1B2A1	0.01	24.14	59.45	1.1012	65.47	62.24	0.95
1A3A1	0.1	24.28	61.45	1.1036	67.81	64.48	0.95
1B3A1	0.1	24.25	61.46	1.1000	67.60	66.10	0.98
Mean							0.950
Standard Deviation							0.018

Table 4.12

Comparison of Computed and Tested Ultimate Loads Based on the Effective Width Formulas in the 1991 AISI Automotive Steel Design Manual for Stub Columns Assembled from Hat Sections (25AK Sheet Steel)

(a) Based on Tensile Yield Stresses (without Considering Cold-Work of Forming)

Spec.	Strain Rate in./in./sec. (1)	w/t (2)	$(P_u)_{comp}$, kips Based on $(F_y)_s$ (3)	$(F_y)_d$ (4)	$(P_u)_{test}$ kips (5)	(5)/(3) (6)	(5)/(4) (7)
1A0B1	0.0001	23.06	28.68	28.68	34.73	1.21	1.21
1B0B1	0.0001	23.03	28.74	28.74	34.68	1.21	1.21
1A1B1	0.001	23.13	28.69	30.23	36.83	1.28	1.22
1B1B1	0.001	23.07	28.72	30.26	36.25	1.26	1.20
1A2B1	0.01	23.17	28.67	32.47	39.42	1.37	1.21
1B2B1	0.01	23.16	28.75	32.56	38.98	1.36	1.20
1A3B1	0.1	23.17	28.75	37.07	43.04	1.50	1.16
1B3B1	0.1	23.02	28.71	37.02	43.09	1.50	1.16
1A0B2	0.0001	42.56	34.50	34.50	37.13	1.08	1.08
1B0B2	0.0001	42.30	34.45	34.45	36.44	1.06	1.06
1A1B2	0.001	42.10	34.47	36.32	39.08	1.13	1.08
1B1B2	0.001	42.35	34.49	36.34	38.74	1.12	1.07
1A2B2	0.01	42.29	34.44	38.89	42.99	1.25	1.11
1B2B2	0.01	42.33	34.42	38.87	42.50	1.23	1.09
1A3B2	0.1	42.30	34.38	43.63	48.46	1.41	1.11
1B3B2	0.1	42.46	34.45	43.69	48.17	1.40	1.10
1A0B3	0.0001	45.21	28.46	28.46	32.63	1.15	1.15
1B0B3	0.0001	45.29	28.51	28.51	32.93	1.16	1.16
1A1B3	0.001	45.35	28.43	29.76	33.61	1.18	1.13
1B1B3	0.001	45.24	28.48	29.81	33.51	1.18	1.12
1A2B3	0.01	45.35	28.44	31.70	36.59	1.29	1.15
1B2B3	0.01	45.37	28.48	31.74	36.64	1.29	1.15
1A3B3	0.1	45.42	28.41	35.42	41.08	1.45	1.16
1B3B3	0.1	45.29	28.52	35.56	40.69	1.43	1.14
1A0B4	0.0001	58.35	36.50	36.50	38.40	1.05	1.05
1B0B4	0.0001	58.31	36.52	36.52	38.89	1.06	1.06
1A1B4	0.001	58.37	36.49	38.18	41.67	1.14	1.09
1B1B4	0.001	58.20	36.53	38.21	40.84	1.12	1.07
1A2B4	0.01	58.19	36.51	40.65	44.65	1.22	1.10
1B2B4	0.01	58.38	32.75	36.78	44.75	1.22	1.10
1A3B4	0.1	58.33	36.48	45.43	48.71	1.34	1.07
1B3B4	0.1	58.30	36.50	45.45	48.56	1.33	1.07
Mean						1.249	1.126
Standard Deviation						0.130	0.052

Table 4.12 (Cont'd)

(b) Based on Tensile Yield Stresses
(with Considering Cold-Work of Forming)

(i) Based on Static Tensile Yield Stresses

Spec.	Strain Rate (in./in./sec.)	w/t	$(F_y)_t$ (ksi)	A_e ($in.^2$)	$(P_u)_{comp}$ (kips)	$(P_u)_{test}$ (kips)	(6)/(5)
	(1)	(2)	(3)	(4)	(5)	(6)	(7)
1A0B1	0.0001	23.06	27.72	1.1658	32.32	34.73	1.07
1B0B1	0.0001	23.03	27.71	1.1683	32.38	34.68	1.07
1A1B1	0.001	23.13	27.72	1.1661	32.32	36.83	1.14
1B1B1	0.001	23.07	27.71	1.1675	32.36	36.25	1.12
1A2B1	0.01	23.17	27.72	1.1653	32.30	39.42	1.22
1B2B1	0.01	23.16	27.71	1.1686	32.38	38.98	1.20
1A3B1	0.1	23.17	27.71	1.1688	32.39	43.04	1.33
1B3B1	0.1	23.02	27.72	1.1672	32.35	43.09	1.33
Mean							1.185
Standard Deviation							0.104

(ii) Based on Dynamic Tensile Yield Stresses

Spec.	Strain Rate (in./in./sec.)	w/t	$(F_y)_t$ (ksi)	A_e ($in.^2$)	$(P_u)_{comp}$ (kips)	$(P_u)_{test}$ (kips)	(6)/(5)
	(1)	(2)	(3)	(4)	(5)	(6)	(7)
1A0B1	0.0001	23.06	27.72	1.1658	32.32	34.73	1.07
1B0B1	0.0001	23.03	27.71	1.1683	32.38	34.68	1.07
1A1B1	0.001	23.13	29.09	1.1661	33.92	36.83	1.09
1B1B1	0.001	23.07	29.09	1.1675	33.96	36.25	1.07
1A2B1	0.01	23.17	31.38	1.1653	36.57	39.42	1.08
1B2B1	0.01	23.16	31.37	1.1686	36.66	38.98	1.06
1A3B1	0.1	23.17	34.58	1.1688	40.42	43.04	1.06
1B3B1	0.1	23.02	34.58	1.1672	40.37	43.09	1.07
Mean							1.071
Standard Deviation							0.010

Table 4.13

Comparison of Computed and Tested Ultimate Loads Based on the Effective Width Formulas in the 1991 AISI Automotive Steel Design Manual for Stub Columns Assembled from Hat Sections (50SK and 25AK Sheet Steels)

(a) Based on Tensile Yield Stresses (without Considering Cold-Work of Forming)

Spec.	Strain Rate in./in./sec. (1)	w/t (2)	$(P_u)_{comp}$, kips Based on $(F_y)_s$ (3)	$(F_y)_d$ (4)	$(P_u)_{test}$ kips (5)	(5)/(3) (6)	(5)/(4) (7)
1A0C1	0.0001	24.41	44.70	44.70	44.94	1.01	1.01
1B0C1	0.0001	24.21	44.66	44.66	44.94	1.01	1.01
1A1C1	0.001	24.36	44.59	45.66	48.36	1.08	1.06
1B1C1	0.001	24.21	44.61	45.68	46.70	1.05	1.02
1A2C1	0.01	24.36	44.66	47.58	50.56	1.13	1.06
1B2C1	0.01	24.39	44.62	47.55	50.12	1.12	1.05
1A3C1	0.1	24.25	44.64	50.49	51.59	1.16	1.02
1B3C1	0.1	24.29	44.47	50.31	53.98	1.21	1.07
1A0C2	0.0001	44.52	50.50	50.50	52.37	1.04	1.04
1B0C2	0.0001	44.66	50.52	50.52	51.39	1.02	1.02
1A1C2	0.001	44.64	50.53	51.74	52.91	1.05	1.02
1B1C2	0.001	44.68	50.55	51.76	52.42	1.04	1.01
1A2C2	0.01	44.68	50.44	53.66	57.16	1.13	1.07
1B2C2	0.01	44.53	50.52	53.74	56.33	1.11	1.05
1A3C2	0.1	44.24	50.56	56.87	60.04	1.19	1.06
1B3C2	0.1	44.41	50.59	56.88	57.94	1.15	1.02
1A0C3	0.0001	47.78	40.67	40.67	42.16	1.04	1.04
1B0C3	0.0001	47.76	40.64	40.64	42.45	1.04	1.04
1A1C3	0.001	47.82	40.59	41.47	43.67	1.08	1.05
1B1C3	0.001	47.78	40.57	41.46	43.38	1.07	1.05
1A2C3	0.01	47.80	40.56	42.94	46.56	1.15	1.08
1B2C3	0.01	47.78	40.60	42.98	47.00	1.16	1.09
1A3C3	0.1	47.80	40.67	45.44	48.17	1.18	1.06
1B3C3	0.1	47.82	40.64	45.41	49.63	1.22	1.09
1A0C4	0.0001	61.49	52.35	52.35	51.83	0.99	0.99
1B0C4	0.0001	61.39	52.28	52.28	51.05	0.98	0.98
1A1C4	0.001	61.53	52.30	53.43	54.62	1.04	1.02
1B1C4	0.001	61.40	52.33	53.46	53.16	1.02	0.99
1A2C4	0.01	61.43	52.34	55.41	57.40	1.10	1.04
1B2C4	0.01	61.60	52.32	55.38	55.50	1.06	1.00
1A3C4	0.1	61.57	52.33	58.46	58.43	1.12	1.00
1B3C4	0.1	61.41	52.37	58.51	60.14	1.15	1.03
Mean						1.091	1.036
Standard Deviation						0.067	0.029

Note: The values of w/t ratio shown in this table are based on the sections fabricated from 50SK sheet steel.

Table 4.13 (Cont'd)

(b) Based on Tensile Yield Stresses
(with Considering Cold-Work of Forming)

(i) Based on Static Tensile Yield Stresses

Spec.	Strain Rate (in./in./sec.)	w/t	$(F_y)_t$ (ksi)	A_e ($in.^2$)	$(P_u)_{comp}$ (kips)	$(P_u)_{test}$ (kips)	(6)/(5)
	(1)	(2)	(3)	(4)	(5)	(6)	(7)
1A0C1	0.0001	24.41	57.86	1.1355	48.11	44.94	0.93
1B0C1	0.0001	24.21	57.86	1.1351	48.08	44.94	0.93
1A1C1	0.001	24.36	57.86	1.1330	48.01	48.36	1.01
1B1C1	0.001	24.21	57.86	1.1337	48.03	46.70	0.97
1A2C1	0.01	24.36	57.86	1.1345	48.07	50.56	1.05
1B2C1	0.01	24.39	57.86	1.1339	48.04	50.12	1.04
1A3C1	0.1	24.25	57.86	1.1340	48.00	51.59	1.07
1B3C1	0.1	24.29	57.87	1.1301	47.89	53.98	1.13
Mean							1.016
Standard Deviation							0.070

(ii) Based on Dynamic Tensile Yield Stresses

Spec.	Strain Rate (in./in./sec.)	w/t	$(F_y)_t$ (ksi)	A_e ($in.^2$)	$(P_u)_{comp}$ (kips)	$(P_u)_{test}$ (kips)	(6)/(5)
	(1)	(2)	(3)	(4)	(5)	(6)	(7)
1A0C1	0.0001	24.41	57.86	1.1355	48.11	44.94	0.93
1B0C1	0.0001	24.21	57.86	1.1351	48.08	44.94	0.93
1A1C1	0.001	24.36	58.25	1.1330	49.02	48.36	0.99
1B1C1	0.001	24.21	58.25	1.1337	49.04	46.70	0.95
1A2C1	0.01	24.36	59.44	1.1345	51.08	50.56	0.99
1B2C1	0.01	24.39	59.45	1.1339	51.05	50.12	0.98
1A3C1	0.1	24.25	61.45	1.1340	54.03	51.59	0.95
1B3C1	0.1	24.29	61.46	1.1301	53.85	53.98	1.00
Mean							0.965
Standard Deviation							0.028

Note: The values of w/t ratio and $(F_y)_t$ shown in this table are based the sections fabricated from 50SK sheet steel.

Table 4.14

Comparison of Computed and Tested Ultimate Loads Based on the Effective Width Formulas in the 1991 AISI Automotive Steel Design Manual for Stub Columns Assembled from Section (50SK Sheet Steel) and Plate (25AK Sheet Steel)

(a) Based on Tensile Yield Stresses (without Considering Cold-Work of Forming)

Spec.	Strain Rate in./in./sec. (1)	w/t (2)	$(P_u)_{comp}$, kips Based on $(F_y)_s$ (3)	$(F_y)_d$ (4)	$(P_u)_{test}$ kips (5)	(5)/(3) (6)	(5)/(4) (7)
1A0D1	0.0001	34.26	34.97	34.97	34.08	0.97	0.97
1B0D1	0.0001	34.19	35.03	35.03	33.71	0.96	0.96
1A1D1	0.001	34.17	35.00	35.64	34.10	0.97	0.96
1B1D1	0.001	34.19	35.02	35.66	34.39	0.98	0.96
1A2D1	0.01	34.21	34.95	36.79	37.03	1.06	1.01
1B2D1	0.01	34.18	34.98	36.82	38.01	1.09	1.03
1A3D1	0.1	34.17	35.03	38.57	39.28	1.12	1.02
1B3D1	0.1	34.23	34.89	38.43	40.25	1.15	1.05
1A0D2	0.0001	40.50	38.40	38.40	37.27	0.98	0.98
1B0D2	0.0001	40.53	37.95	37.95	37.91	1.00	1.00
1A1D2	0.001	40.49	38.04	38.75	37.83	0.99	0.98
1B1D2	0.001	40.54	37.94	38.65	38.79	1.02	1.00
1A2D2	0.01	40.49	37.96	40.00	40.69	1.07	1.02
1B2D2	0.01	40.54	37.93	39.97	40.25	1.06	1.01
1A3D2	0.1	40.47	37.93	41.71	41.28	1.09	0.99
1B3D2	0.1	40.50	37.95	41.73	43.28	1.14	1.04
1A0D3	0.0001	59.63	42.43	42.43	41.82	0.99	0.99
1B0D3	0.0001	59.69	42.45	42.45	42.50	1.00	1.00
1A1D3	0.001	59.68	42.50	43.15	44.06	1.04	1.02
1B1D3	0.001	59.69	42.47	43.11	44.16	1.04	1.02
1A2D3	0.01	59.72	42.47	44.32	45.04	1.06	1.02
1B2D3	0.01	59.72	42.48	44.33	46.17	1.09	1.04
1A3D3	0.1	59.72	42.53	46.00	48.02	1.13	1.04
1B3D3	0.1	59.73	42.50	45.97	48.56	1.14	1.06
Mean						1.048	1.007
Standard Deviation						0.061	0.029

Note: The values of w/t ratio shown in this table are based on the sections fabricated from 25AK sheet steel.

Table 4.14 (Cont'd)

(b) Based on Tensile Yield Stresses
(with Considering Cold-Work of Forming)

(i) Based on Static Tensile Yield Stresses

Spec.	Strain Rate (in./in./sec.)	w/t	$(F_y)_t$ (ksi)	A_e ($in.^2$)	$(P_u)_{comp}$ (kips)	$(P_u)_{test}$ (kips)	(6)/(5)
	(1)	(2)	(3)	(4)	(5)	(6)	(7)
1A0D1	0.0001	17.51	58.07	0.7874	36.56	34.08	0.93
1B0D1	0.0001	17.52	58.06	0.7883	36.62	33.71	0.92
1A1D1	0.001	17.41	58.07	0.7878	36.60	34.10	0.93
1B1D1	0.001	17.68	58.06	0.7882	36.62	34.39	0.94
1A2D1	0.01	17.41	58.07	0.7869	36.54	37.03	1.01
1B2D1	0.01	17.56	58.07	0.7873	36.57	38.01	1.04
1A3D1	0.1	17.44	58.06	0.7885	36.62	39.28	1.07
1B3D1	0.1	17.56	58.08	0.7857	36.49	40.25	1.10
Mean							0.993
Standard Deviation							0.072

(ii) Based on Dynamic Tensile Yield Stresses

Spec.	Strain Rate (in./in./sec.)	w/t	$(F_y)_t$ (ksi)	A_e ($in.^2$)	$(P_u)_{comp}$ (kips)	$(P_u)_{test}$ (kips)	(6)/(5)
	(1)	(2)	(3)	(4)	(5)	(6)	(7)
1A0D1	0.0001	17.51	58.07	0.7874	36.56	34.08	0.93
1B0D1	0.0001	17.52	58.06	0.7883	36.62	33.71	0.92
1A1D1	0.001	17.41	58.44	0.7878	37.15	34.10	0.92
1B1D1	0.001	17.68	58.44	0.7882	37.17	34.39	0.93
1A2D1	0.01	17.41	59.65	0.7869	38.24	37.03	0.97
1B2D1	0.01	17.56	59.65	0.7873	38.27	38.01	0.99
1A3D1	0.1	17.44	61.67	0.7885	40.43	39.28	0.97
1B3D1	0.1	17.56	61.69	0.7857	40.23	40.25	1.00
Mean							0.954
Standard Deviation							0.032

Note: The values of w/t ratio shown in this table are based on the sections fabricated from 50SK sheet steel.

Table 4.15

Comparison of Computed and Tested Ultimate Loads Based on the Effective Width Formulas in the 1991 AISI Automotive Steel Design Manual for Stub Columns Assembled from Section (25AK Sheet Steel) and Plate (50SK Sheet Steel)

(a) Based on Tensile Yield Stresses (without Considering Cold-Work of Forming)

Spec.	Strain Rate in./in./sec. (1)	w/t (2)	$(P_u)_{comp}$, kips Based on $(F_y)_s$ (3)	$(F_y)_d$ (4)	$(P_u)_{test}$ kips (5)	(5)/(3) (6)	(5)/(4) (7)
1A0E1	0.0001	29.05	24.65	24.65	24.72	1.00	1.00
1B0E1	0.0001	29.08	24.64	24.64	25.50	1.03	1.03
1A1E1	0.001	29.03	24.67	25.46	26.62	1.08	1.05
1B1E1	0.001	28.97	24.64	25.43	26.09	1.06	1.03
1A2E1	0.01	29.03	24.68	26.74	27.85	1.13	1.04
1B2E1	0.01	29.01	24.67	26.74	27.80	1.13	1.04
1A3E1	0.1	29.03	24.67	28.93	30.04	1.22	1.04
1B3E1	0.1	28.99	24.68	28.95	29.51	1.20	1.02
1A0E2	0.0001	42.50	28.07	28.07	30.87	1.10	1.10
1B0E2	0.0001	42.53	28.12	28.12	30.87	1.10	1.10
1A1E2	0.001	42.64	28.06	28.93	32.14	1.15	1.11
1B1E2	0.001	42.55	28.08	28.95	31.12	1.11	1.07
1A2E2	0.01	41.50	28.10	30.34	34.49	1.23	1.14
1B2E2	0.01	42.51	28.11	30.35	33.22	1.18	1.09
1A3E2	0.1	42.51	28.10	32.82	35.96	1.28	1.10
1B3E2	0.1	42.49	28.11	32.84	35.66	1.27	1.09
1A0E3	0.0001	62.74	32.00	32.00	31.17	0.97	0.97
1B0E3	0.0001	62.78	31.95	31.95	31.02	0.97	0.97
1A1E3	0.001	62.73	32.02	33.05	32.54	1.02	0.98
1B1E3	0.001	62.78	31.97	32.99	31.56	0.99	0.96
1A2E3	0.01	62.73	32.00	34.59	35.08	1.10	1.01
1B2E3	0.01	62.74	31.92	34.50	34.39	1.08	1.00
1A3E3	0.1	62.72	31.96	37.16	36.79	1.15	0.99
1B3E3	0.1	62.76	31.92	37.13	36.93	1.16	0.99
Mean						1.113	1.038
Standard Deviation						0.090	0.052

Note: The values of w/t ratio shown in this table are based on the sections fabricated from 50SK sheet steel.

Table 4.15 (Cont'd)

(b) Based on Tensile Yield Stresses
(with Considering Cold-Work of Forming)

(i) Based on Static Tensile Yield Stresses

Spec.	Strain Rate (in./in./sec.)	w/t	$(F_y)_t$ (ksi)	A_e ($in.^2$)	$(P_u)_{comp}$ (kips)	$(P_u)_{test}$ (kips)	(6)/(5)
	(1)	(2)	(3)	(4)	(5)	(6)	(7)
1A0E1	0.0001	9.67	28.21	0.7278	26.48	24.72	0.93
1B0E1	0.0001	10.22	28.21	0.7274	26.47	25.50	0.96
1A1E1	0.001	10.10	28.20	0.7275	26.50	26.62	1.00
1B1E1	0.001	10.10	28.21	0.7276	26.47	26.09	0.99
1A2E1	0.01	9.74	28.20	0.7285	26.50	27.85	1.05
1B2E1	0.01	9.98	28.20	0.7285	26.50	27.80	1.05
1A3E1	0.1	10.20	28.20	0.7282	26.49	30.04	1.13
1B3E1	0.1	10.19	28.20	0.7287	26.50	29.51	1.11
Mean							1.028
Standard Deviation							0.070

(ii) Based on Dynamic Tensile Yield Stresses

Spec.	Strain Rate (in./in./sec.)	w/t	$(F_y)_t$ (ksi)	A_e ($in.^2$)	$(P_u)_{comp}$ (kips)	$(P_u)_{test}$ (kips)	(6)/(5)
	(1)	(2)	(3)	(4)	(5)	(6)	(7)
1A0E1	0.0001	9.67	28.21	0.7278	26.48	24.72	0.93
1B0E1	0.0001	10.22	28.21	0.7274	26.47	25.50	0.96
1A1E1	0.001	10.10	29.57	0.7275	27.33	26.62	0.97
1B1E1	0.001	10.10	29.58	0.7276	27.28	26.09	0.96
1A2E1	0.01	9.74	31.87	0.7285	28.77	27.85	0.97
1B2E1	0.01	9.98	31.87	0.7285	28.77	27.80	0.97
1A3E1	0.1	10.20	35.09	0.7282	30.66	30.04	0.98
1B3E1	0.1	10.19	35.08	0.7287	30.67	29.51	0.96
Mean							0.963
Standard Deviation							0.015

Note: The values of w/t ratio shown in this table are based on the sections fabricated from 25AK sheet steel.

Table 4.15 (Cont'd)

(b) Based on Tensile Yield Stresses
(with Considering Cold-Work of Forming)

(i) Based on Static Tensile Yield Stresses

Spec.	Strain Rate (in./in./sec.)	w/t	$(F_y)_t$ (ksi)	A_e ($in.^2$)	$(P_u)_{comp}$ (kips)	$(P_u)_{test}$ (kips)	(6)/(5)
	(1)	(2)	(3)	(4)	(5)	(6)	(7)
1A0E1	0.0001	9.67	28.21	0.7278	26.48	24.72	0.93
1B0E1	0.0001	10.22	28.21	0.7274	26.47	25.50	0.96
1A1E1	0.001	10.10	28.20	0.7275	26.50	26.62	1.00
1B1E1	0.001	10.10	28.21	0.7276	26.47	26.09	0.99
1A2E1	0.01	9.74	28.20	0.7285	26.50	27.85	1.05
1B2E1	0.01	9.98	28.20	0.7285	26.50	27.80	1.05
1A3E1	0.1	10.20	28.20	0.7282	26.49	30.04	1.13
1B3E1	0.1	10.19	28.20	0.7287	26.50	29.51	1.11
Mean							1.028
Standard Deviation							0.070

(ii) Based on Dynamic Tensile Yield Stresses

Spec.	Strain Rate (in./in./sec.)	w/t	$(F_y)_t$ (ksi)	A_e ($in.^2$)	$(P_u)_{comp}$ (kips)	$(P_u)_{test}$ (kips)	(6)/(5)
	(1)	(2)	(3)	(4)	(5)	(6)	(7)
1A0E1	0.0001	9.67	28.21	0.7278	26.48	24.72	0.93
1B0E1	0.0001	10.22	28.21	0.7274	26.47	25.50	0.96
1A1E1	0.001	10.10	29.57	0.7275	27.33	26.62	0.97
1B1E1	0.001	10.10	29.58	0.7276	27.28	26.09	0.96
1A2E1	0.01	9.74	31.87	0.7285	28.77	27.85	0.97
1B2E1	0.01	9.98	31.87	0.7285	28.77	27.80	0.97
1A3E1	0.1	10.20	35.09	0.7282	30.66	30.04	0.98
1B3E1	0.1	10.19	35.08	0.7287	30.67	29.51	0.96
Mean							0.963
Standard Deviation							0.015

Note: The values of w/t ratio shown in this table are based on the sections fabricated from 25AK sheet steel.

Table 4.16

Comparison of Tested Ultimate and Mean Crushing Loads for Box-Shaped Stub Columns Assembled from Hat Sections (50SK Sheet Steel)

Spec.	w/t	P_u (kips) (1)	P_{mean} (Kips) (2)	(1)/(2) (3)	Type of Failure Mode	Spacing of Connection
1A0A1	24.30	59.89	*****	N/A	F	2.0"
1B0A1	24.40	59.50	23.50	2.53	F	2.0"
1A1A1	24.30	60.97	22.43	2.72	F	2.0"
1B1A1	24.32	60.04	22.49	2.67	F	2.0"
1A2A1	24.26	63.51	23.96	2.65	F	2.0"
1B2A1	24.14	62.24	21.52	N/A	F,L	2.0"
1A3A1	24.28	64.48	24.21	2.66	F	2.0"
1B3A1	24.25	66.10	24.28	2.72	F	2.0"
1A0A2	44.36	65.02	16.01	N/A	F,B	2.5"
1B0A2	44.47	65.68	22.51	2.93	F	2.5"
1A1A2	44.55	68.51	23.01	2.98	F	2.5"
1B1A2	44.53	68.64	19.74	N/A	F,T	2.5"
1A2A2	44.63	70.25	20.62	N/A	F,O	2.5"
1B2A2	44.41	70.20	19.27	N/A	F,O	2.5"
1A3A2	44.47	72.59	19.63	N/A	F,T	2.5"
1B3A2	44.44	72.59	20.11	N/A	F,O	2.5"
1A0A3	47.79	53.25	10.54	N/A	B	2.0"
1B0A3	47.87	52.32	21.71	2.41	F	2.0"
1A1A3	47.68	54.81	14.99	N/A	F,B	2.0"
1B1A3	47.83	53.69	22.57	2.38	F	2.0"
1A2A3	47.87	56.08	18.43	N/A	F,B	2.0"
1B2A3	47.86	54.23	22.01	2.46	F	2.0"
1A3A3	47.79	58.23	11.44	N/A	B	2.0"
1B3A3	47.82	57.74	15.44	N/A	F,B	2.0"
1A0A4	61.56	65.22	17.51	N/A	F,O	3.0"
1B0A4	61.44	64.88	22.29	2.91	F	3.0"
1A1A4	61.24	66.93	22.43	2.98	F	3.0"
1B1A4	61.39	65.22	16.71	N/A	F,O	3.0"
1A2A4	61.41	70.59	15.58	N/A	F,T	3.0"
1B2A4	61.53	71.13	20.26	N/A	F,T	3.0"
1A3A4	61.49	72.45	24.76	2.93	F	3.0"
1B3A4	61.51	72.50	23.63	3.07	F	3.0"

Note: F - Folding B - Bending T - Twisting
O - Openning L - Lateral Buckling

Table 4.17

Comparison of Tested Ultimate and Mean Crushing Loads for Box-Shaped Stub Columns Assembled from Hat Sections (25AK Sheet Steel)

Spec.	w/t	P_u (kips) (1)	P_{mean} (Kips) (2)	(1)/(2) (3)	Type of Failure Mode	Spacing of Connection
1A0B1	23.06	34.73	15.09	2.30	F	2.0"
1B0B1	23.03	34.68	14.54	2.39	F	2.0"
1A1B1	23.13	36.83	14.48	2.54	F	2.0"
1B1B1	23.08	36.25	13.85	2.62	F	2.0"
1A2B1	23.17	39.42	16.51	2.39	F	2.0"
1B2B1	23.16	38.98	13.27	N/A	F,T	2.0"
1A3B1	23.17	43.04	16.73	2.57	F	2.0"
1B3B1	23.02	43.09	15.25	N/A	F,T	2.0"
1A0B2	42.56	37.13	14.25	2.61	F	2.5"
1B0B2	42.30	36.44	14.87	2.45	F	2.5"
1A1B2	42.10	39.08	11.43	N/A	F,B	2.5"
1B1B2	42.35	38.74	15.52	2.50	F	2.5"
1A2B2	42.29	42.99	16.89	2.55	F	2.5"
1B2B2	42.33	42.50	16.22	2.62	F	2.5"
1A3B2	42.30	48.46	17.00	2.85	F	2.5"
1B3B2	42.46	48.17	18.14	2.66	F	2.5"
1A0B3	45.21	32.63	13.47	2.42	F	2.0"
1B0B3	45.29	32.93	13.51	2.44	F	2.0"
1A1B3	45.35	33.61	14.33	2.35	F	2.0"
1B1B3	45.24	33.51	14.50	2.31	F	2.0"
1A2B3	45.35	36.59	14.66	2.50	F	2.0"
1B2B3	45.37	36.64	15.48	2.37	F	2.0"
1A3B3	45.42	41.08	15.32	2.68	B	2.0"
1B3B3	45.29	40.69	14.18	N/A	F,B	2.0"
1A0B4	58.35	38.40	14.79	2.60	F	3.0"
1B0B4	58.31	38.89	12.75	N/A	F,B	3.0"
1A1B4	58.37	41.67	15.63	2.67	F	3.0"
1B1B4	58.20	40.84	14.74	2.77	F	3.0"
1A2B4	58.19	44.65	15.37	2.91	F	3.0"
1B2B4	58.38	44.75	16.19	2.76	F	3.0"
1A3B4	58.33	48.71	15.38	N/A	F,B	3.0"
1B3B4	58.30	48.56	15.25	N/A	F,B	3.0"

Note: F - Folding B - Bending T - Twisting
O - Openning L - Lateral Buckling

Table 4.18

Comparison of Tested Ultimate and Mean Crushing Loads for Box-Shaped Stub Columns Assembled from Hat Sections (50SK and 25AK Sheet Steels)

Spec.	w/t (50SK)	P_u (kips) (1)	P_{mean} (Kips) (2)	(1)/(2) (3)	Type of Failure Mode	Spacing of Connection
1A0C1	24.41	44.94	18.04	2.49	F	2.0"
1B0C1	24.21	44.94	18.10	2.48	F	2.0"
1A1C1	24.36	48.36	19.08	2.53	F	2.0"
1B1C1	24.21	46.70	18.18	2.57	F	2.0"
1A2C1	24.36	50.56	19.64	2.57	F	2.0"
1B2C1	24.39	50.12	18.81	2.66	F	2.0"
1A3C1	24.25	51.59	20.02	2.58	F	2.0"
1B3C1	24.29	53.98	19.95	2.71	F	2.0"
1A0C2	44.52	52.37	18.54	2.82	F	2.5"
1B0C2	44.66	51.39	14.67	N/A	F,O	2.5"
1A1C2	44.64	52.91	18.01	2.94	F	2.5"
1B1C2	44.68	52.42	17.32	N/A	F,L	2.5"
1A2C2	44.68	57.16	16.09	N/A	F,O	2.5"
1B2C2	44.53	56.33	17.93	N/A	F,O	2.5"
1A3C2	44.24	60.04	19.84	3.03	F	2.5"
1B3C2	44.41	57.94	16.81	N/A	F,L	2.5"
1A0C3	47.78	42.16	12.02	N/A	F,B	2.0"
1B0C3	47.76	42.45	12.65	N/A	F,B	2.0"
1A1C3	47.82	43.67	9.86	N/A	F,B	2.0"
1B1C3	47.78	43.38	11.08	N/A	F,B	2.0"
1A2C3	47.80	46.56	12.66	N/A	F,B	2.0"
1B2C3	47.78	47.00	12.92	N/A	F,B	2.0"
1A3C3	47.80	48.17	12.13	N/A	F,B	2.0"
1B3C3	47.82	49.63	16.13	N/A	F,B	2.0"
1A0C4	61.49	51.83	20.51	2.53	F	3.0"
1B0C4	61.39	51.05	19.66	2.60	F	3.0"
1A1C4	61.53	54.62	19.53	2.80	F	3.0"
1B1C4	61.40	53.16	18.38	2.89	F	3.0"
1A2C4	61.42	57.40	18.93	3.03	F	3.0"
1B2C4	61.60	55.50	19.95	2.78	F	3.0"
1A3C4	61.57	58.43	14.86	N/A	F,T	3.0"
1B3C4	61.41	60.14	21.67	2.78	F	3.0"

Note: F - Folding B - Bending T - Twisting
O - Openning L - Lateral Buckling

Table 4.19

Comparison of Tested Ultimate and Mean Crushing Loads for Hat-Shaped Stub Columns Assembled from Hat Section (50SK Sheet Steel) and Plate (25AK Sheet Steel)

Spec.	w/t (50SK)	P_u (kips) (1)	P_{mean} (Kips) (2)	(1)/(2) (3)	Type of Failure Mode	Spacing of Connection
1A0D1	34.26	34.08	13.12	2.60	F	1.0"
1B0D1	34.19	33.71	7.39	N/A	F,L	1.0"
1A1D1	34.17	34.10	12.82	2.66	F	1.0"
1B1D1	34.19	34.39	13.40	2.57	F	1.0"
1A2D1	34.21	37.03	10.36	N/A	F,L	1.0"
1B2D1	34.18	38.01	14.31	2.66	F	1.0"
1A3D1	34.17	39.28	14.48	2.71	F	1.0"
1B3D1	34.23	40.25	14.88	2.70	F	1.0"
1A0D2	40.54	37.27	13.22	2.82	F	1.0"
1B0D2	40.53	37.91	13.93	2.72	F	1.0"
1A1D2	40.49	37.83	13.60	2.78	F	1.0"
1B1D2	40.54	38.79	13.80	2.81	F	1.0"
1A2D2	40.49	40.69	14.08	2.89	F	1.0"
1B2D2	40.54	40.25	14.29	2.82	F	1.0"
1A3D2	40.47	41.28	14.22	2.90	F	1.0"
1B3D2	40.50	43.28	15.20	2.85	F	1.0"
1A0D3	59.63	41.82	15.18	2.75	F	1.25"
1B0D3	59.69	42.50	15.79	2.69	F	1.25"
1A1D3	59.68	44.06	14.80	2.98	F	1.25"
1B1D3	59.69	44.16	15.26	2.89	F	1.25"
1A2D3	59.72	45.04	15.54	2.90	F	1.25"
1B2D3	59.72	46.17	14.67	N/A	F,B	1.25"
1A3D3	59.72	48.02	15.82	3.04	F	1.25"
1B3D3	59.73	48.59	15.73	3.09	F	1.25"

Note: F - Folding B - Bending T - Twisting
O - Openning L - Lateral Buckling

Table 4.20

Comparison of Tested Ultimate and Mean Crushing Loads for Hat-Shaped Stub Columns Assembled from Hat Section (50SK Sheet Steel) and Plate (25AK Sheet Steel)

Spec.	w/t (25AK)	P_u (kips) (1)	P_{mean} (Kips) (2)	(1)/(2) (3)	Type of Failure Mode	Spacing of Connection
1A0E1	29.05	24.72	9.26	2.67	F	1.0"
1B0E1	29.08	25.50	9.96	2.56	F	1.0"
1A1E1	29.03	26.62	10.57	2.52	F	1.0"
1B1E1	28.97	26.09	10.00	2.61	F	1.0"
1A2E1	29.03	27.85	11.09	2.51	F	1.0"
1B2E1	29.01	27.80	11.07	2.51	F	1.0"
1A3E1	29.03	30.04	11.35	2.65	F	1.0"
1B3E1	28.99	29.51	11.90	2.48	F	1.0"
1A0E2	42.50	30.87	10.26	3.01	F	1.0"
1B0E2	42.53	30.87	10.38	2.97	F	1.0"
1A1E2	42.64	32.14	10.86	2.96	F	1.0"
1B1E2	42.55	31.12	10.93	2.85	F	1.0"
1A2E2	42.50	34.49	10.96	3.15	F	1.0"
1B2E2	42.51	33.22	11.66	2.85	F	1.0"
1A3E2	42.51	35.96	12.39	2.90	F	1.0"
1B3E2	42.49	35.66	11.08	N/A	F,B	1.0"
1A0E3	62.74	31.17	10.33	3.02	F	1.25"
1B0E3	62.78	31.02	11.37	2.73	F	1.25"
1A1E3	62.73	32.54	11.75	2.77	F	1.25"
1B1E3	62.78	31.56	11.37	2.78	F	1.25"
1A2E3	62.73	35.08	11.65	3.01	F	1.25"
1B2E3	62.74	34.39	13.16	2.61	F	1.25"
1A3E3	62.72	36.79	12.80	2.87	F	1.25"
1B3E3	62.76	36.93	11.83	N/A	F,B	1.25"

Note: F - Folding B - Bending T - Twisting
O - Openning L - Lateral Buckling

Table 4.21

Comparison of Computed and Tested Mean Crushing Loads for Box-Shaped Stub Columns Assembled from Hat Sections (50SK Sheet Steel)

Strain Rate in./in./sec.	$(P_u)_{comp}$ (Kips) (1)	$(P_m)_{comp}$ (Kips) (2)	$(P_m)_{test}$ (Kips) (3)	(3)/(2) (4)
A1 Specimens				
0.0001	60.76	25.22	23.50	0.93
0.1	63.97	26.55	24.25	0.91
25.97	69.98	29.05	28.21	0.97
39.37	70.49	29.26	30.13	1.03
A2 Specimens				
0.0001	66.58	24.09	22.51	0.93
0.1	69.89	25.29	N/A	N/A
A3 Specimens				
0.0001	52.76	21.60	21.71	1.01
0.1	55.24	22.62	N/A	N/A
25.97	59.54	24.38	28.55	1.17
39.37	59.50	24.53	29.00	1.18
A4 Specimens				
0.0001	68.08	25.77	22.29	0.87
0.1	71.49	27.06	24.20	0.89

Note: $(P_u)_{comp}$ calculated based on Equation 4.5
$(P_m)_{comp}$ calculated based on Equation 4.13

Table 4.22

Comparison of Computed and Tested Mean Crushing Loads for Box-Shaped Stub Columns Assembled from Hat Sections (25AK Sheet Steel)

Strain Rate in./in./sec.	$(P_u)_{comp}$ (Kips) (1)	$(P_m)_{comp}$ (Kips) (2)	$(P_m)_{test}$ (Kips) (3)	(3)/(2) (4)
B1 Specimens				
0.0001	32.35*	13.38	14.82	1.11
0.1	40.40*	16.71	15.99	0.96
25.97	57.06*	23.60	26.31	1.12
39.37	58.27*	24.10	27.65	1.15
B2 Specimens				
0.0001	34.48	12.48	14.56	1.17
0.1	43.66	15.80	17.57	1.11
B3 Specimens				
0.0001	28.49	11.65	13.49	1.16
0.1	35.49	14.51	14.75	1.02
25.97	48.56	19.85	24.28	1.22
39.37	49.32	20.16	24.96	1.24
B4 Specimens				
0.0001	36.51	13.81	14.79	1.07
0.1	45.44	17.19	N/A	N/A

Note: The supscript "*" represents the values calculated by considering the cold-work effect.

$(P_u)_{comp}$ calculated based on Equation 4.5
$(P_m)_{comp}$ calculated based on Equation 4.13

Table 4.23

Comparison of Computed and Tested Mean Crushing Loads for Box-Shaped Stub Columns Assembled from Hat Sections (50SK and 25AK Sheet Steels)

Strain Rate in./in./sec.	$(P_u)_{comp}$ (Kips) (1)	$(P_m)_{comp}$ (Kips) (2)	$(P_m)_{test}$ (Kips) (3)	(3)/(2) (4)
C1 Specimens				
0.0001	44.68	18.52	18.07	0.98
0.1	50.40	20.89	19.99	0.96
25.97	61.68	25.56	26.53	1.04
39.37	62.51	25.91	27.43	1.06
C2 Specimens				
0.0001	50.51	18.28	18.54	1.01
0.1	56.88	20.59	19.84	0.96
C3 Specimens				
0.0001	40.66	16.64	N/A	N/A
0.1	45.43	18.59	N/A	N/A
25.97	54.05	22.12	27.20	1.23
39.37	54.61	22.34	28.33	1.27
C4 Specimens				
0.0001	52.32	19.80	20.09	1.02
0.1	58.49	22.13	21.67	0.98

Note: $(P_u)_{comp}$ calculated based on Equation 4.6
$(P_m)_{comp}$ calculated based on Equation 4.13

Table 4.24

Comparison of Computed and Tested Mean Crushing Loads for Hat-Shaped Stub Columns Assembled from Hat Section (50SK Sheet Steel) and Plate (25AK Sheet Steel)

Strain Rate in./in./sec.	$(P_u)_{comp}$ (Kips) (1)	$(P_m)_{comp}$ (Kips) (2)	$(P_m)_{test}$ (Kips) (3)	(3)/(2) (4)
D1 Specimens				
0.0001	35.00	12.64	13.12	1.04
0.1	38.50	13.90	14.68	1.06
25.97	44.84	16.19	17.09	1.06
39.37	45.29	16.35	18.66	1.14
D2 Specimens				
0.0001	38.18	14.04	13.58	0.97
0.1	41.72	15.34	14.71	0.96
D3 Specimens				
0.0001	42.44	17.40	15.49	0.89
0.1	45.99	18.86	15.78	0.84

Note: $(P_u)_{comp}$ calculated based on Equation 4.6
$(P_m)_{comp}$ calculated based on Equation 4.13

Table 4.25

Comparison of Computed and Tested Mean Crushing Loads for Hat-Shaped Stub Columns Assembled from Hat Section (25AK Sheet Steel) and Plate (50SK Sheet Steel)

Strain Rate in./in./sec.	$(P_u)_{comp}$ (Kips) (1)	$(P_m)_{comp}$ (Kips) (2)	$(P_m)_{test}$ (Kips) (3)	(3)/(2) (4)
E1 Specimens				
0.0001	24.65	9.85	9.61	0.98
0.1	28.94	11.56	11.63	1.01
25.97	44.31	17.70	16.41	0.93
39.37	44.61	17.82	16.86	0.95
E2 Specimens				
0.0001	28.10	10.34	10.32	1.00
0.1	32.83	12.08	12.39	1.03
E3 Specimens				
0.0001	31.98	13.11	11.37	0.87
0.1	37.15	15.23	12.80	0.84

Note: $(P_u)_{comp}$ calculated based on Equation 4.6
$(P_m)_{comp}$ calculated based on Equation 4.13

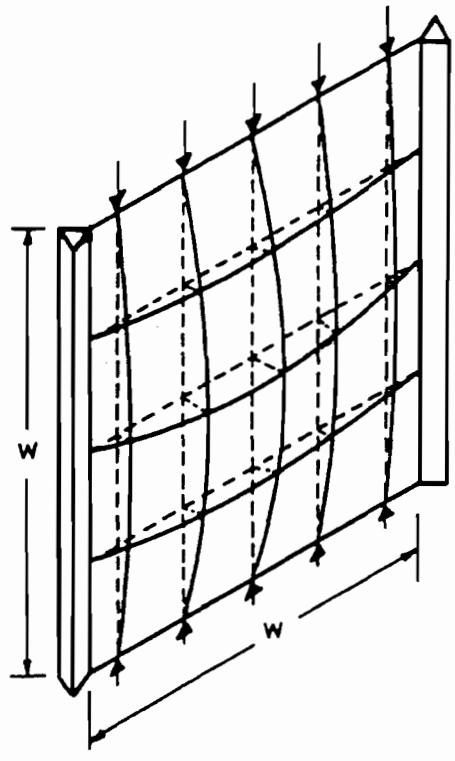

Figure 2.1 Strut and Bar Grid Model Simply Supported Along Its Edges and Subjected to End Loading[11]

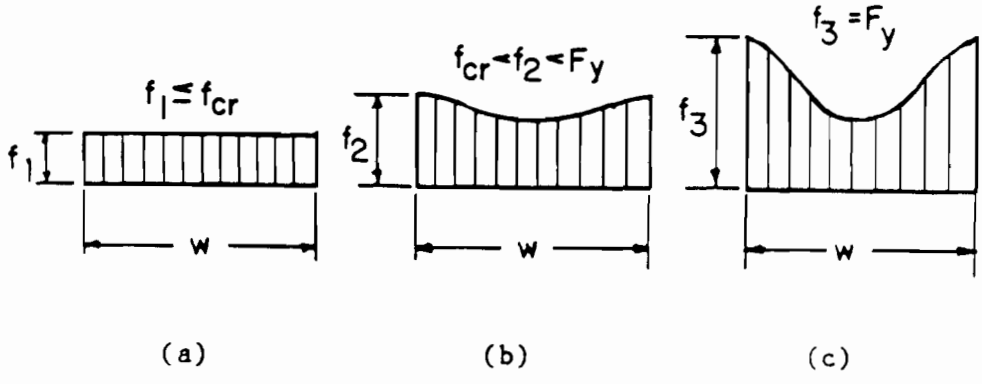

Figure 2.2 Consective Stages of Stress Distribution in a Stiffened Compression Element[11]

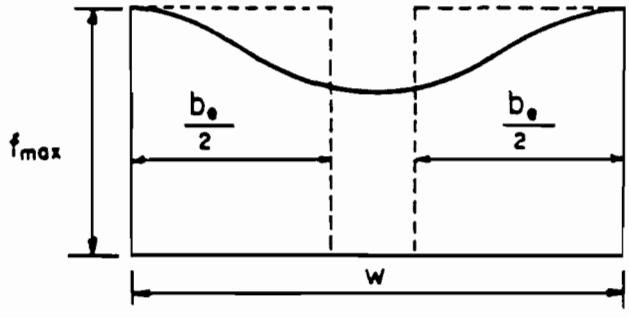

Figure 2.3 Effective Design Width of a Stiffened Compression Element[11]

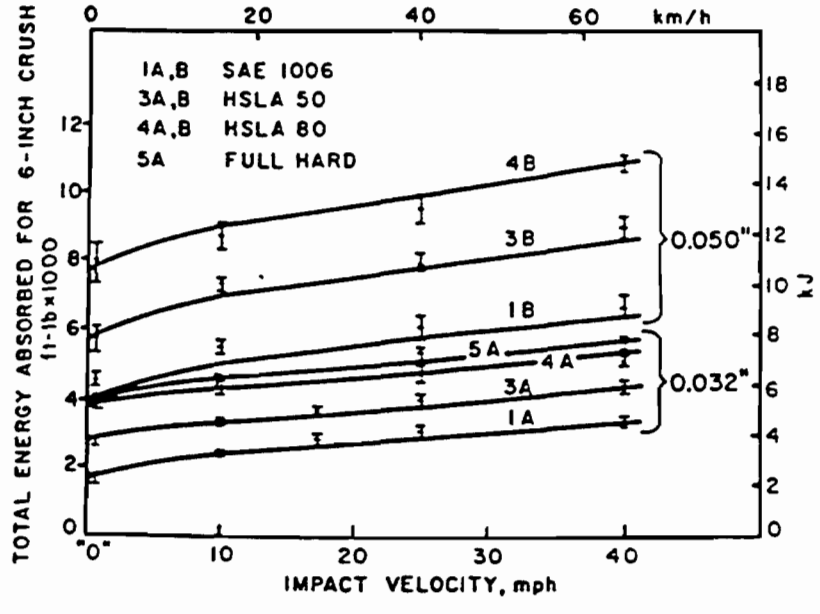

Figure 2.4 Effect of Impact Velocity on the Energy Absorbed for Several Steels[4]

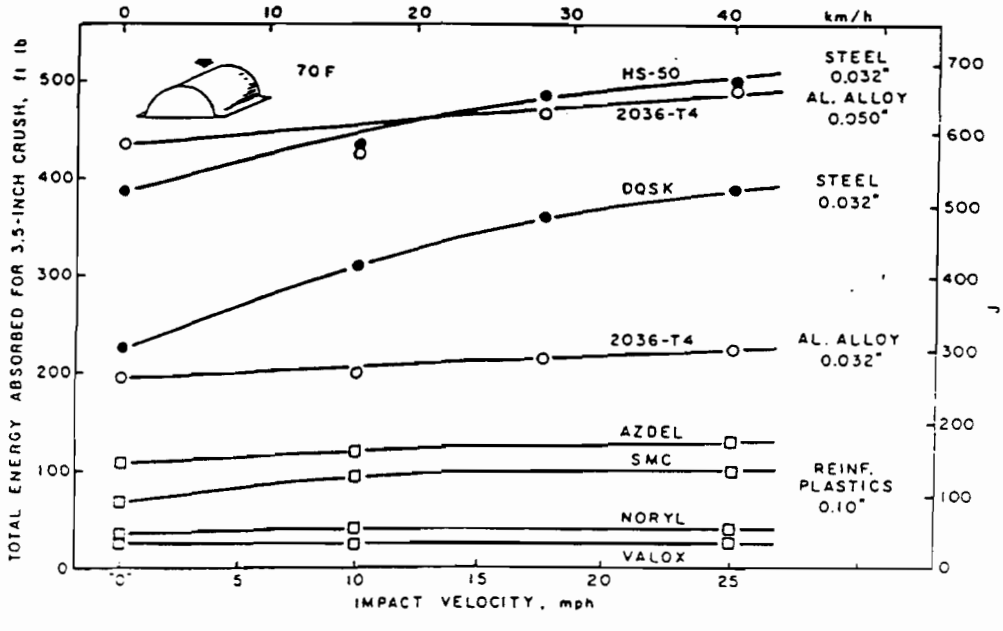

Figure 2.5 Effect of Impact Velocity on the Energy Absorption of Several Materials[27]

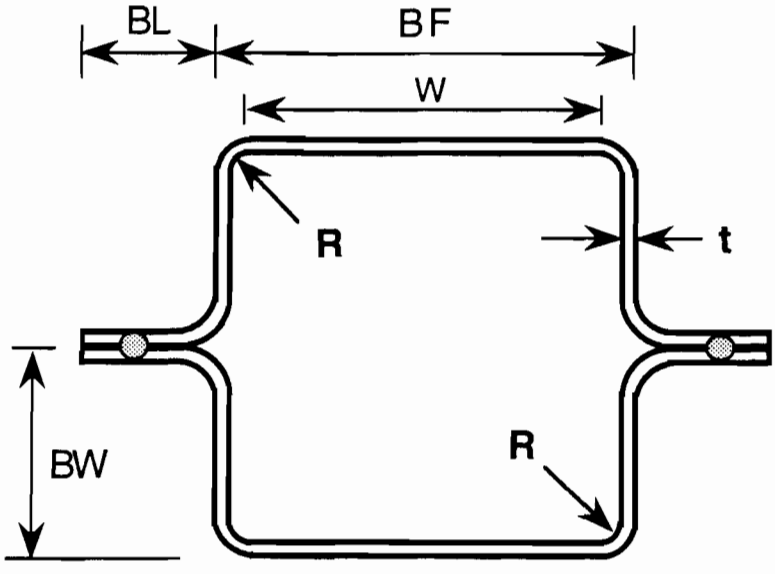

(a) Box-Shaped Stub Column

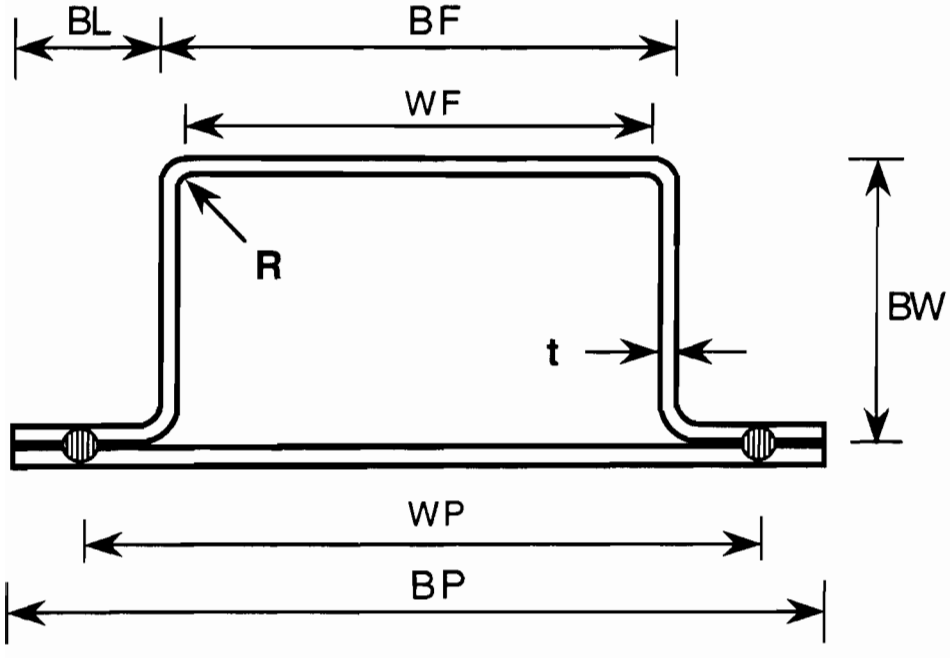

(b) Hat-Shaped Stub Column

Figure 3.1 Configuration of Stub Column Specimens

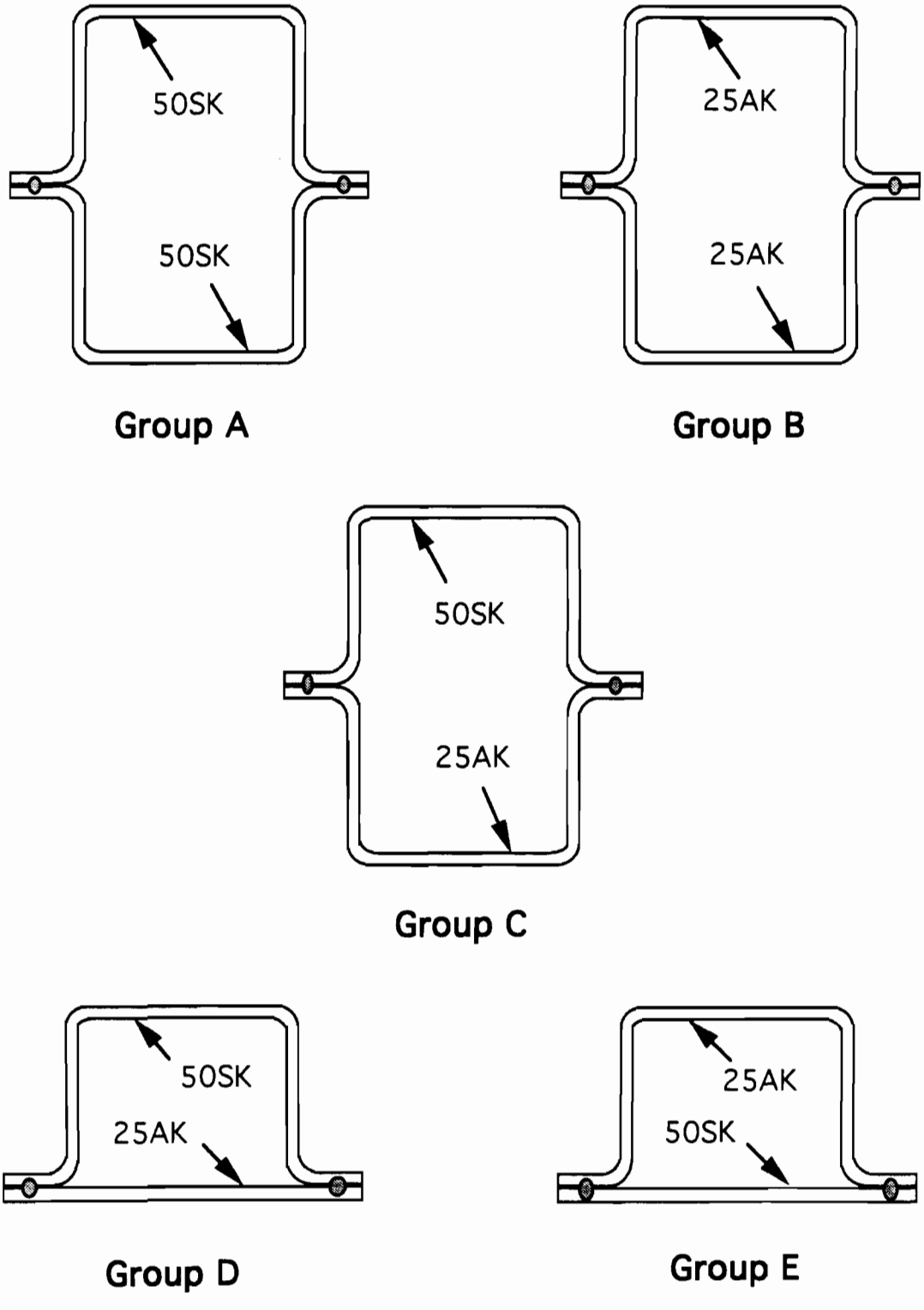

Figure 3.2 Cross Section of Stub Columns Used in This Study

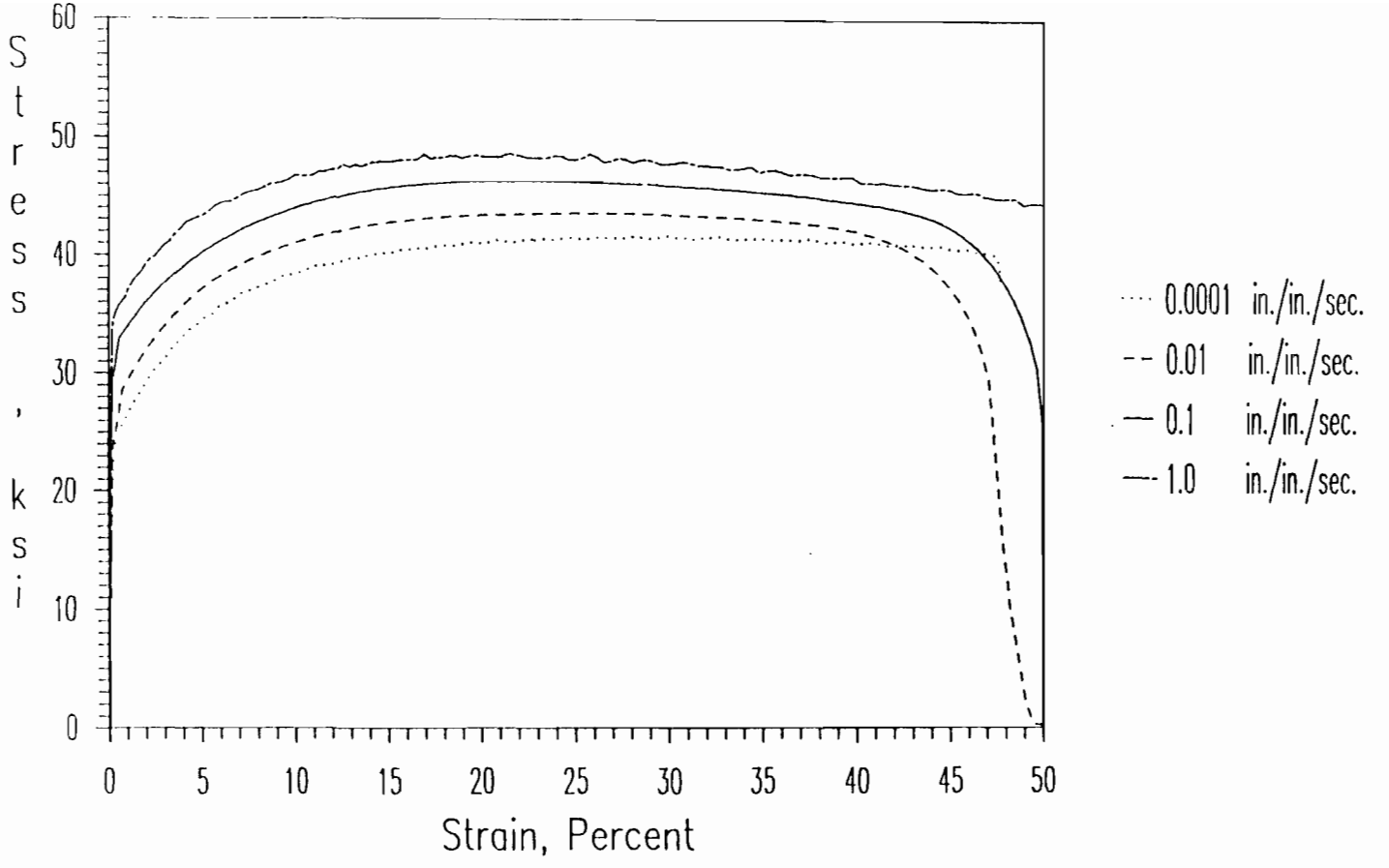

Figure 3.3 Stress-Strain Curves for 25AK Steel in the Longitudinal Tension under Different Strain Rates

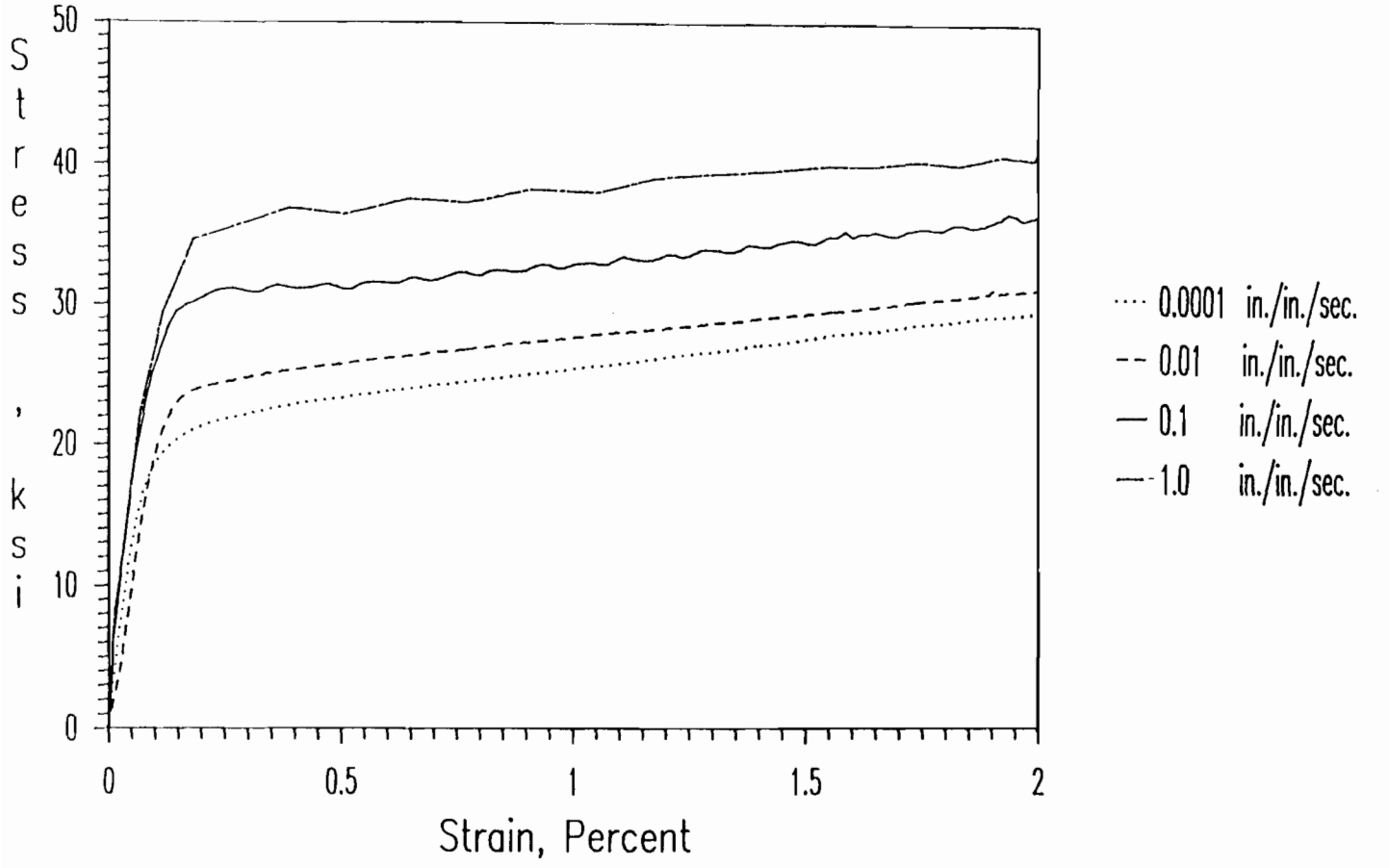

Figure 3.4 Stress-Strain Curves for 25AK Steel in the Longitudinal Compression under Different Strain Rates

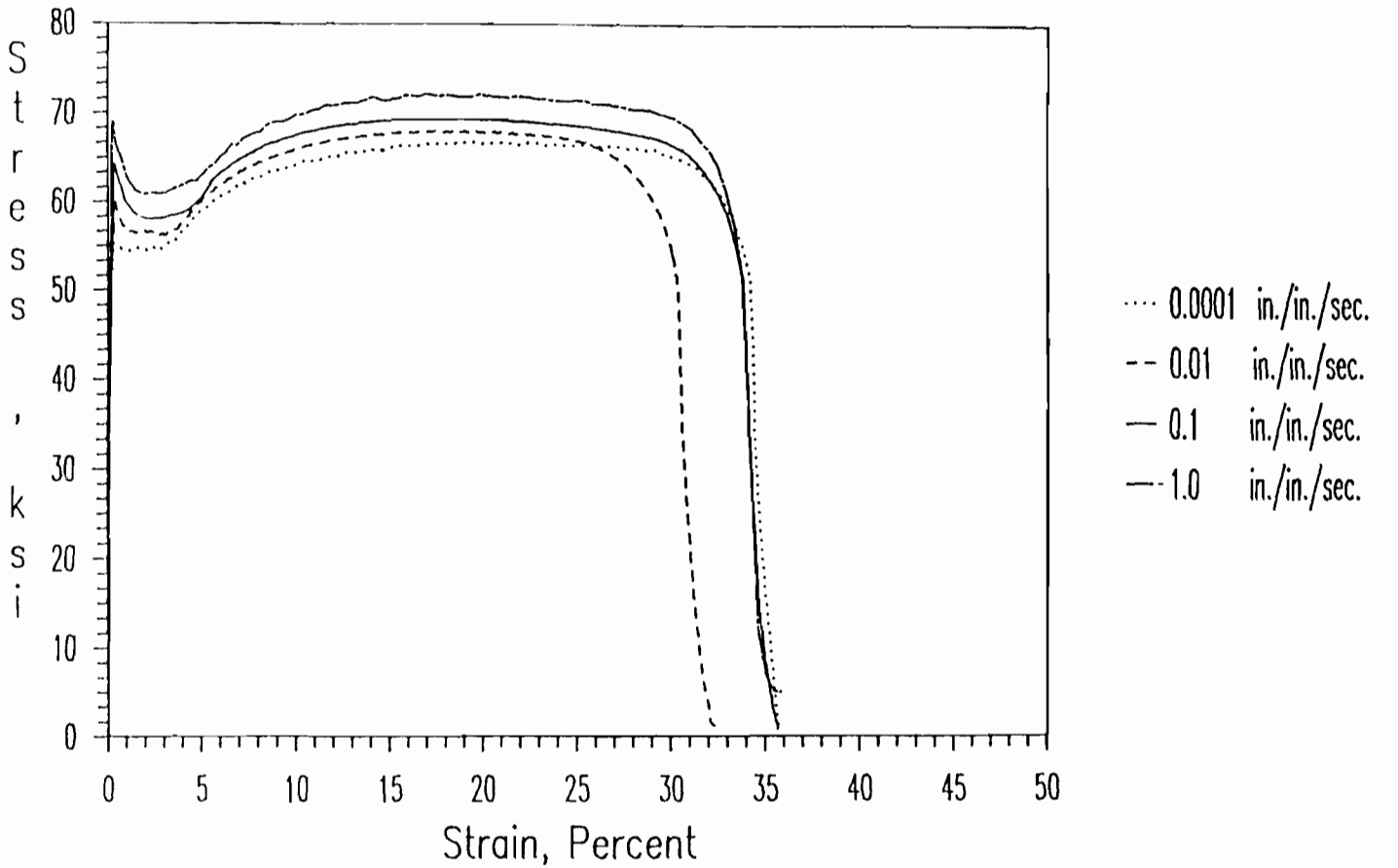

Figure 3.5 Stress-Strain Curves for 50SK Steel in the Longitudinal Tension under Different Strain Rates

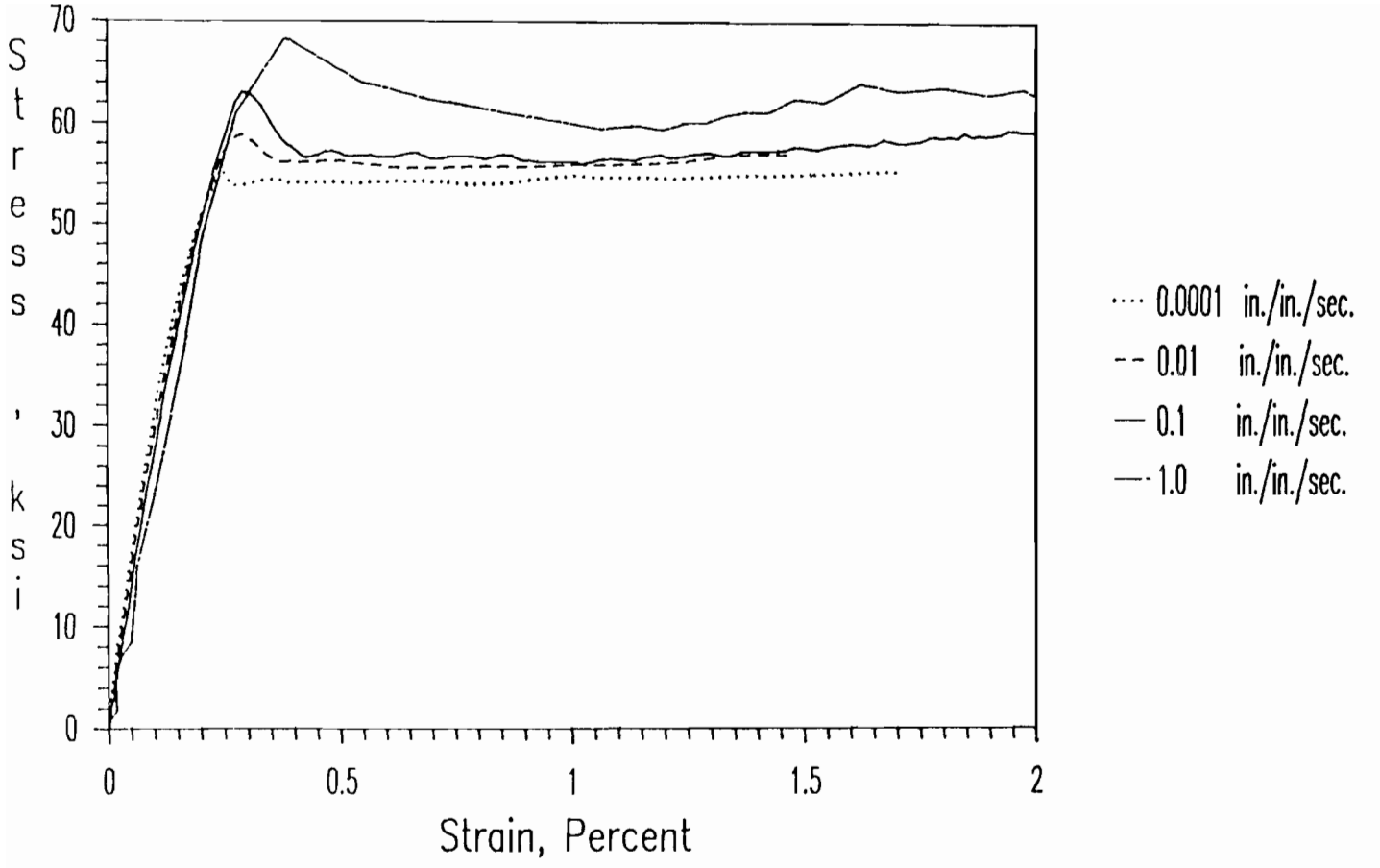

Figure 3.6 Stress-Strain Curves for 50SK Steel in the Longitudinal Compression under Different Strain Rates

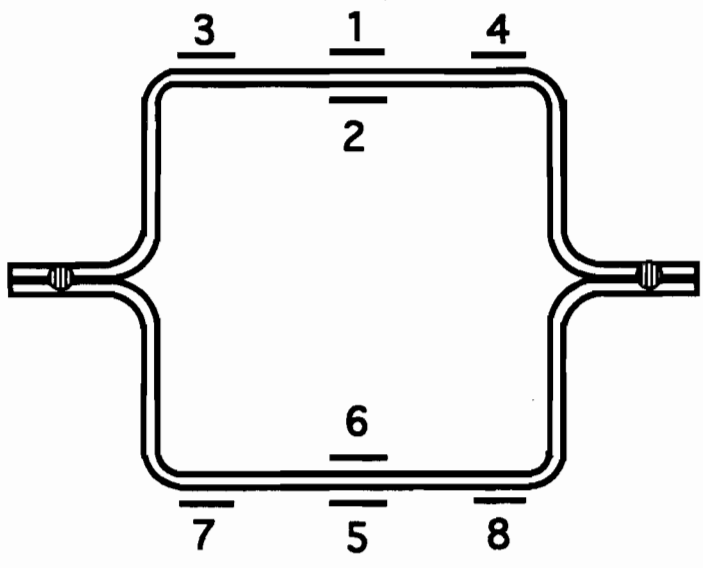

(a) Box-Shaped Stub Column

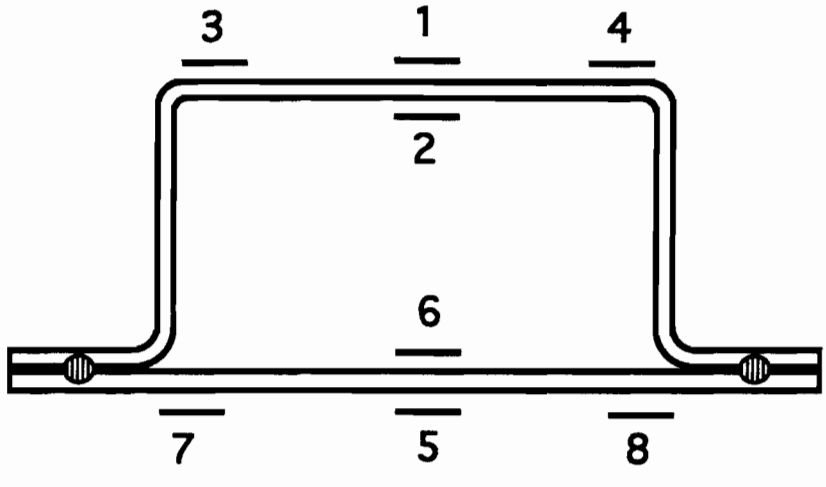

(b) Hat-Shaped Stub Column

Figure 3.7 Locations of Strain Gages at Midheight of Stub Columns

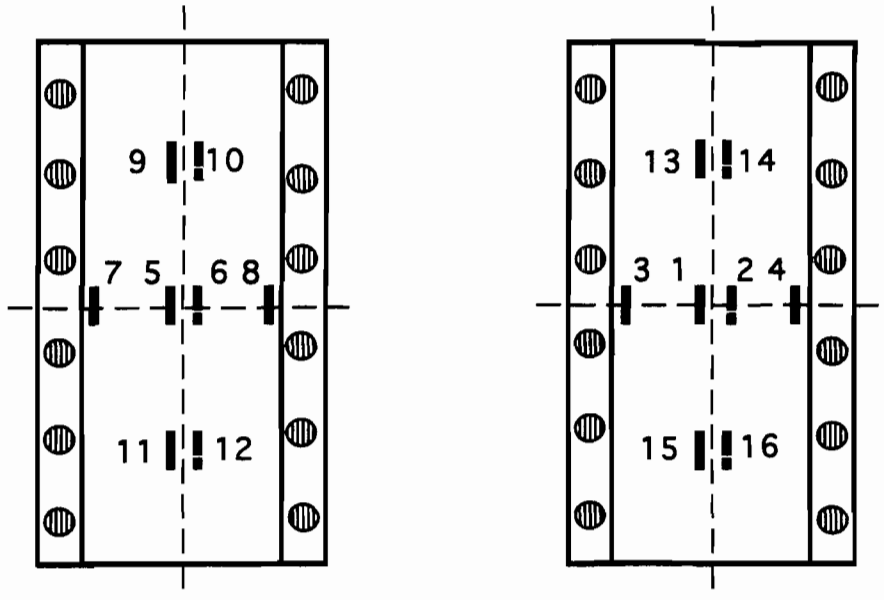

(a) Box-Shaped Stub Column

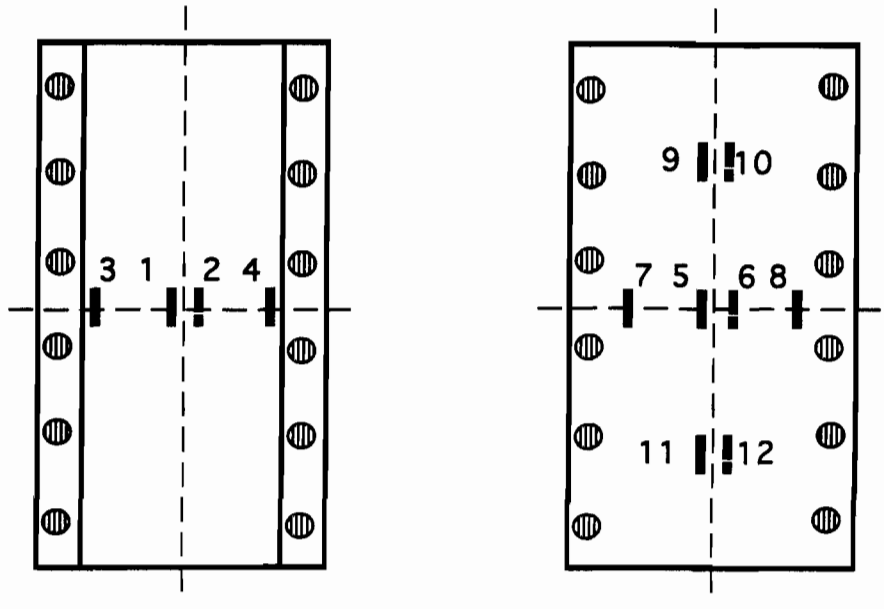

(b) Hat-Shaped Stub Column

Figure 3.8 Locations of Strain Gages along the Specimen Length for Stub Columns Having Large w/t Ratios

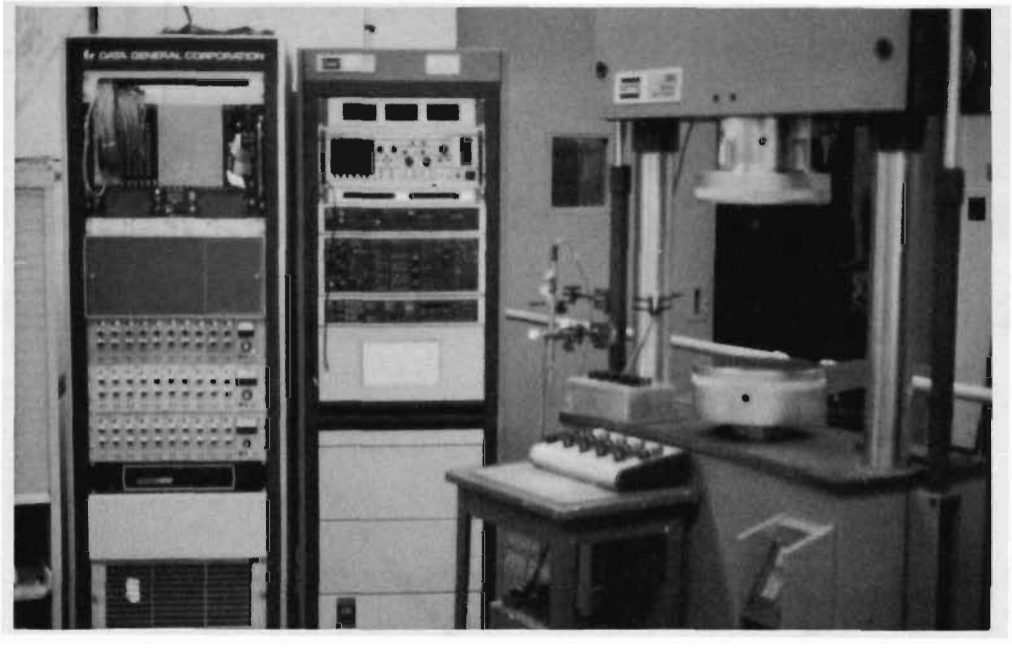

Figure 3.9 880 Material Test System and Data Acquisition System

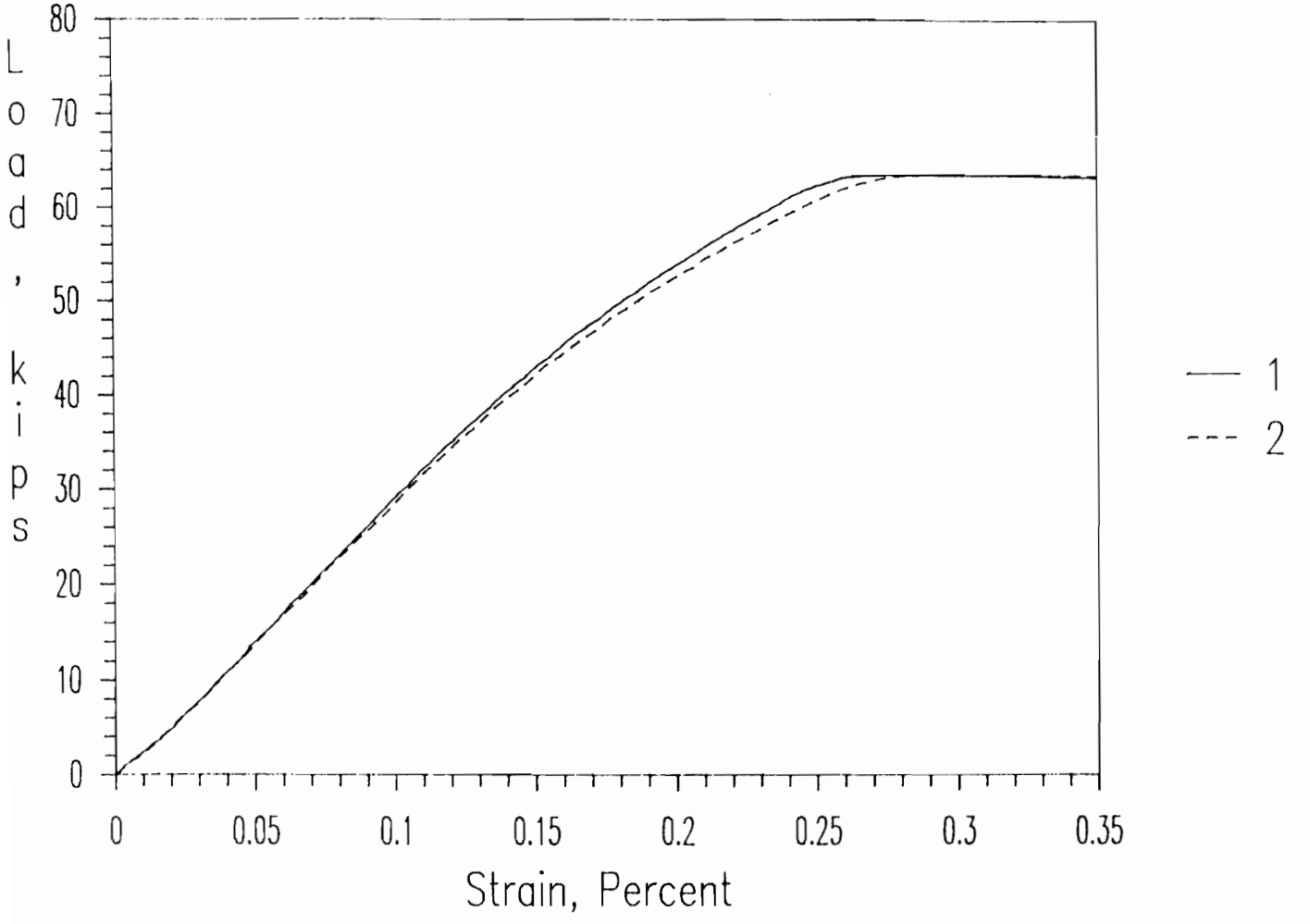

Figure 3.10 Load-Strain Curves of Strain Gages #1 and #2 Installed at the Center of Stiffened Elements (Spec. 1A0A1)

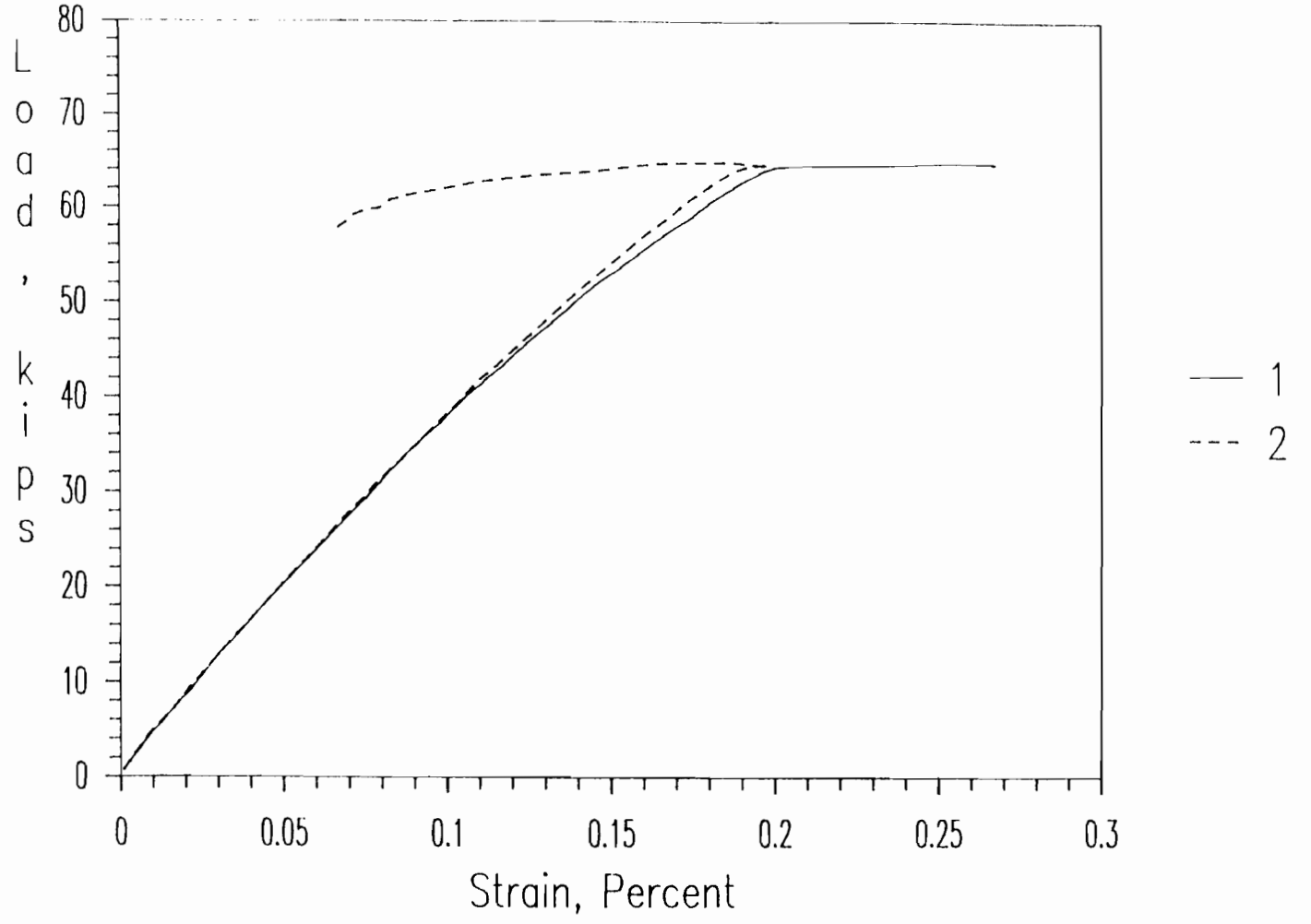

Figure 3.11 Load-Strain Curves of Strain Gages #5 and #6 Installed at the Center of Stiffened Elements (Spec. 1A2A2)

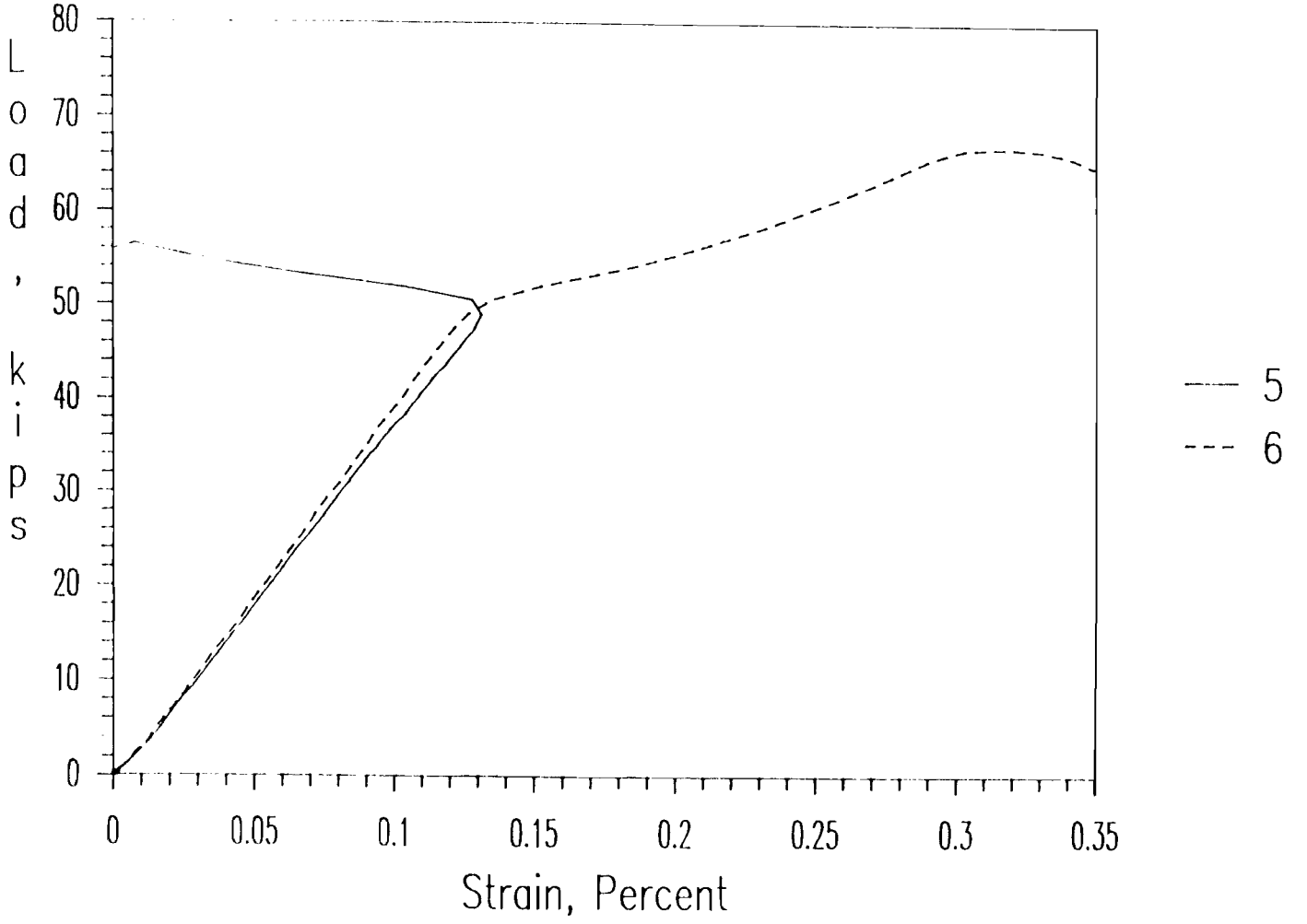

Figure 3.12 Load-Strain Curves of Strain Gages #5 and #6 Installed at the Center of Stiffened Elements (Spec. 1A0A4)

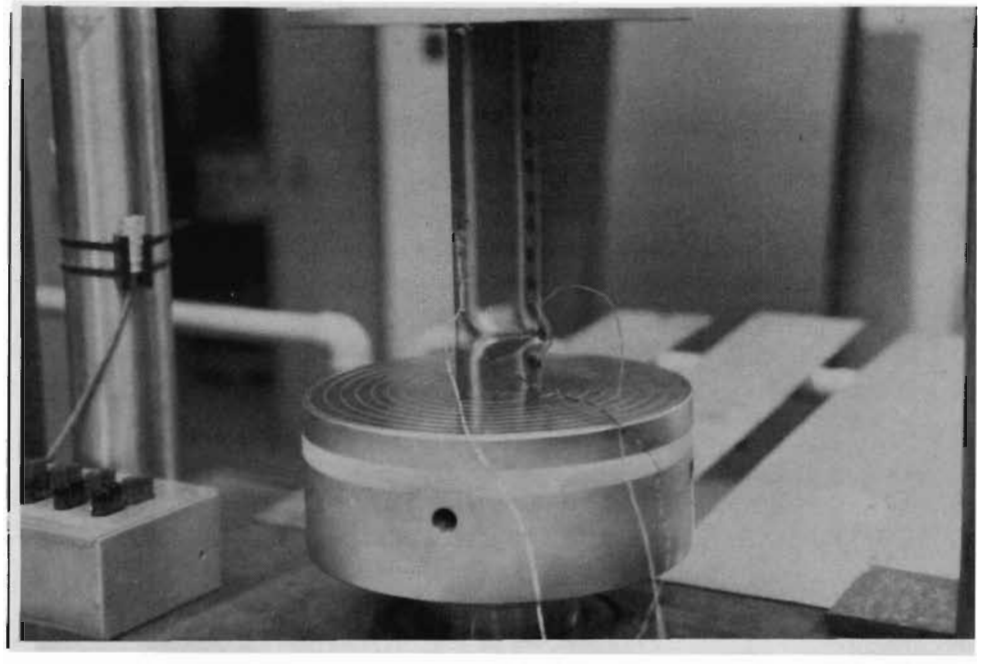

Figure 3.13 Photograph of a Stub Column with small w/t Ratio at Beginning of Buckling (Spec. 1B1E1)

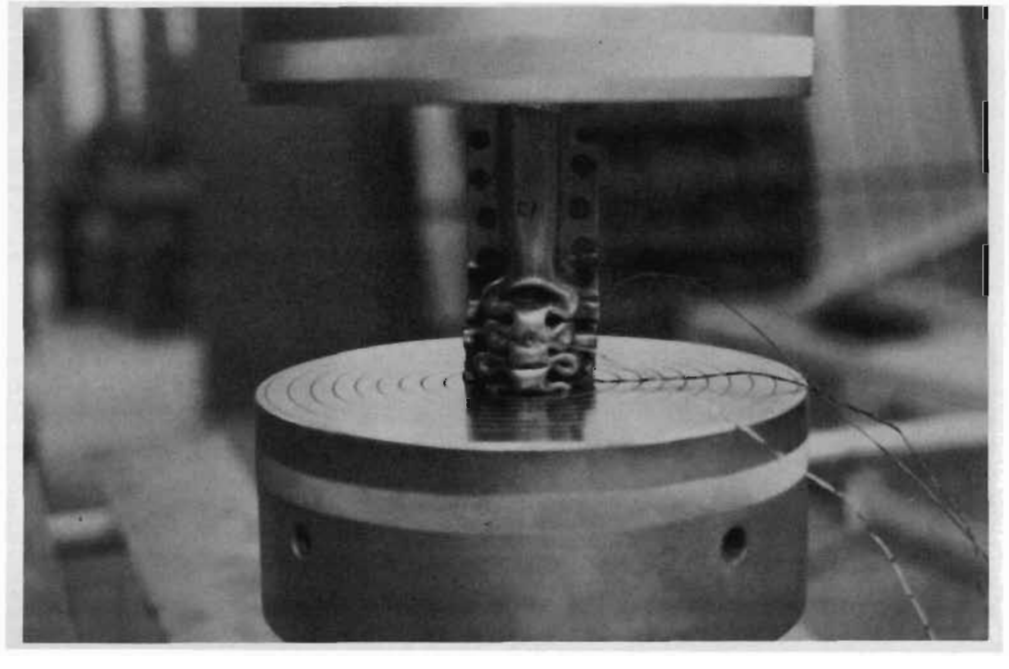

Figure 3.14 Typical Failure of a Stub Column with small w/t Ratio (Spec. 1B1E1)

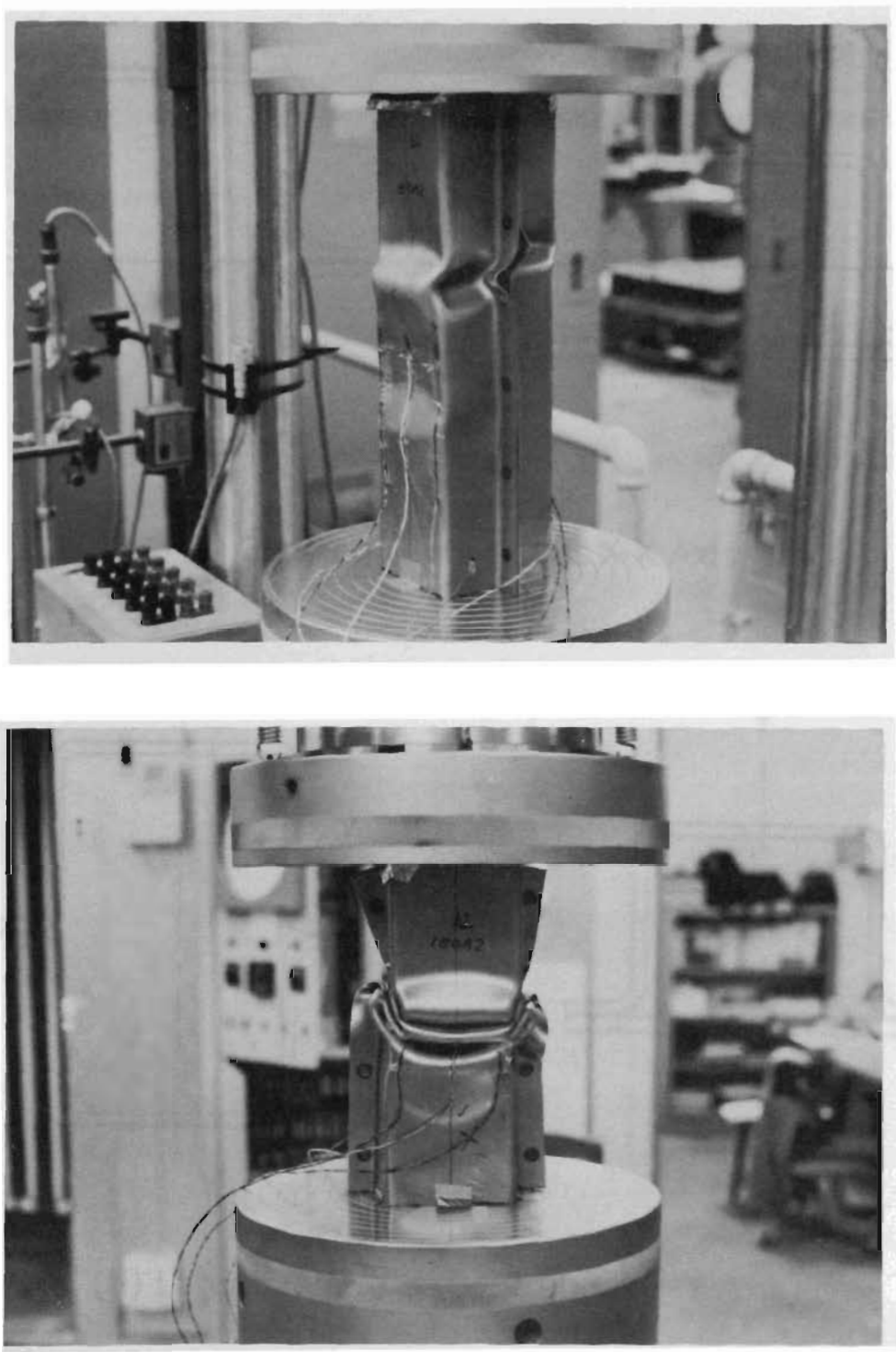

Figure 3.15 Typical Failure of a Stub Column with Large w/t Ratio (Spec. 1B0A2)

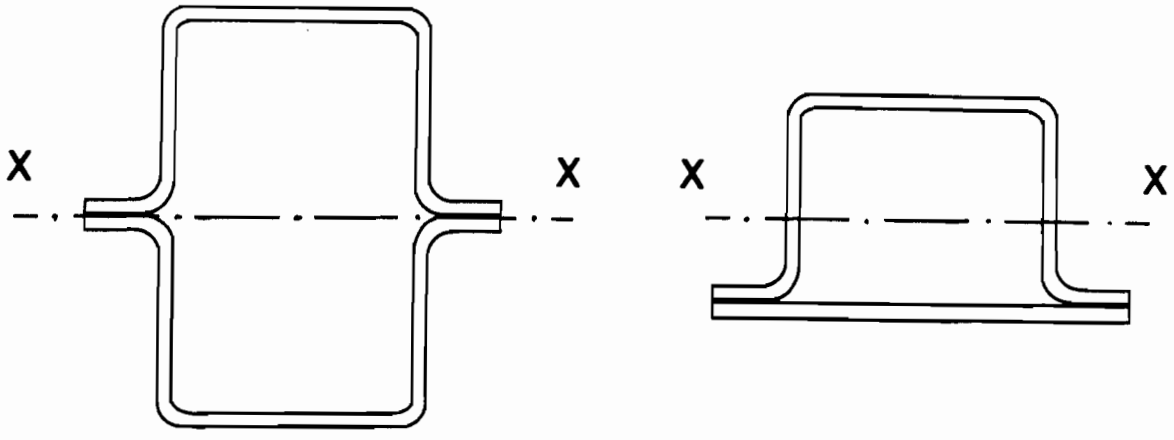

(a) Bending (Bent about X-X Axis)

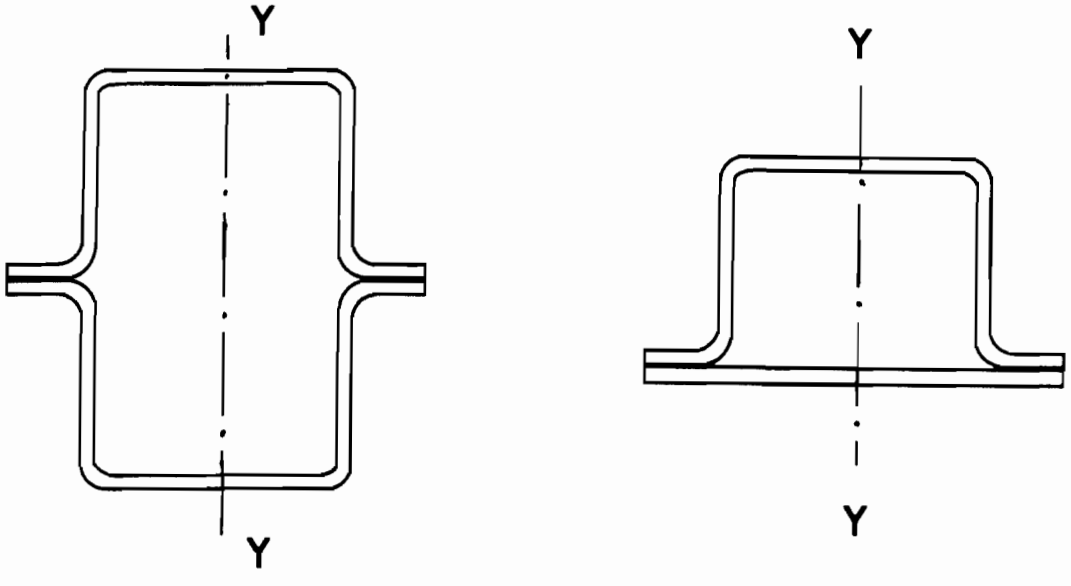

(b) Lateral Buckling (Bent about Y-Y Axis)

Figure 3.16 Definition of Bending and Lateral Buckling of Stub Columns Used in This Study

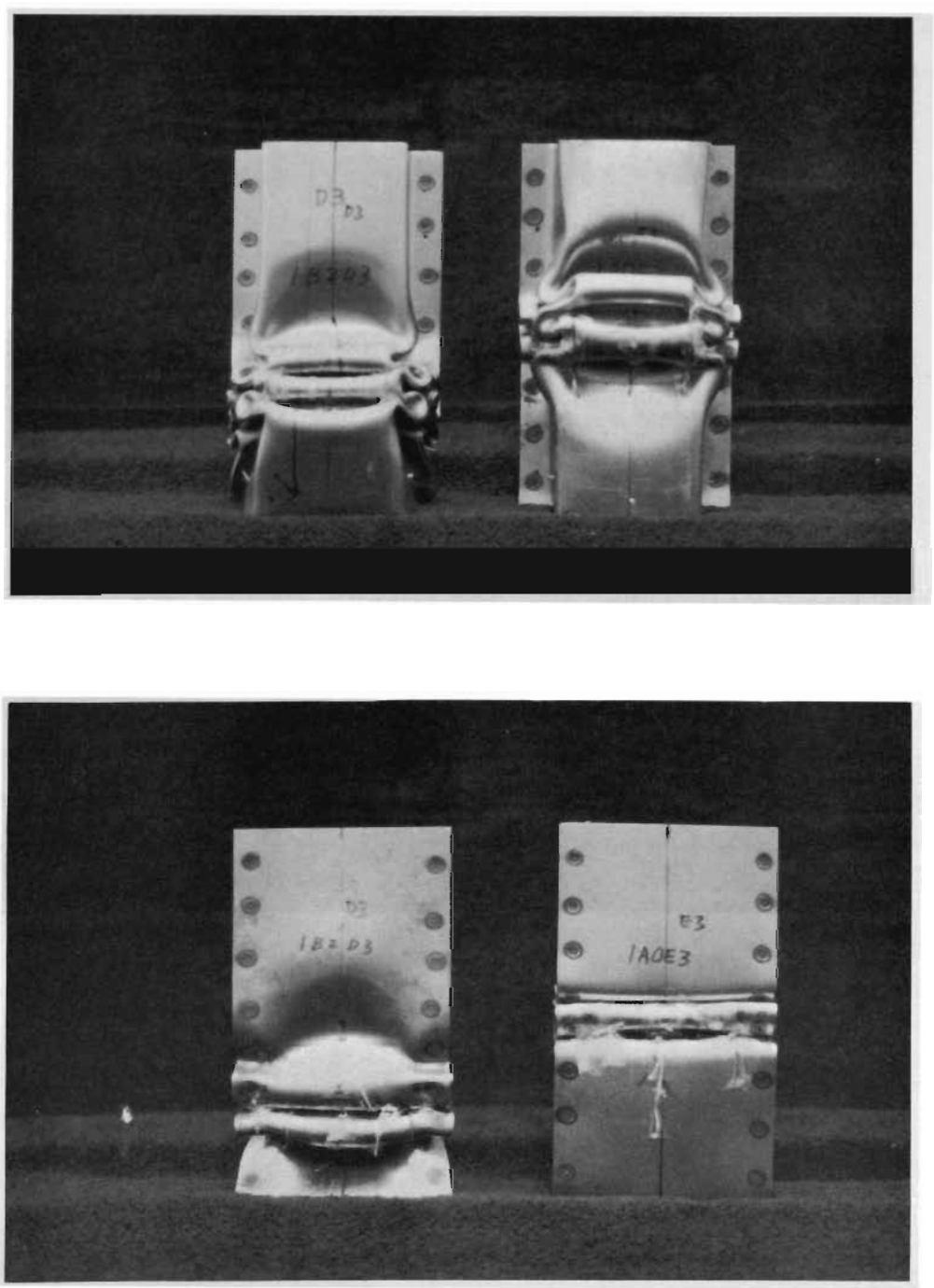

Figure 3.17 Typical Folding Type of Stub Column Specimens (Spec. 1B2D3 and 1A0E3)

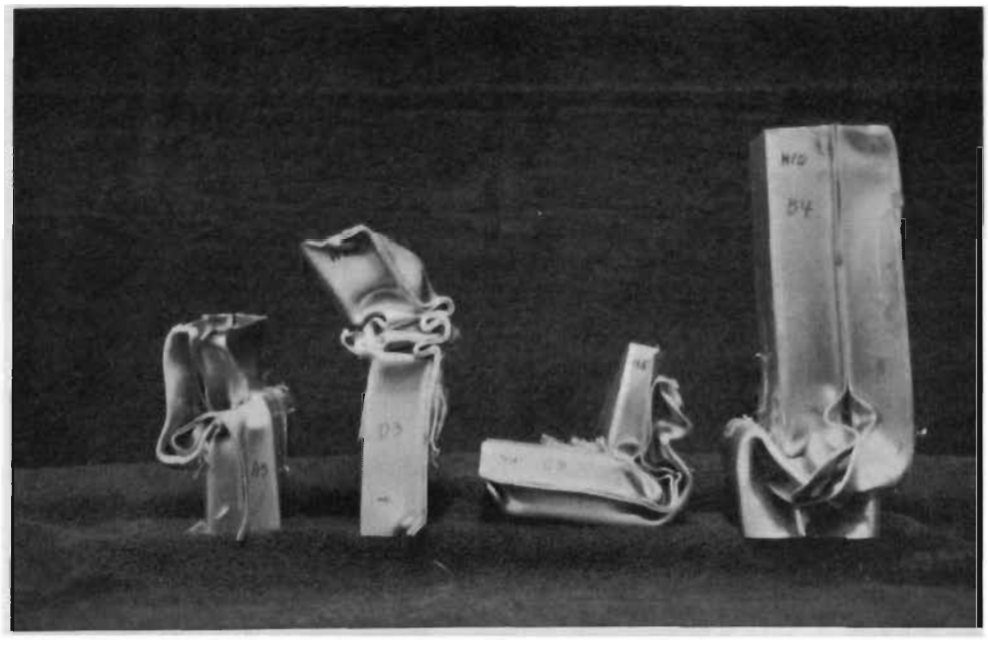

Figure 3.18 Typical Bending Type of Stub Column Specimens (Spec. 1A1A3, 1B2D3, 1B0C3, and 1B0B4)

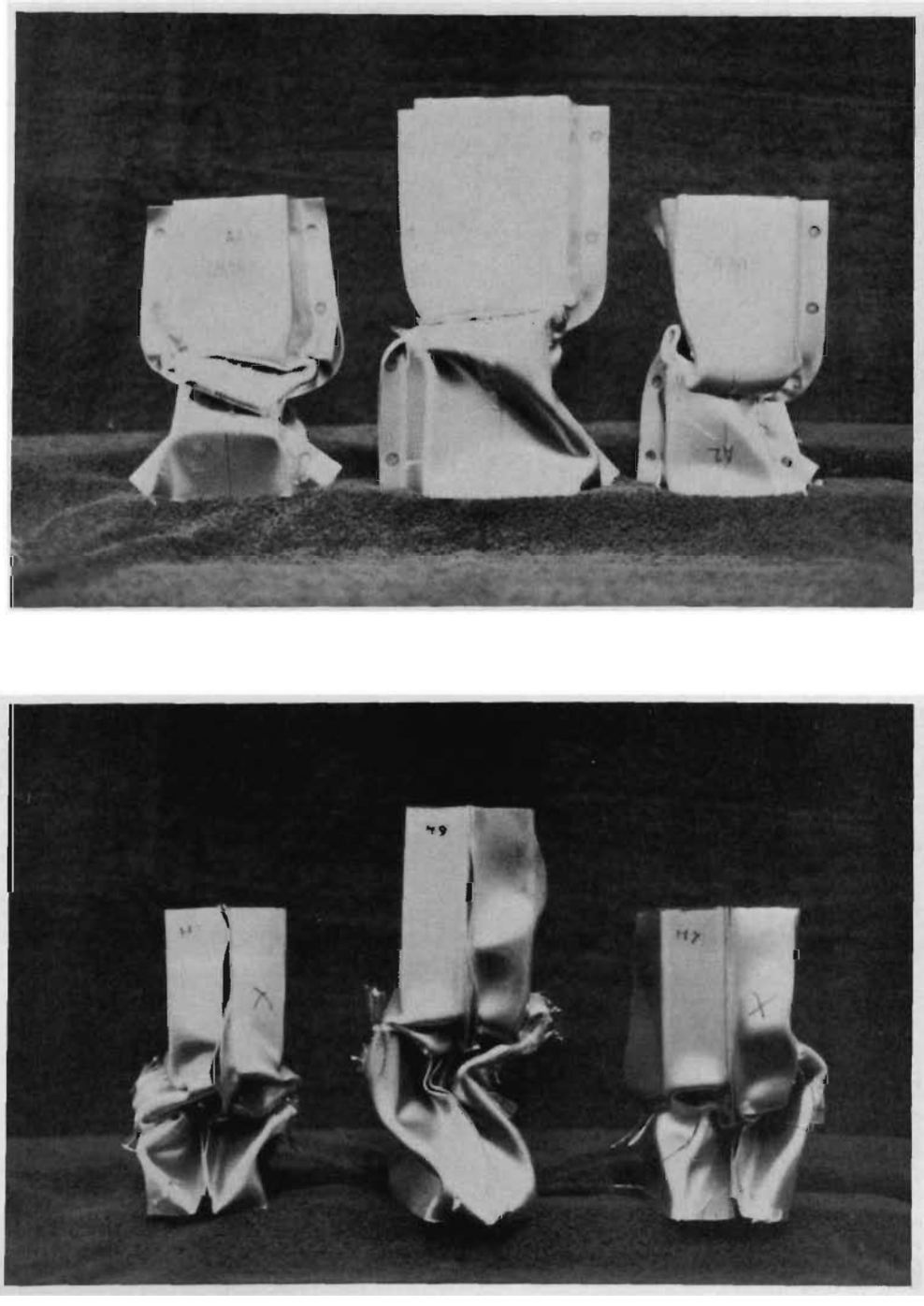

Figure 3.19 Typical Twisting Type of Stub Column Specimens (Spec. 1B1A2, 1A3C4, and 1A3A2)

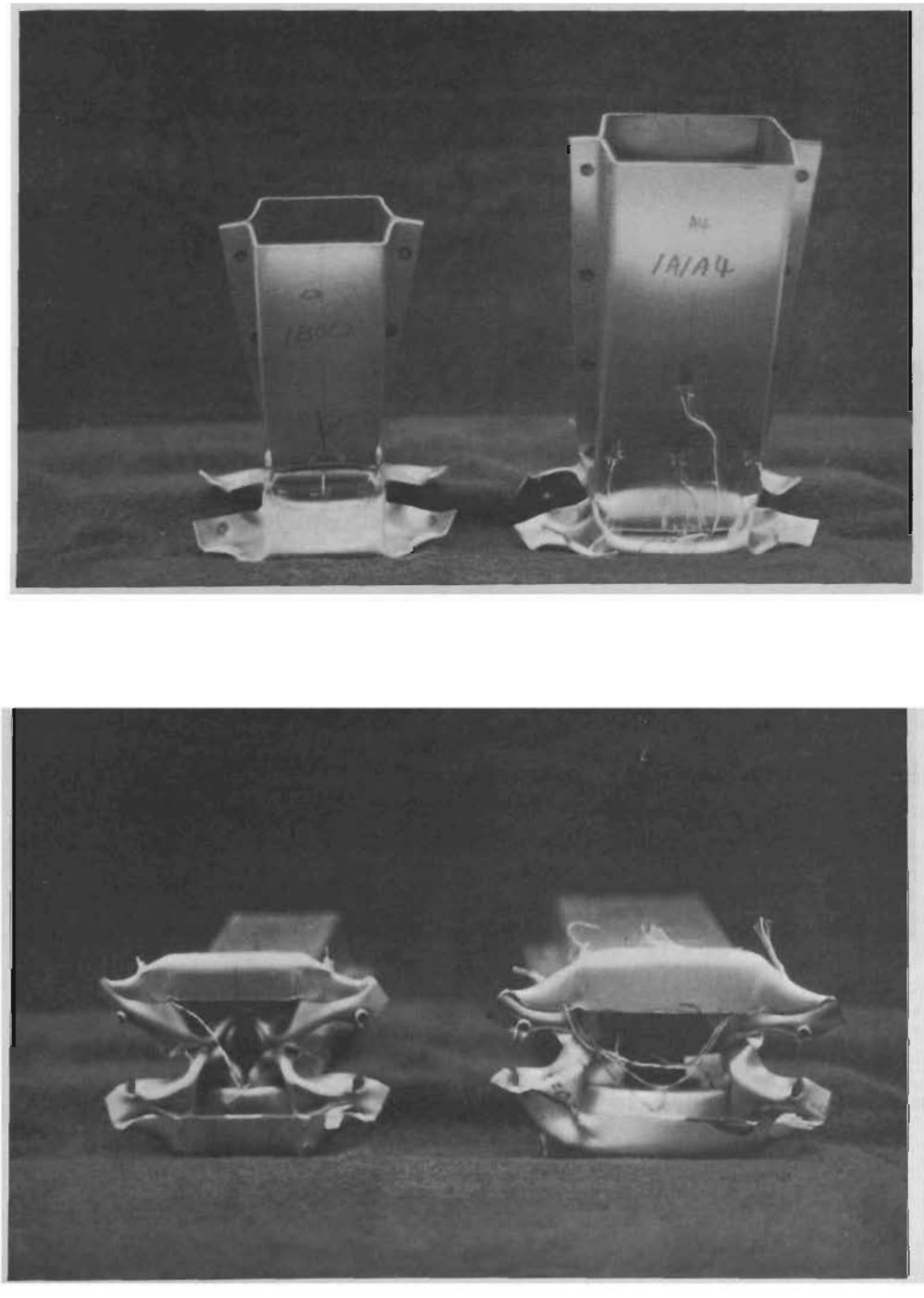

Figure 3.20 Typical Openning Type of Stub Column Specimens (Spec. 1B0C2 and 1A1A4)

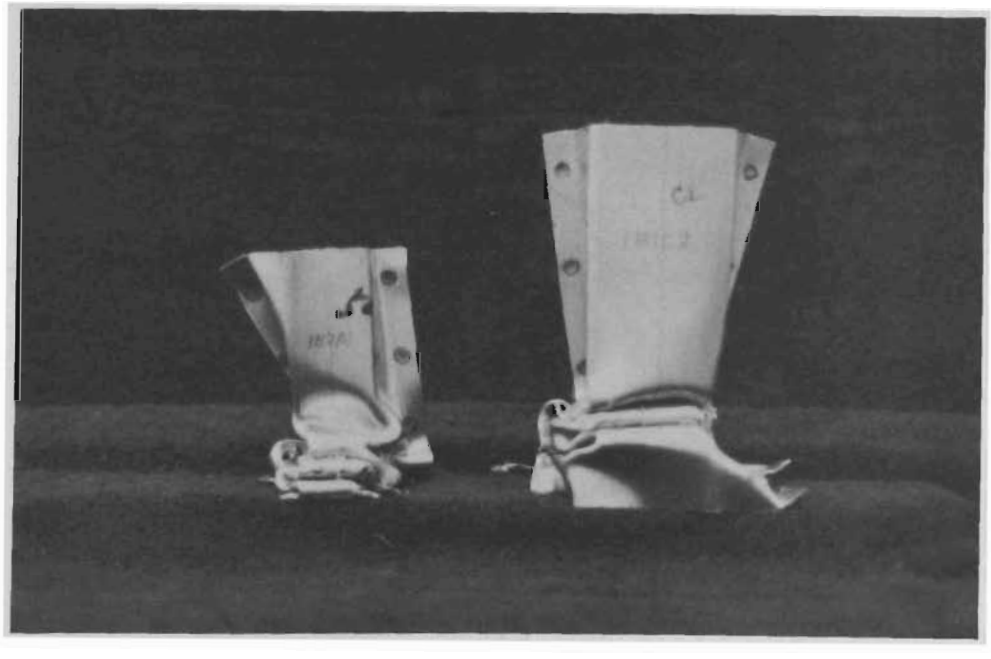

Figure 3.21 Typical Lateral Buckling Type of Stub Column Specimens (Spec. 1B2A1 and 1B1C2)

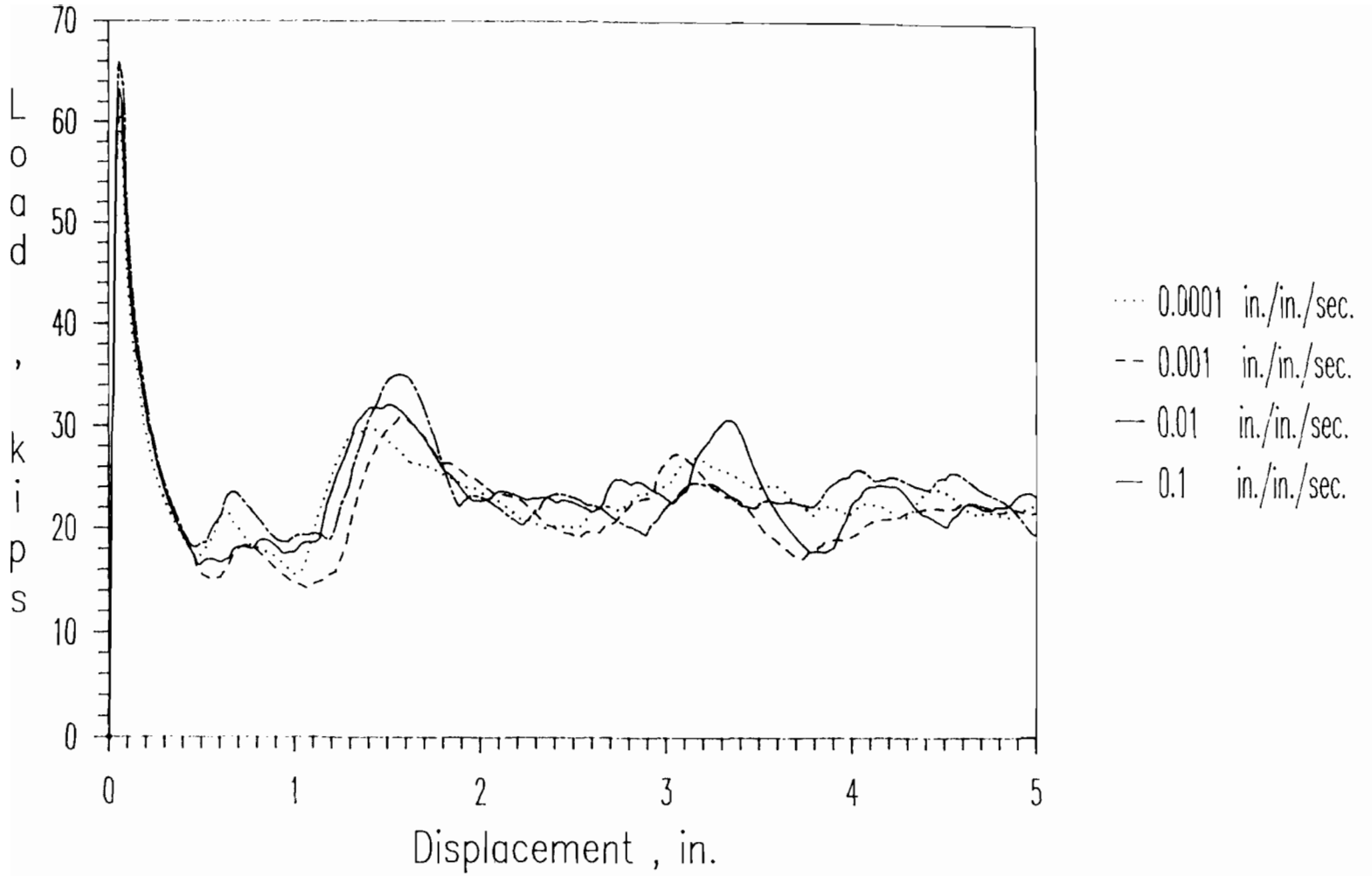

Figure 3.22 Load-Displacement Curves for Stub Column Specimens (Case 1 of Group A)

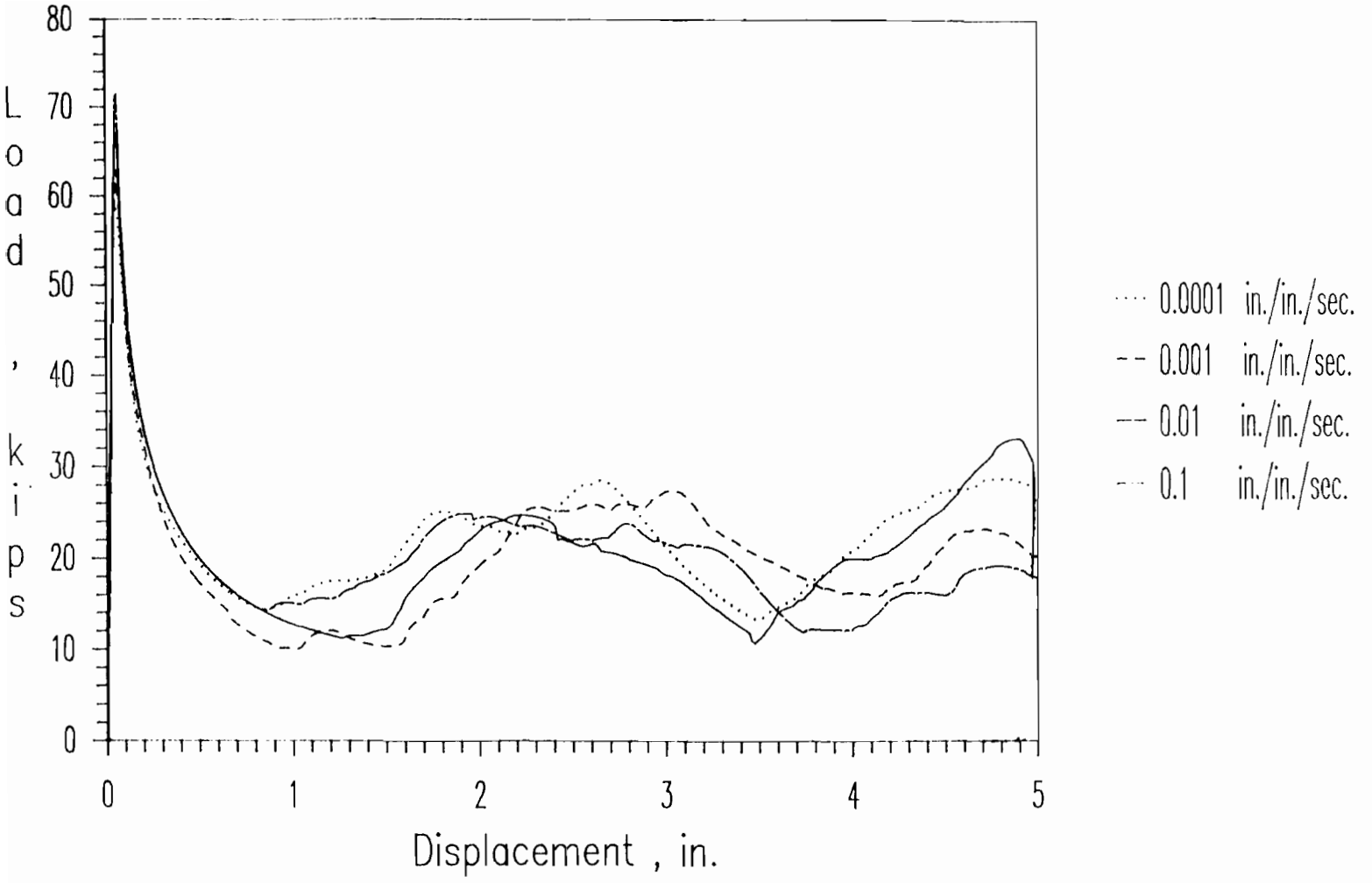

Figure 3.23 Load-Displacement Curves for Stub Column Specimens (Case 2 of Group A)

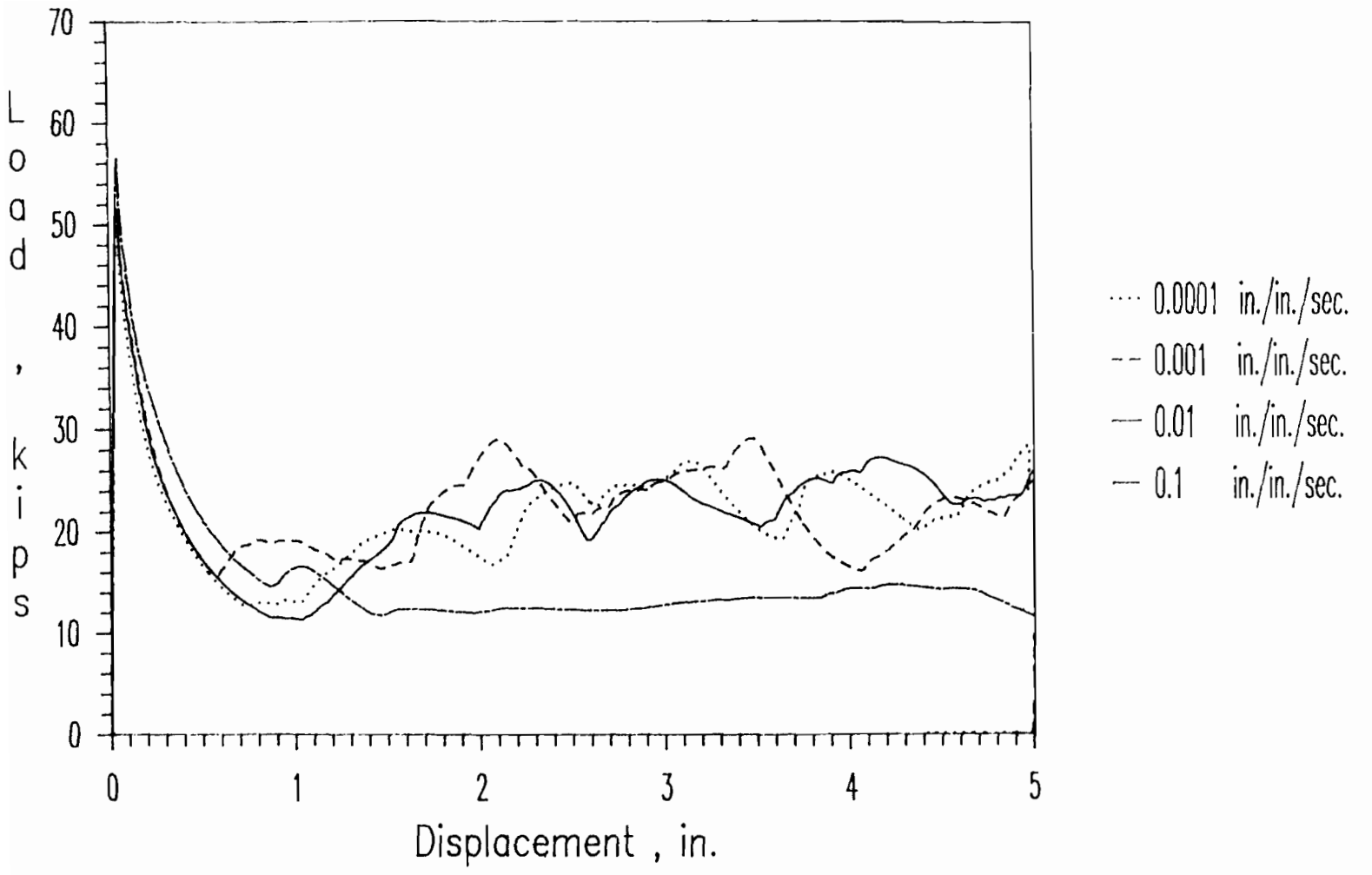

Figure 3.24 Load-Displacement Curves for Stub Column Specimens (Case 3 of Group A)

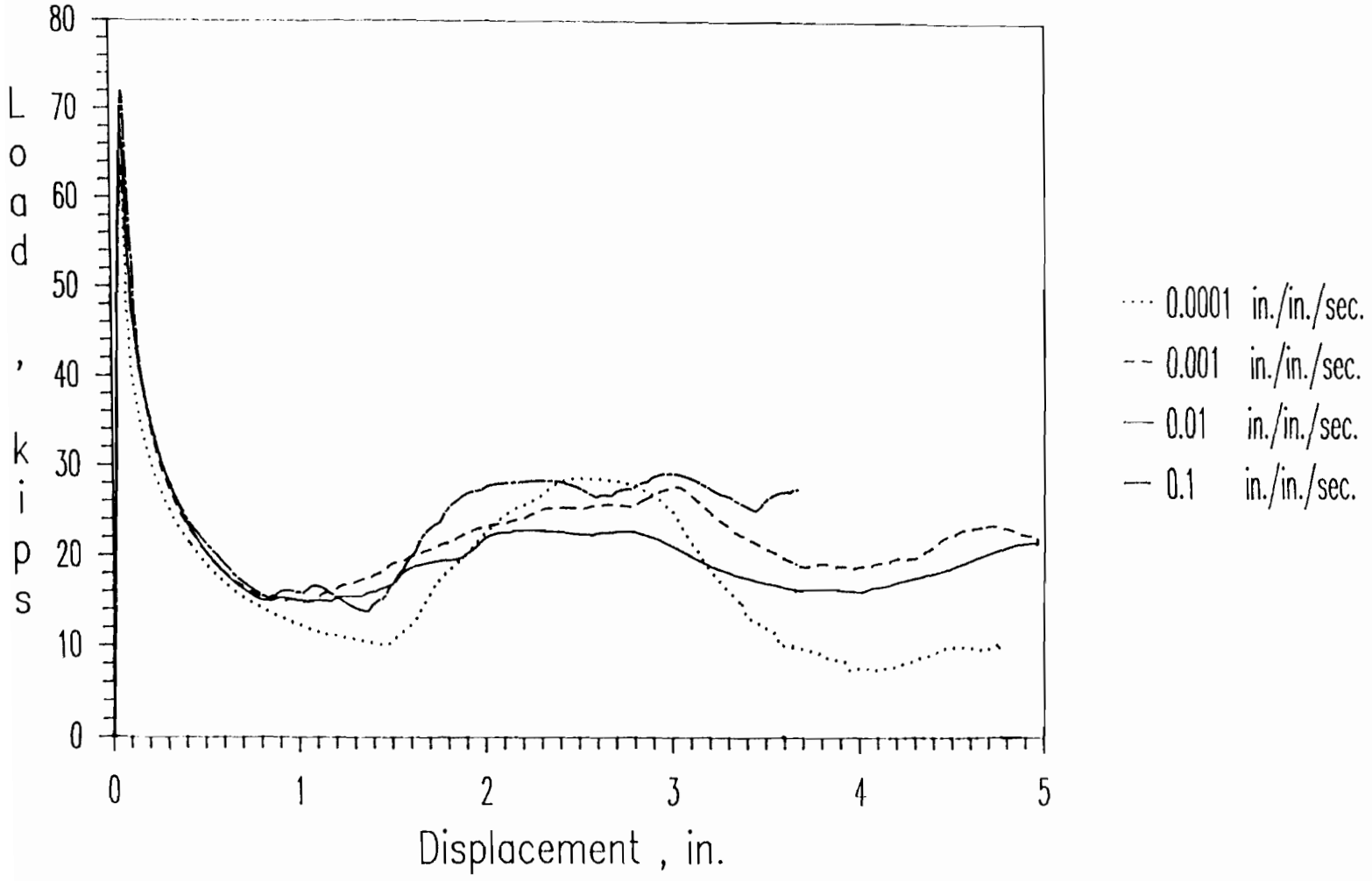

Figure 3.25 Load-Displacement Curves for Stub Column Specimens (Case 4 of Group A)

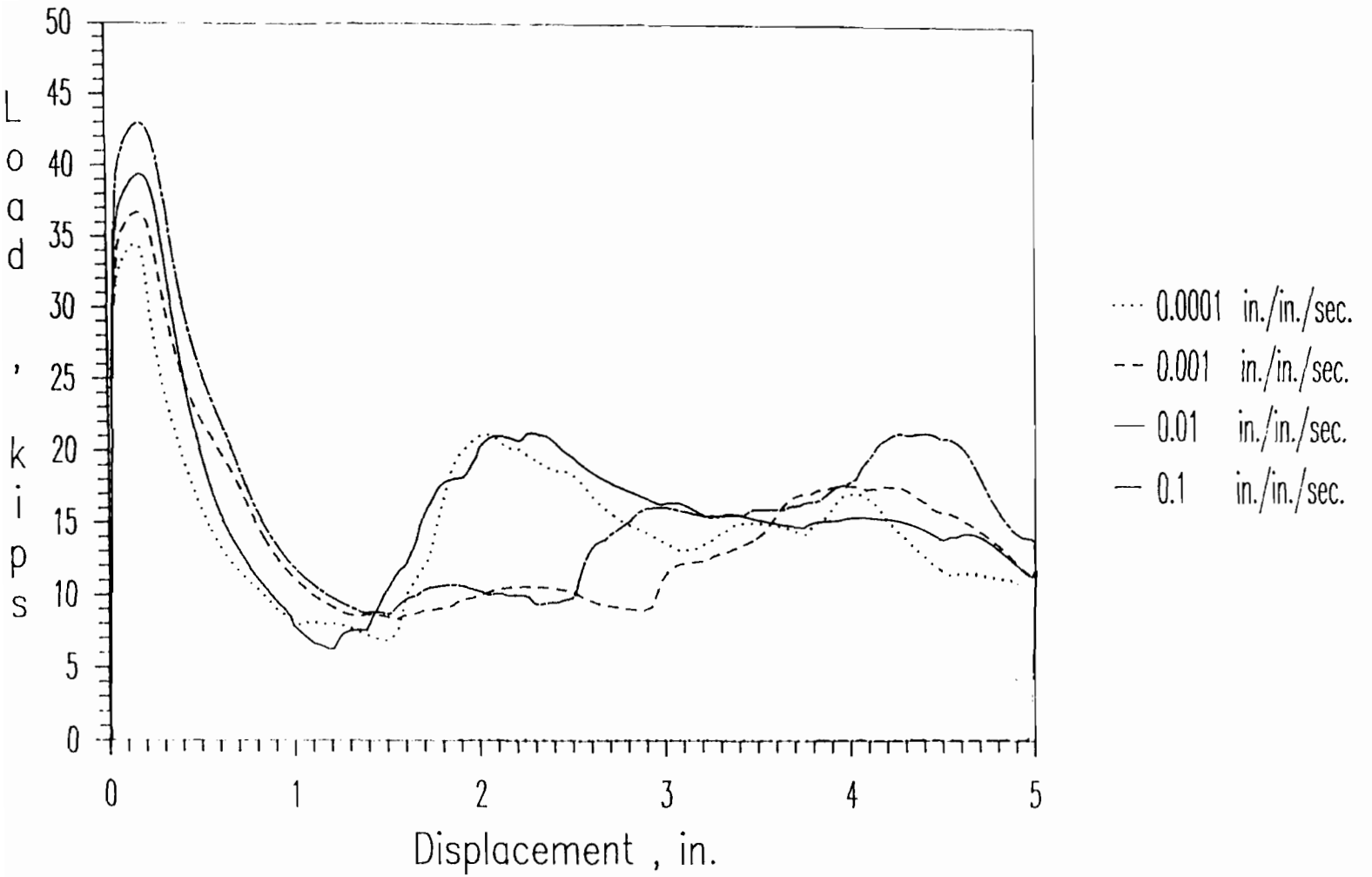

Figure 3.26 Load-Displacement Curves for Stub Column Specimens (Case 1 of Group B)

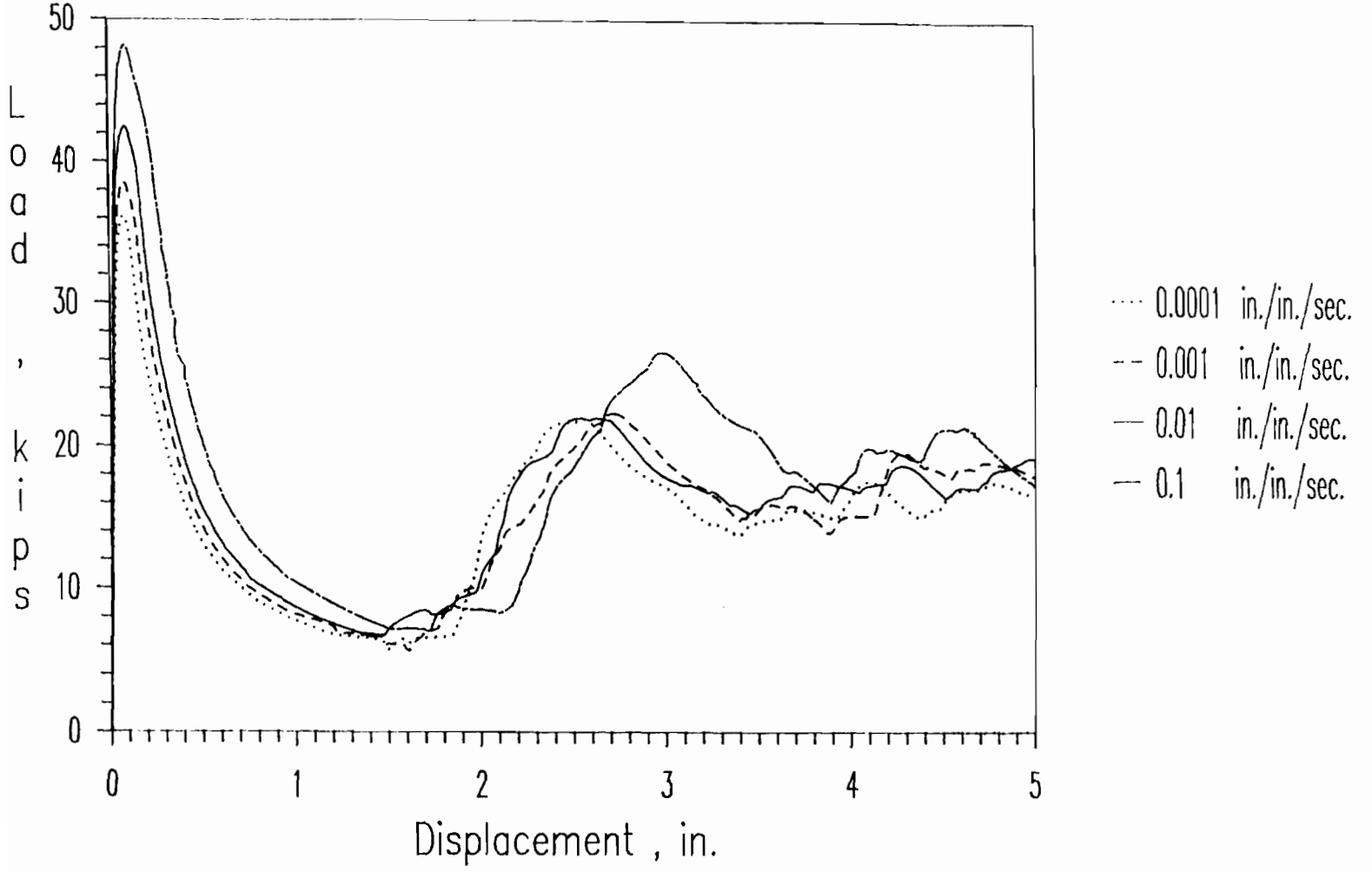

Figure 3.27 Load-Displacement Curves for Stub Column Specimens (Case 2 of Group B)

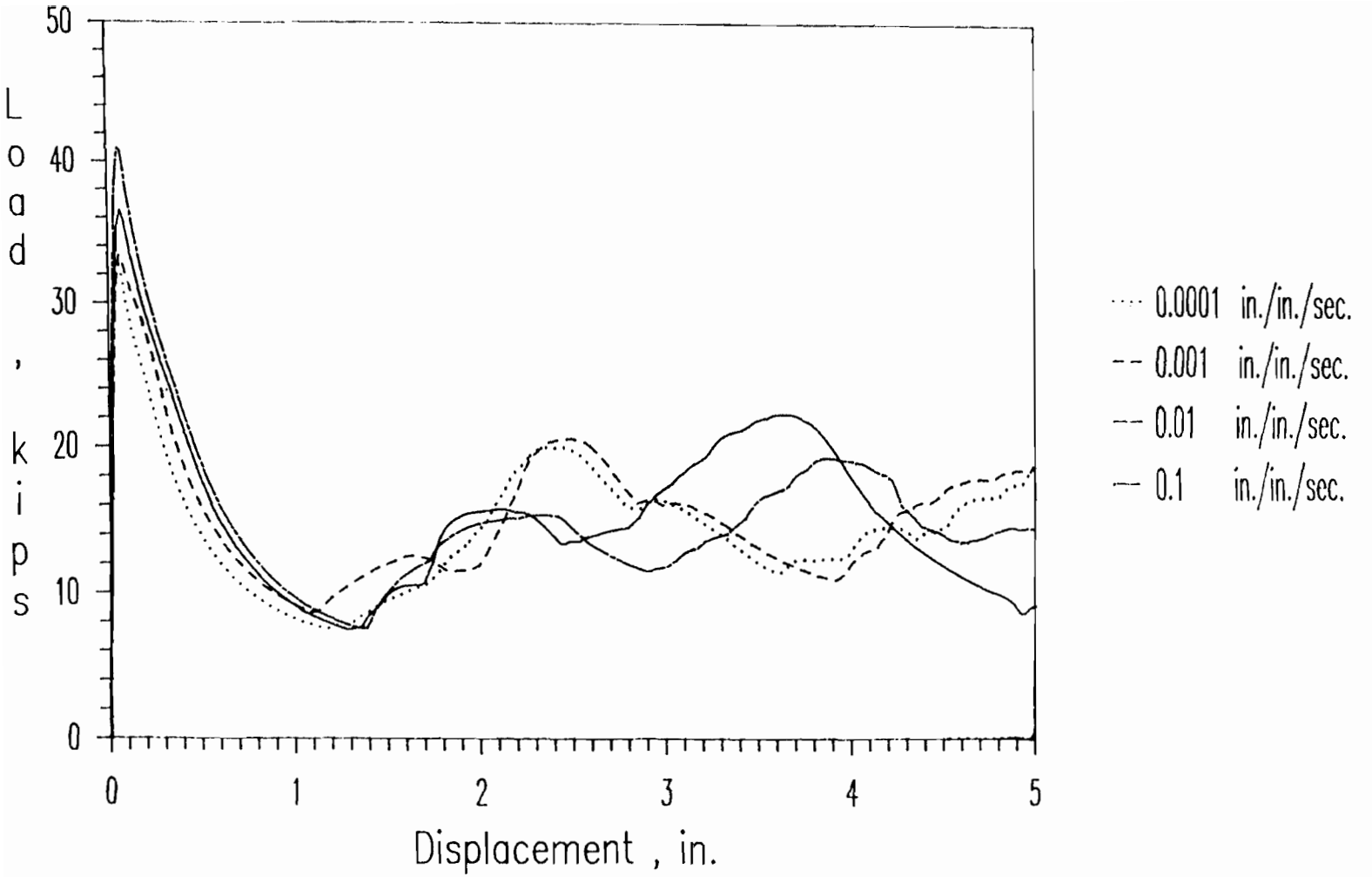

Figure 3.28 Load-Displacement Curves for Stub Column Specimens (Case 3 of Group B)

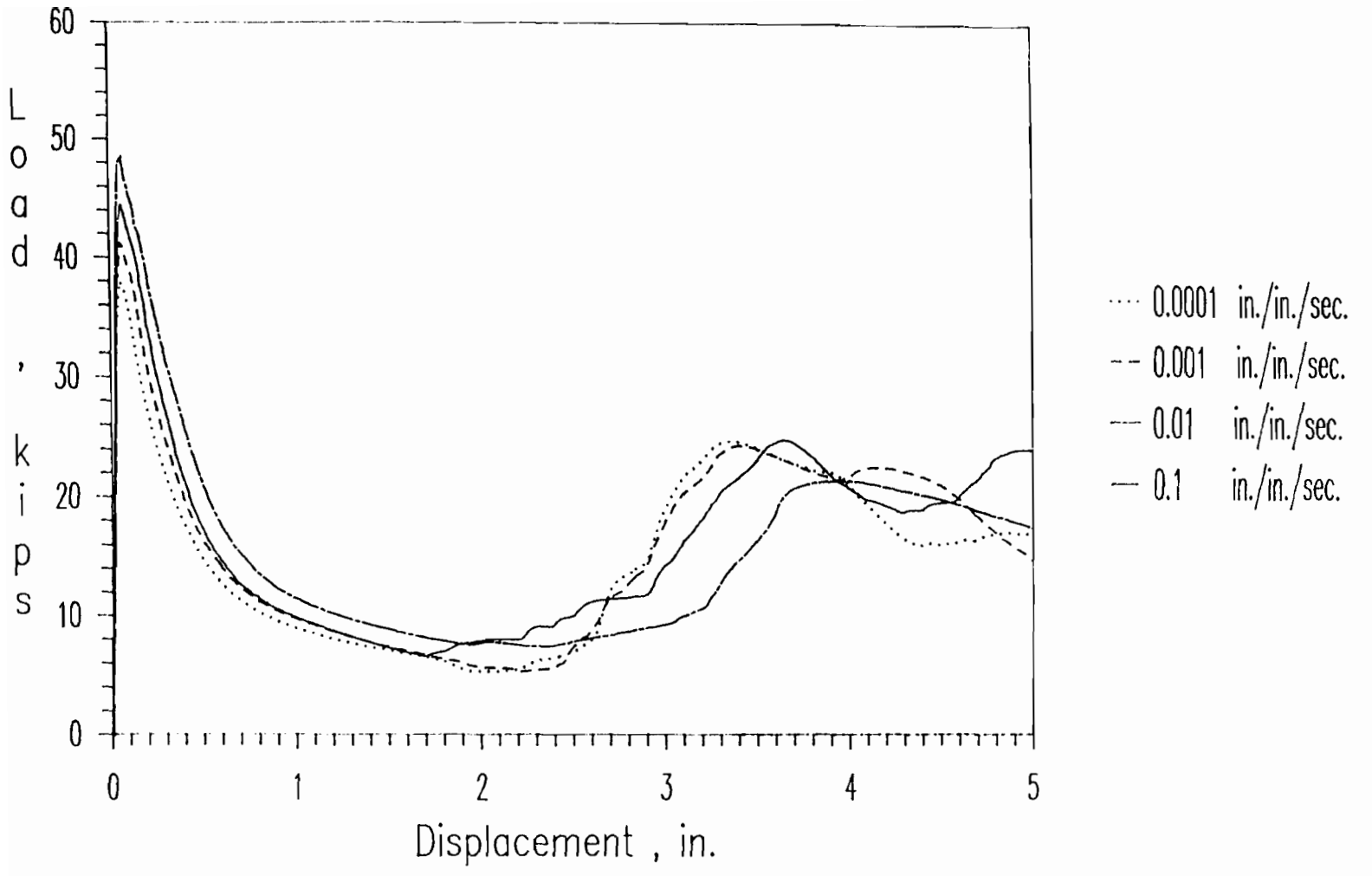

Figure 3.29 Load-Displacement Curves for Stub Column Specimens (Case 4 of Group B)

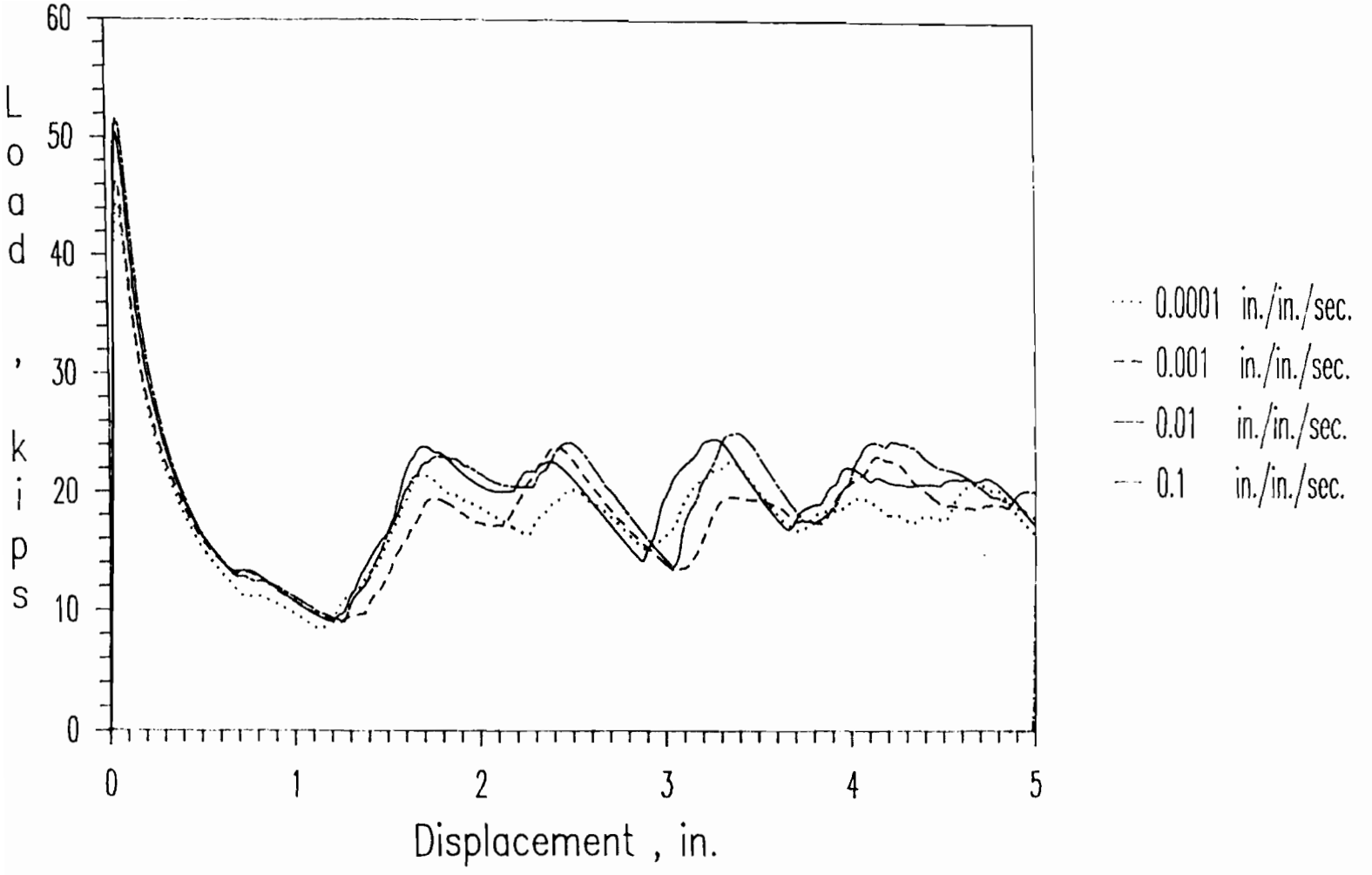

Figure 3.30 Load-Displacement Curves for Stub Column Specimens (Case 1 of Group C)

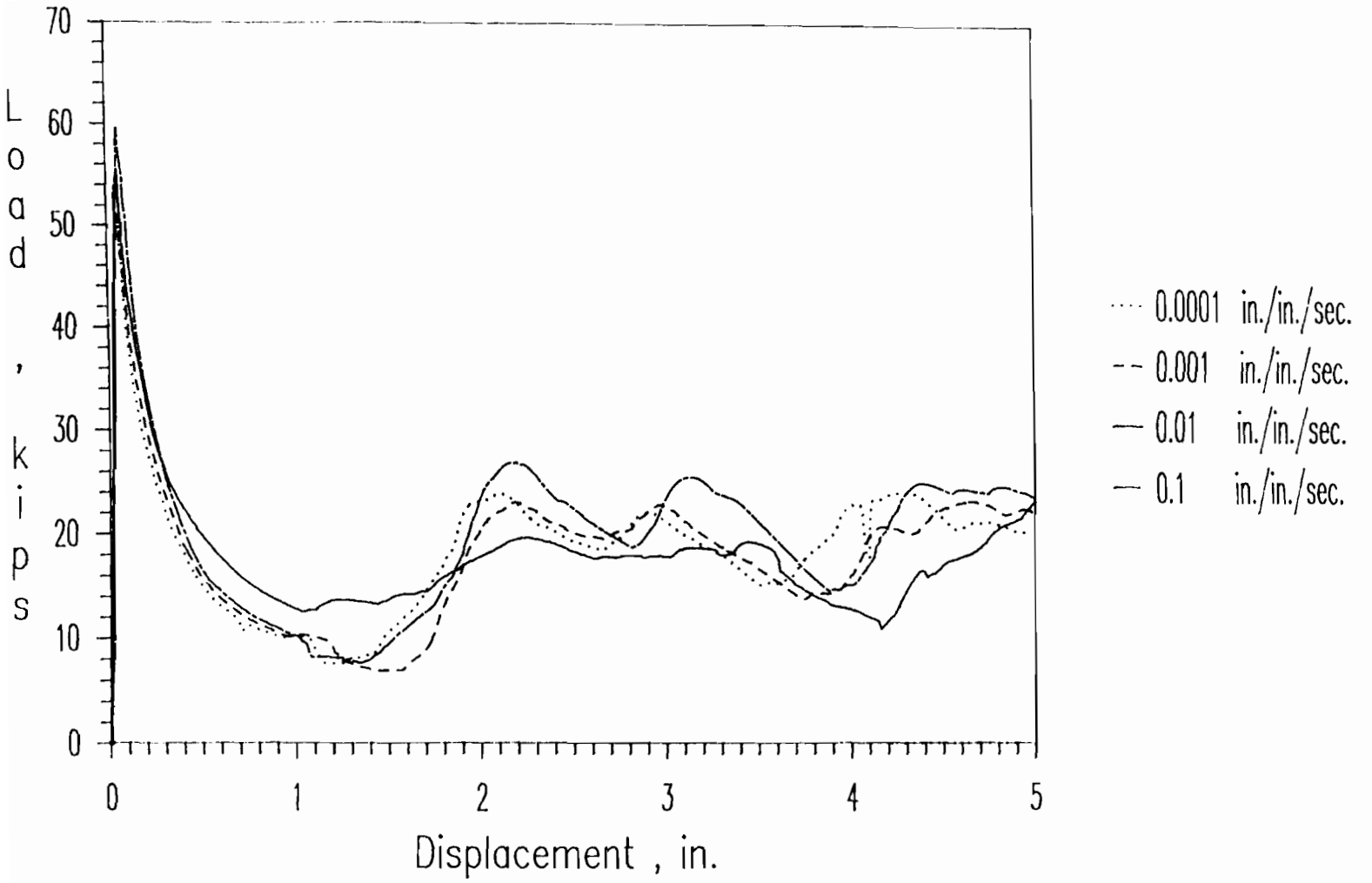

Figure 3.31 Load-Displacement Curves for Stub Column Specimens (Case 2 of Group C)

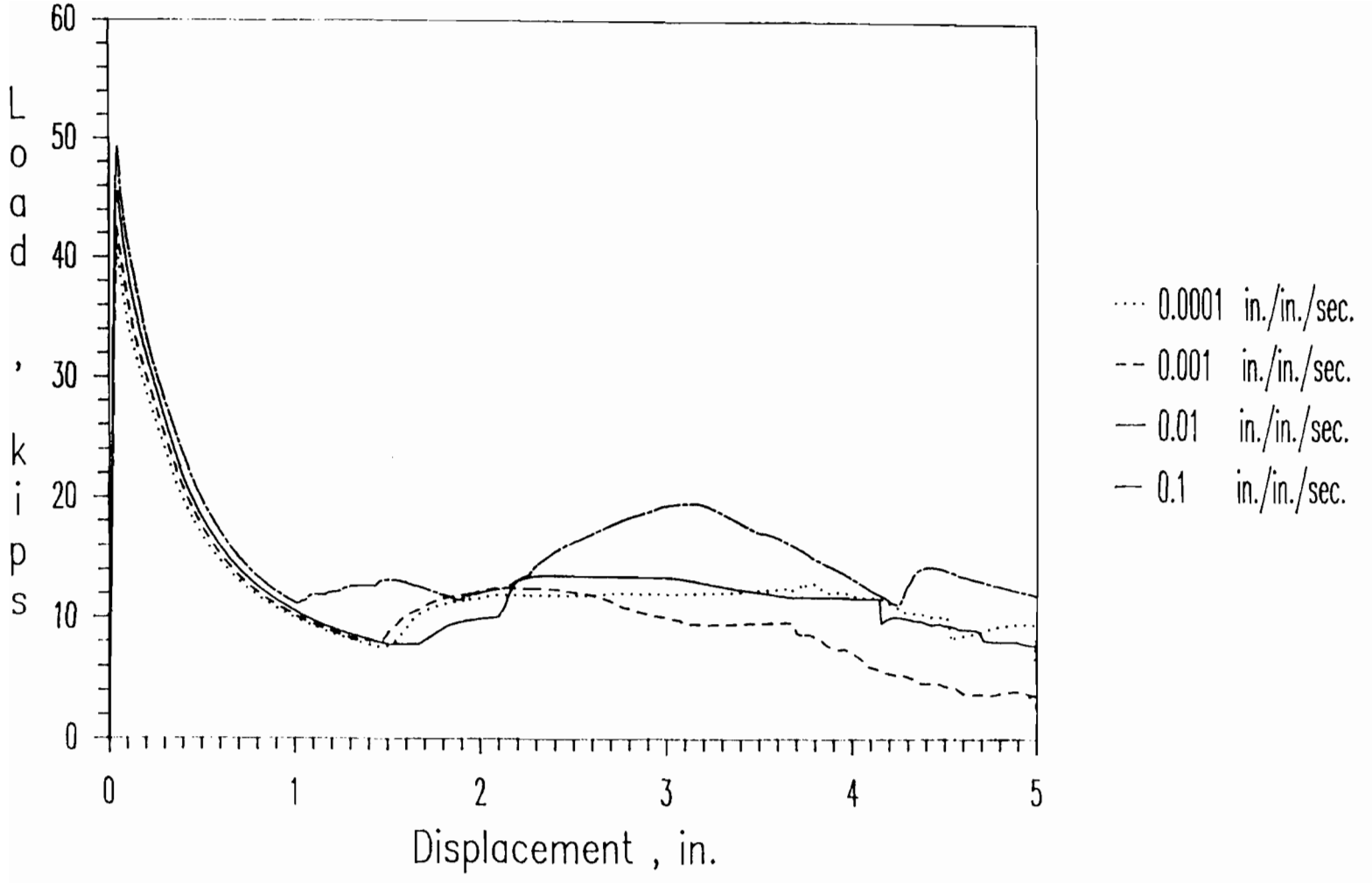

Figure 3.32 Load-Displacement Curves for Stub Column Specimens (Case 3 of Group C)

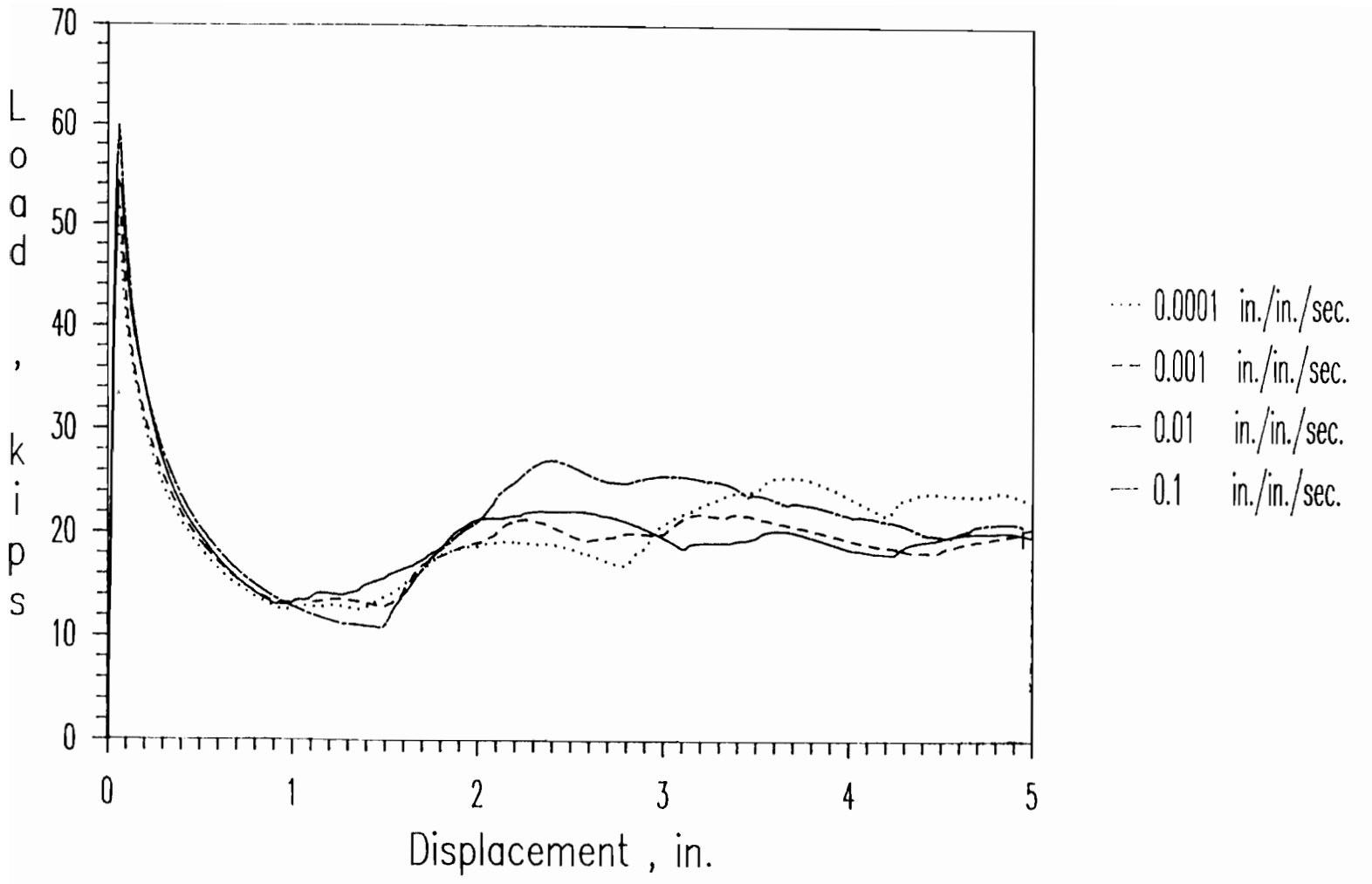

Figure 3.33 Load-Displacement Curves for Stub Column Specimens (Case 4 of Group C)

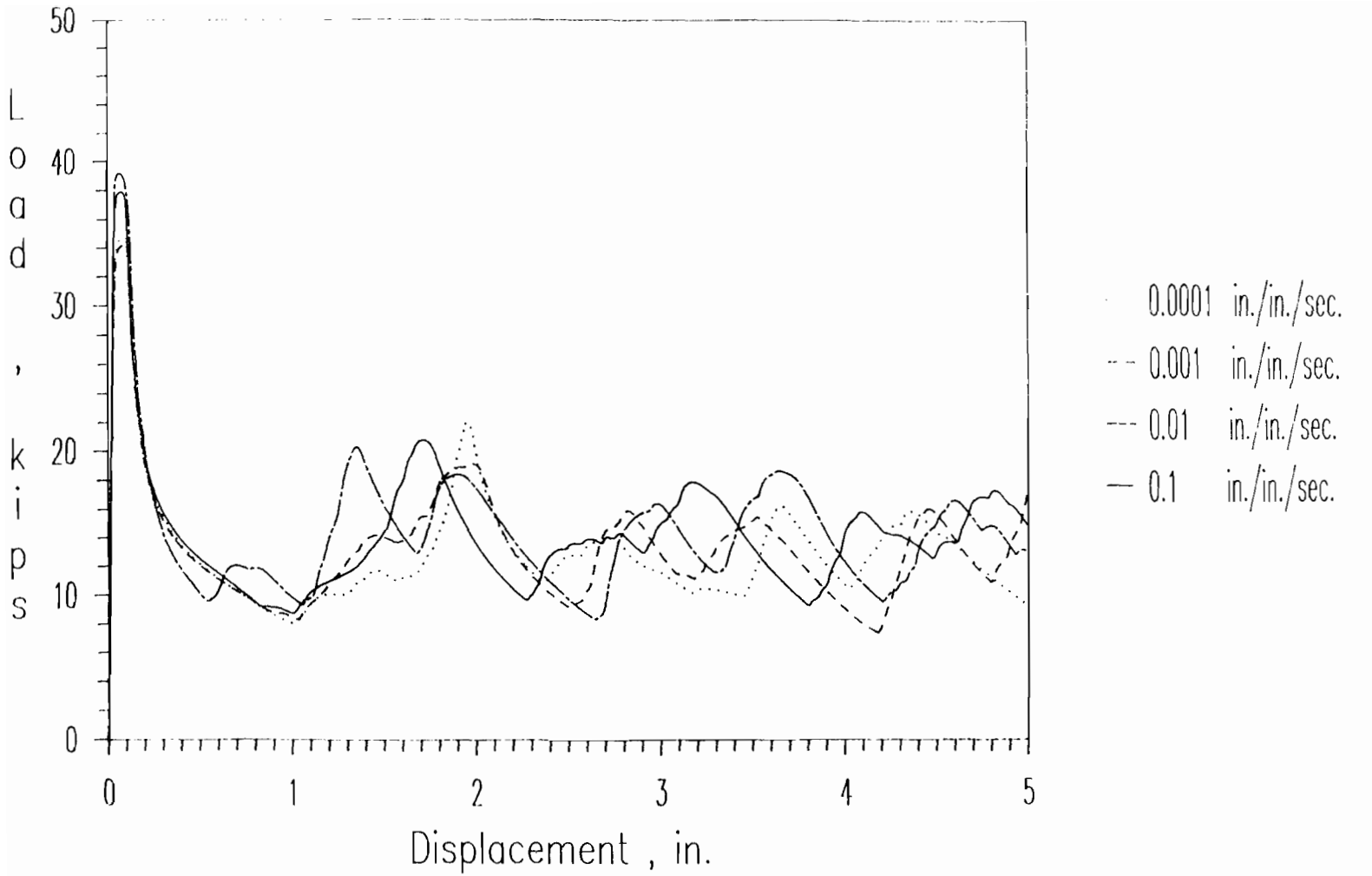

Figure 3.34 Load-Displacement Curves for Stub Column Specimens (Case 1 of Group D)

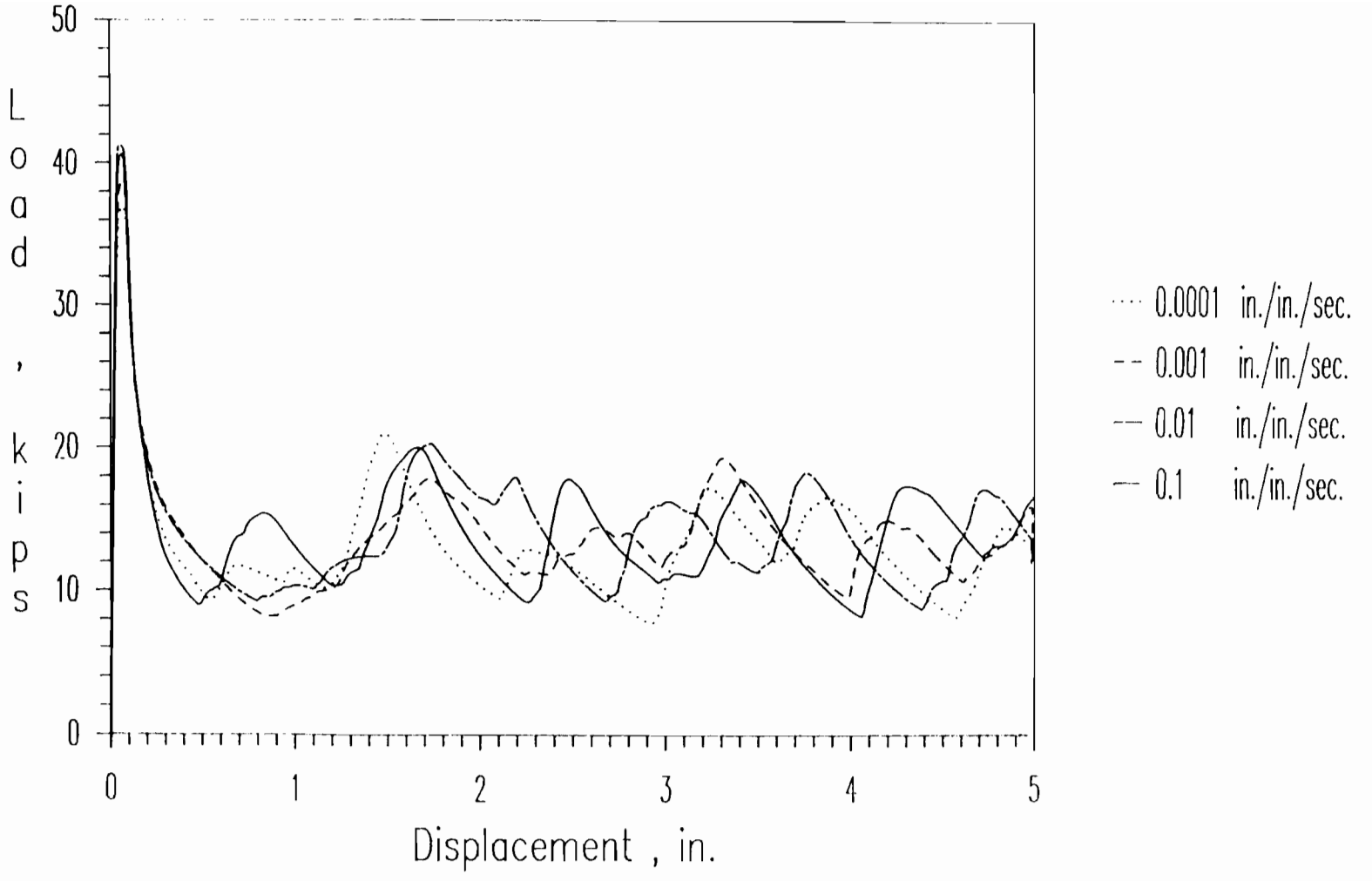

Figure 3.35 Load-Displacement Curves for Stub Column Specimens (Case 2 of Group D)

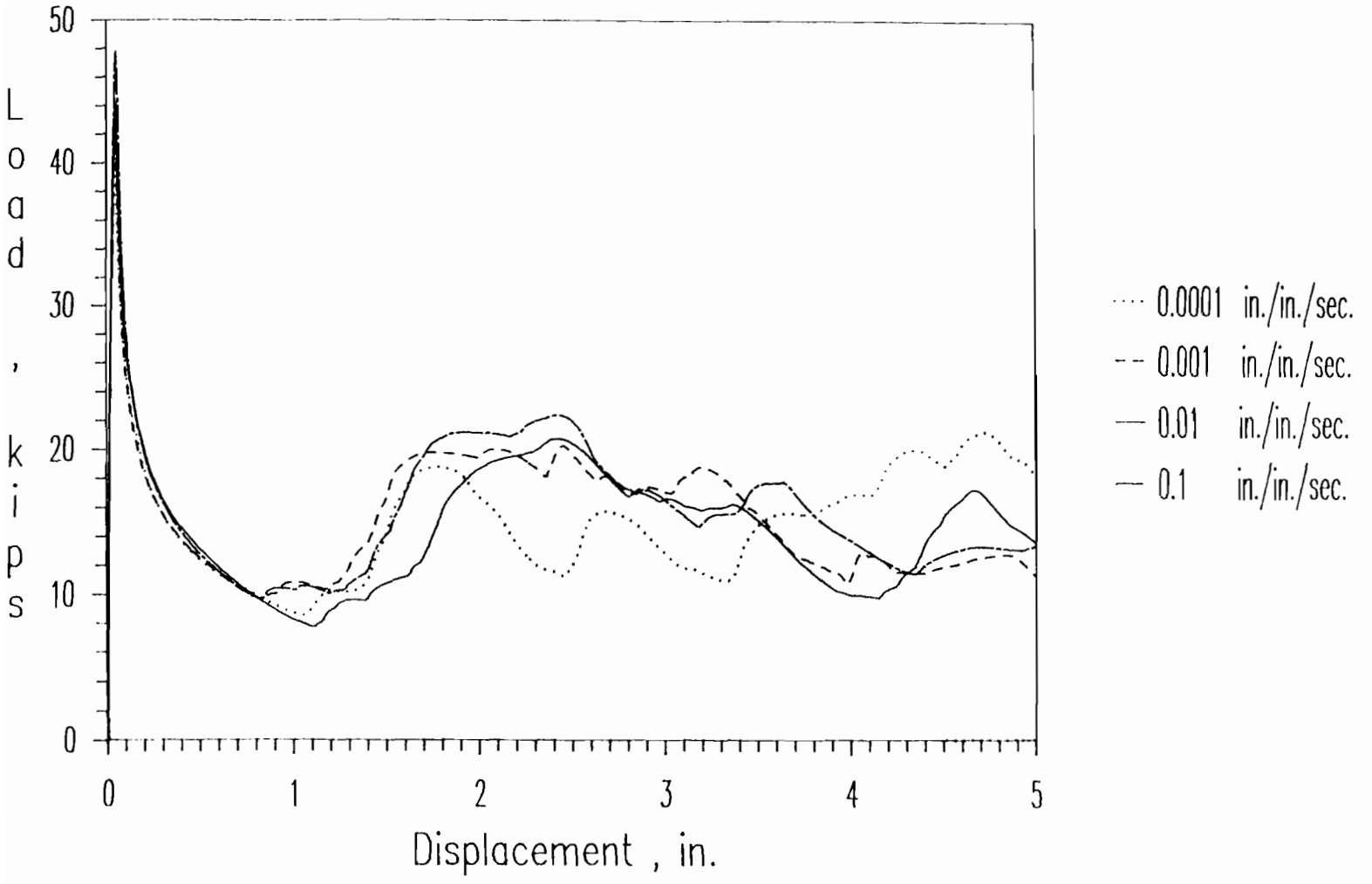

Figure 3.36 Load-Displacement Curves for Stub Column Specimens (Case 3 of Group D)

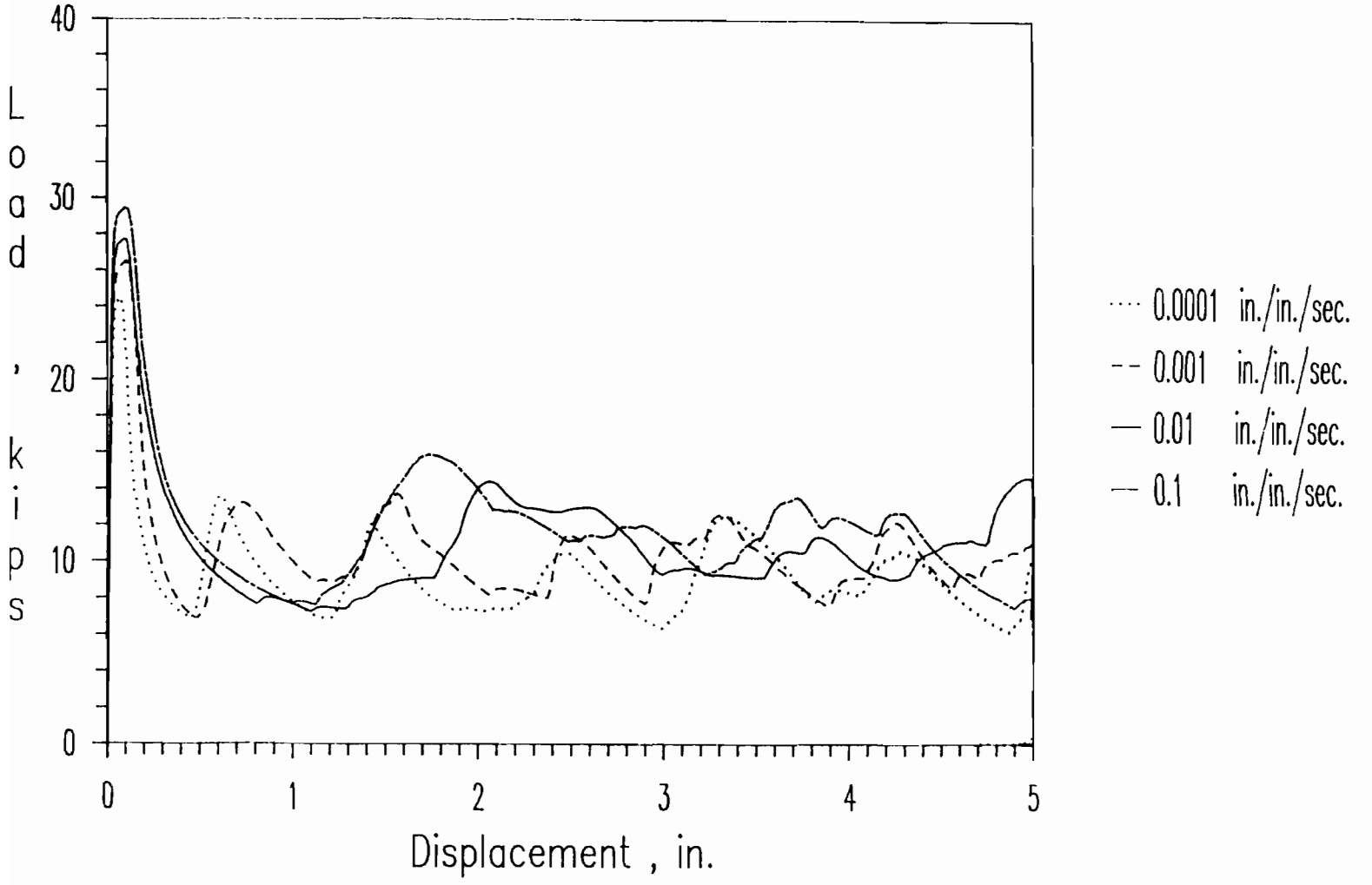

Figure 3.37 Load-Displacement Curves for Stub Column Specimens (Case 1 of Group E)

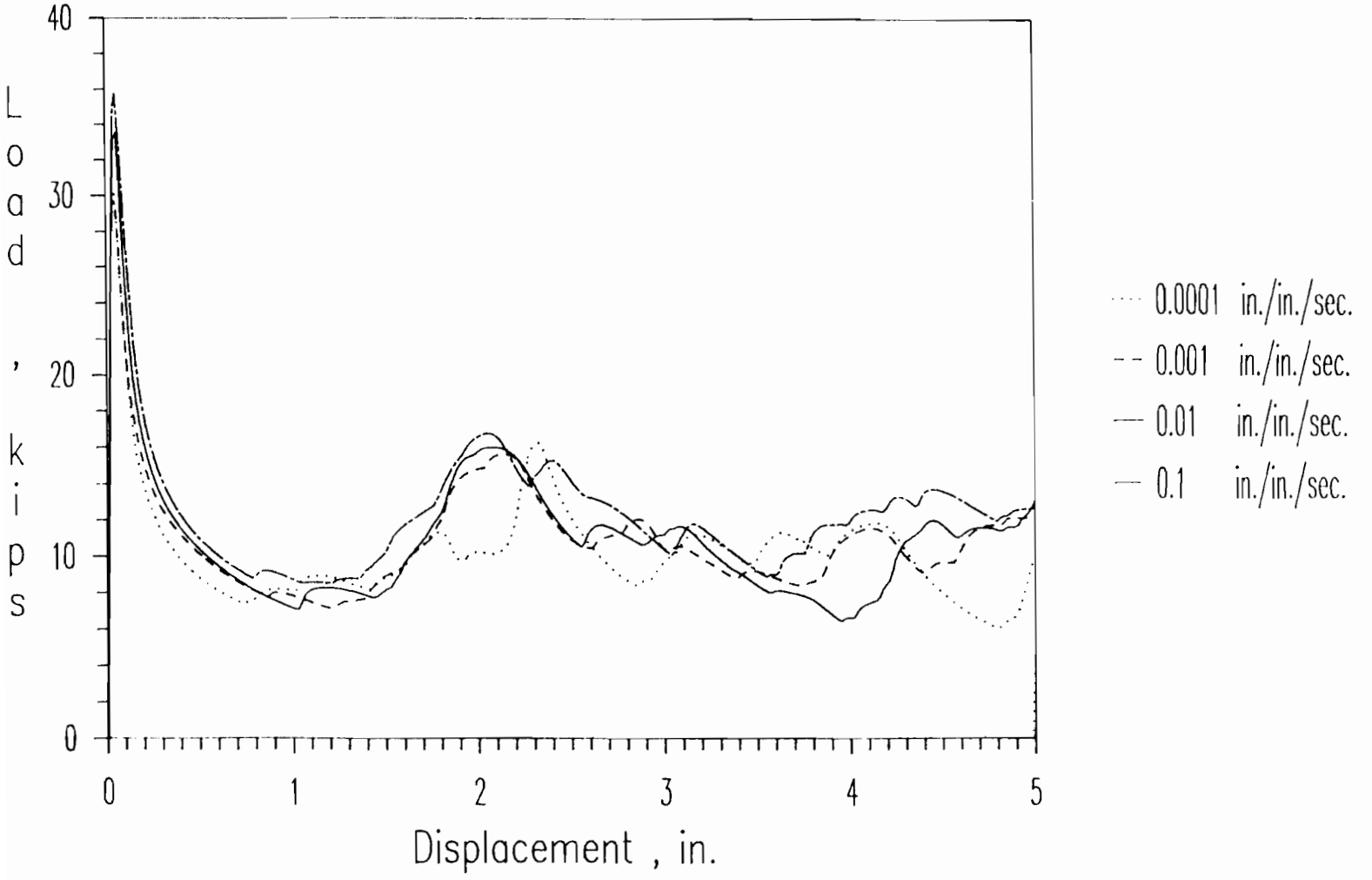

Figure 3.38 Load-Displacement Curves for Stub Column Specimens (Case 2 of Group E)

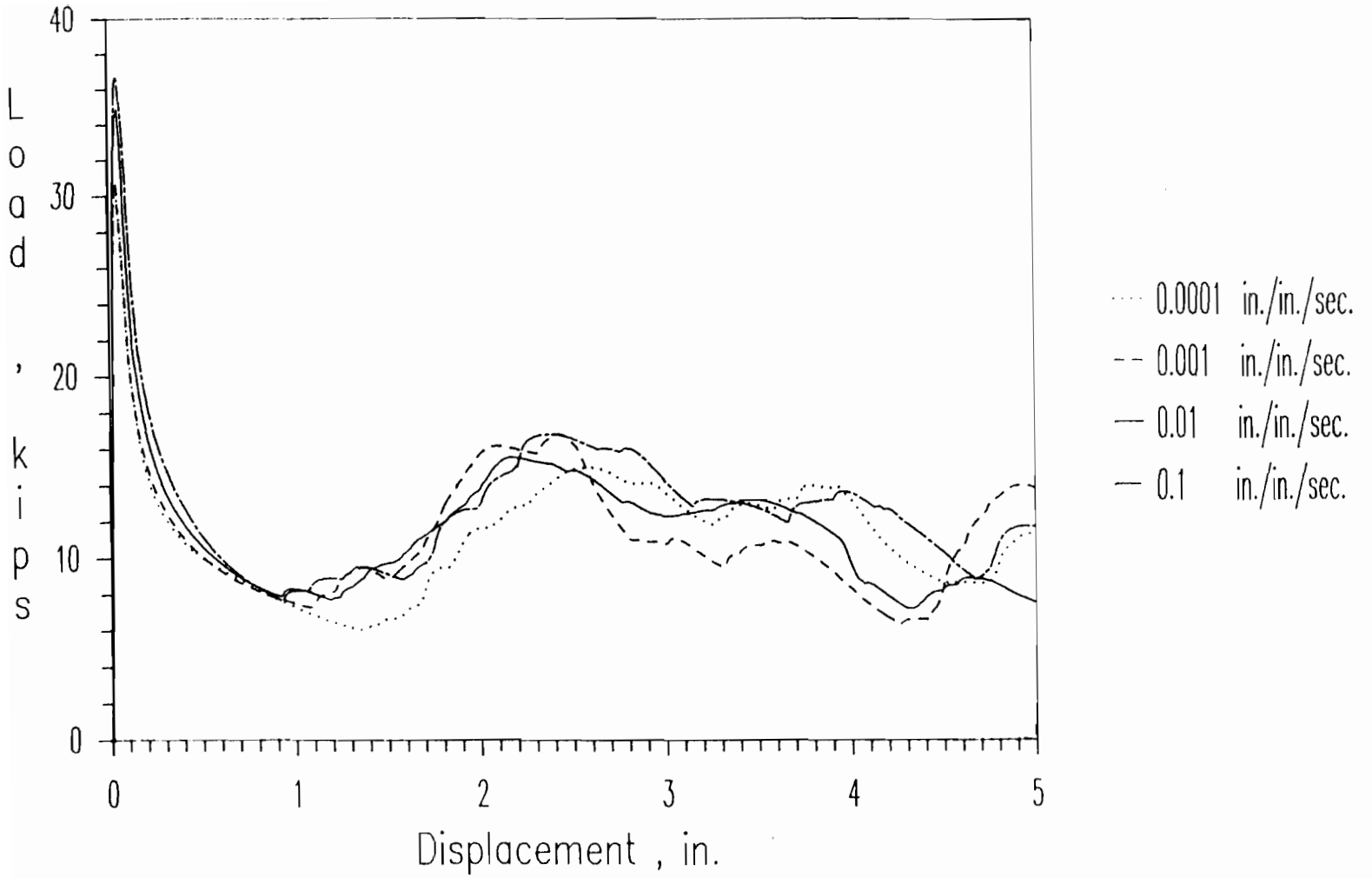

Figure 3.39 Load-Displacement Curves for Stub Column Specimens (Case 3 of Group E)

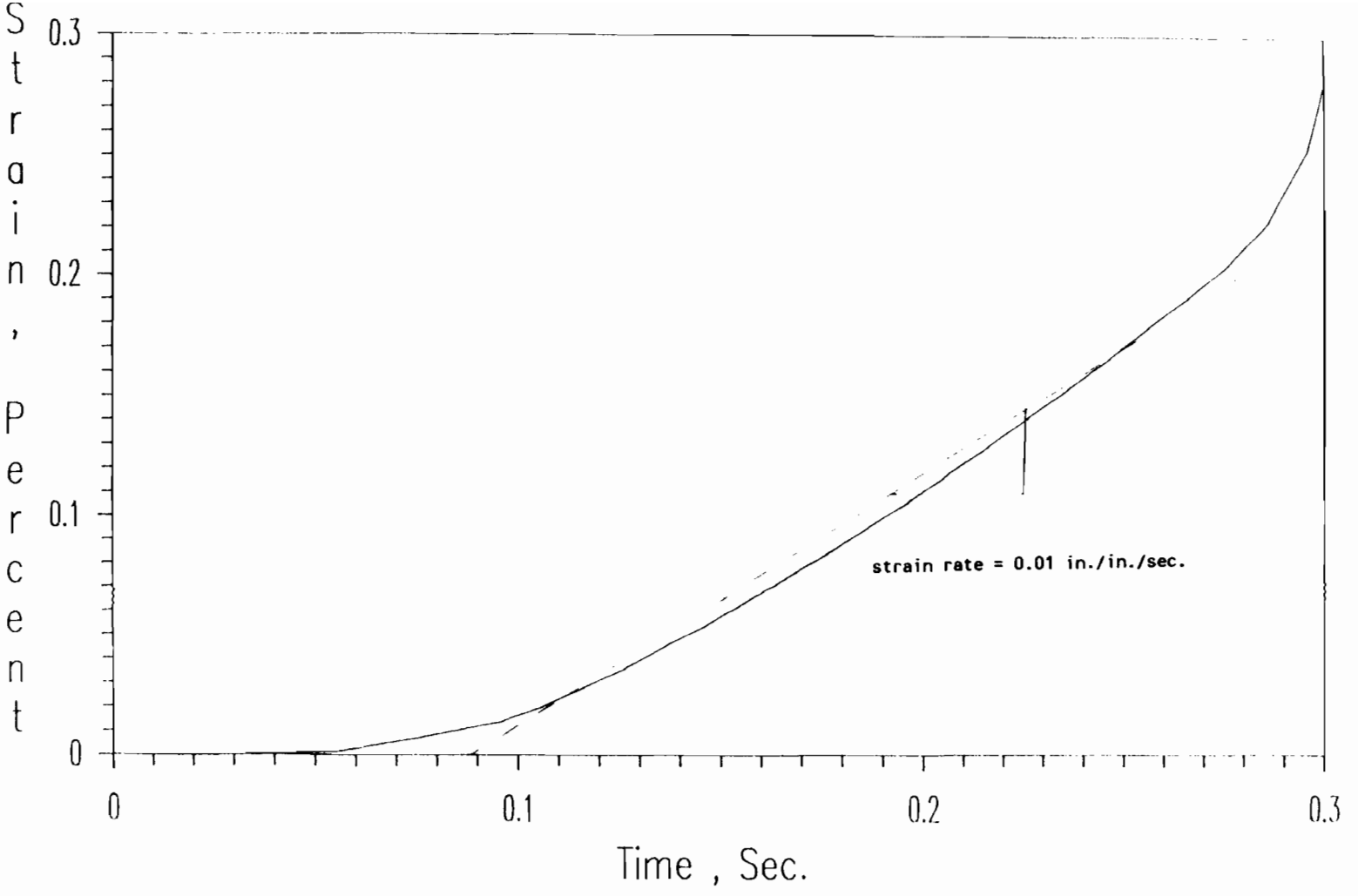

Figure 3.40 Typical Plot of Strain-Time Relationship for the Stub Column Tested under 0.01 in./in./sec. (Spec. 1B2D3)

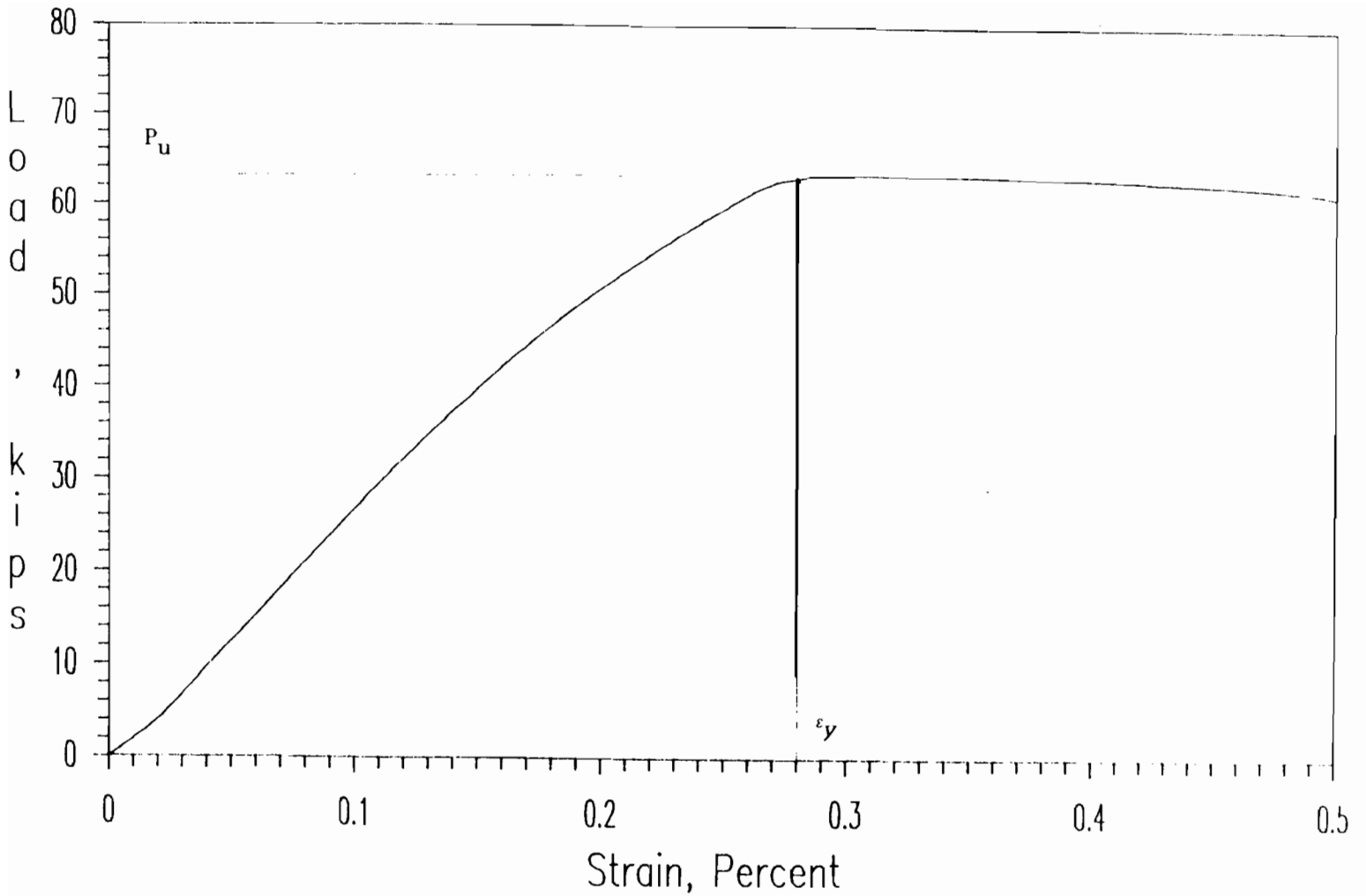

Figure 4.1 Load-Strain Curve of Box-Shaped Stub Column Fabricated from 50SK Sheet Steel (Spec. 1A2A1)

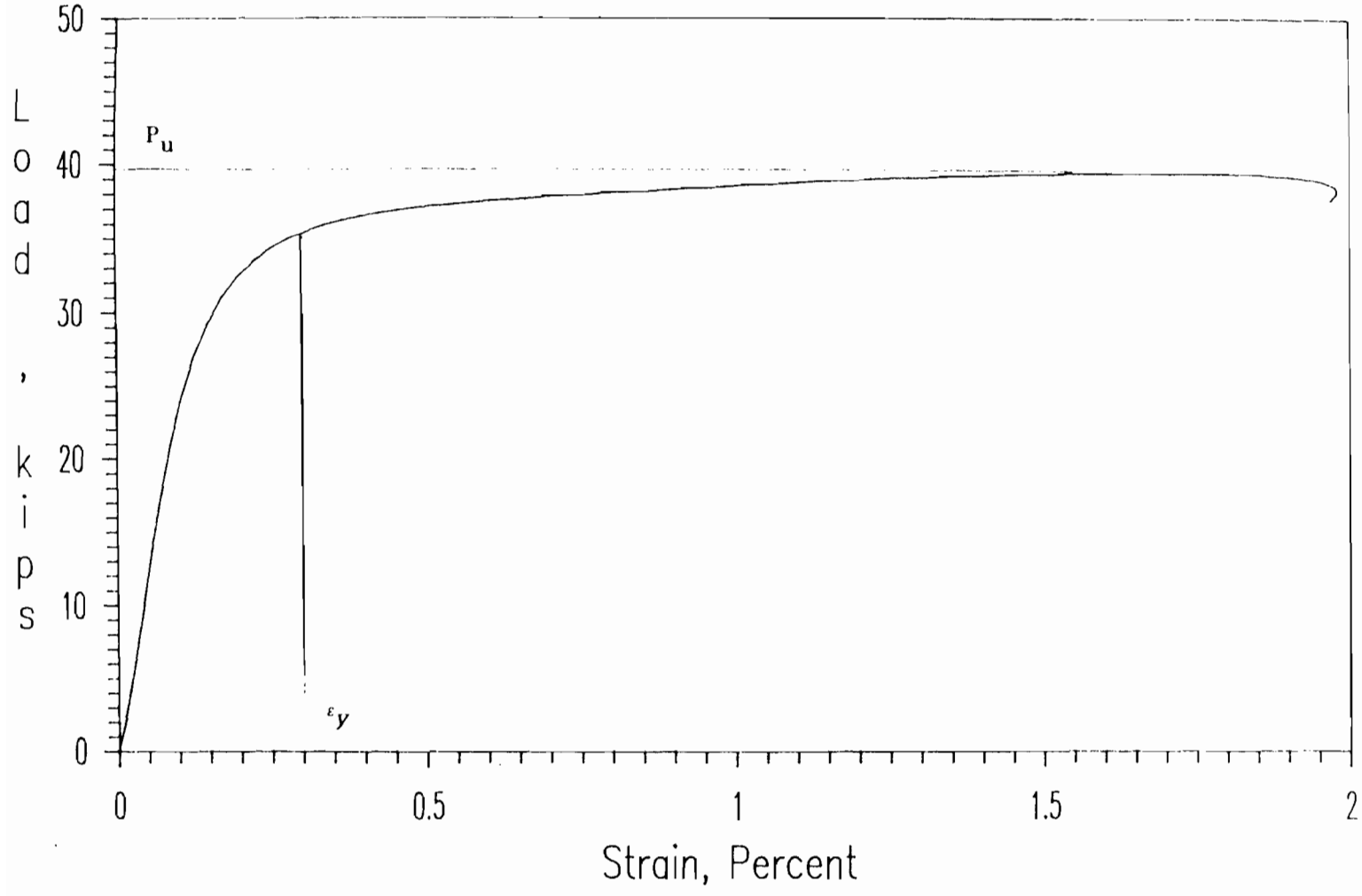

Figure 4.2 Load-Strain Curve of Box-Shaped Stub Column Fabricated from 25AK Sheet Steel (Spec. 1A2A1)

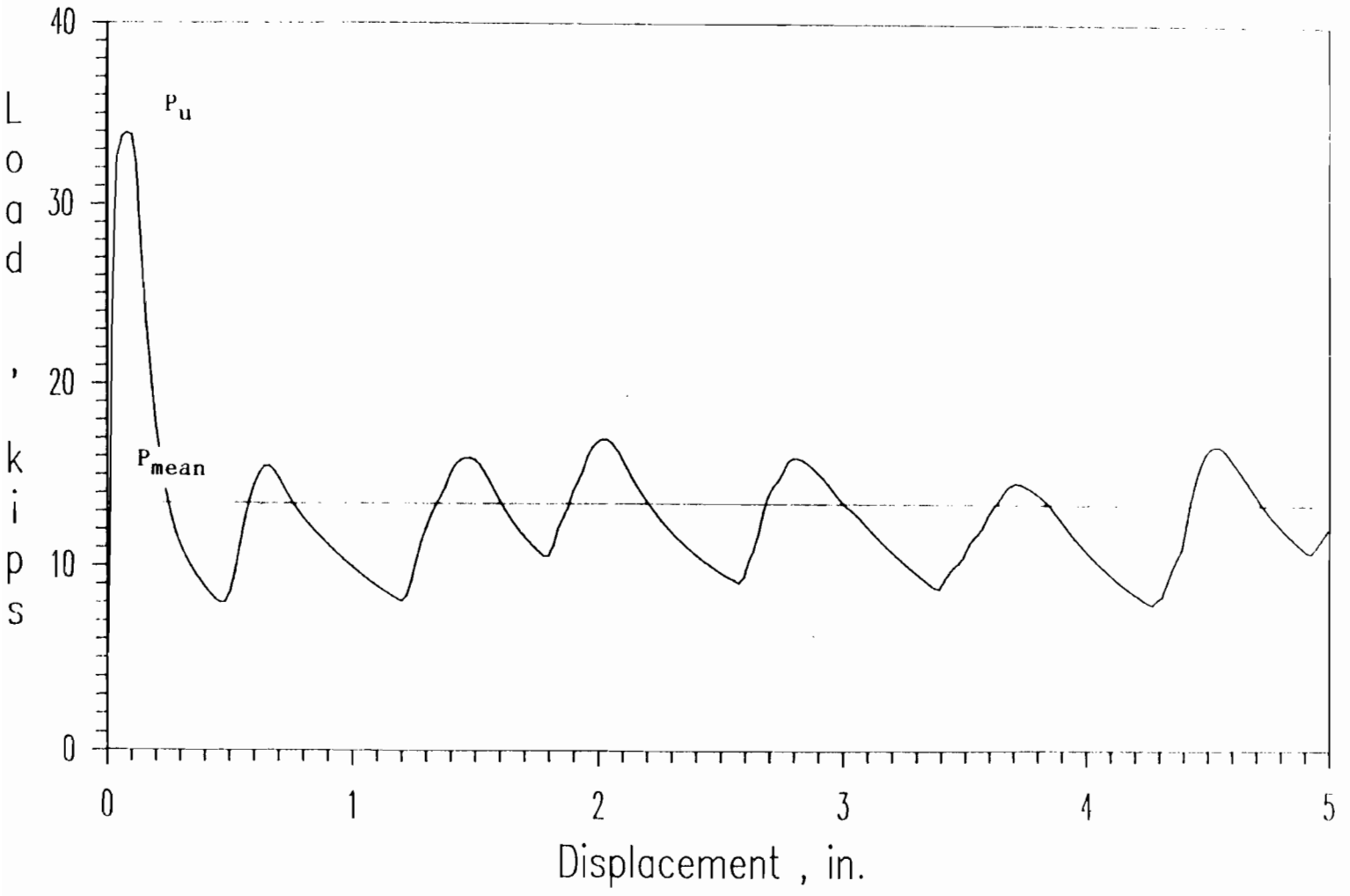

Figure 4.3 Typical Load-Displacement Curve of Hat-Shaped Stub Column (Spec. 1A1D1)

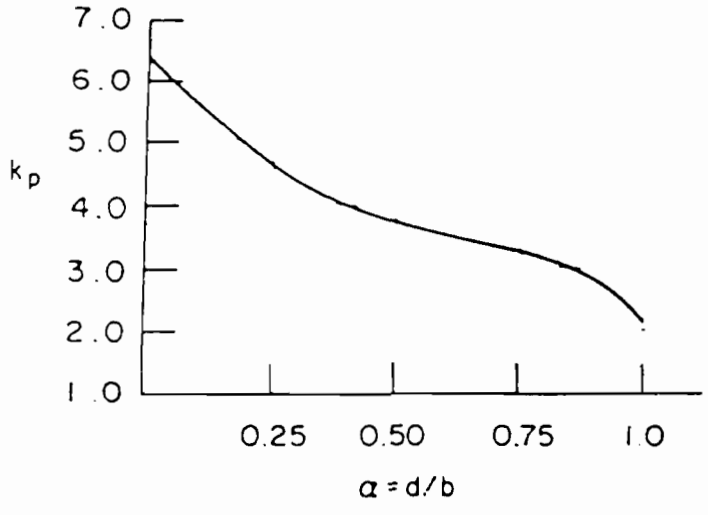

Figure 4.4 Crippling Plate Coefficient vs. Aspect Ratio (d/b)[32]

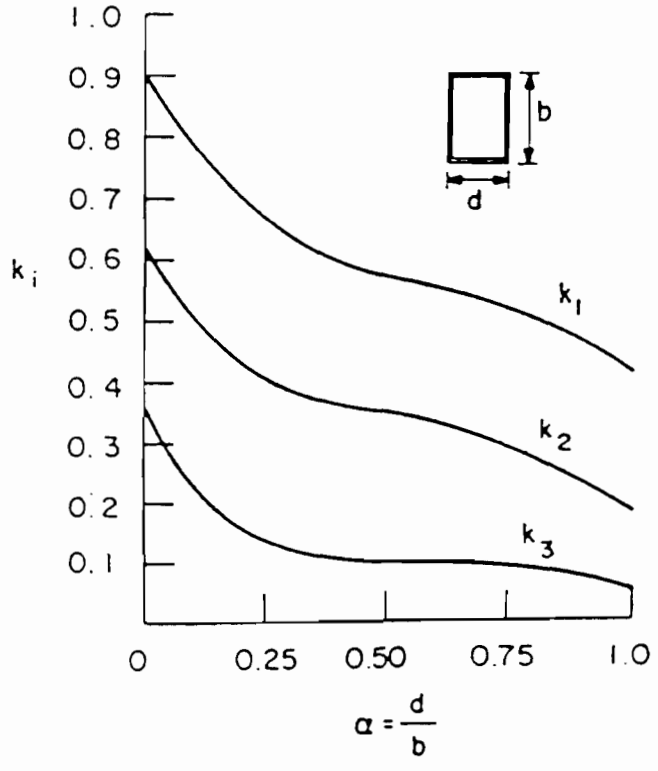

Figure 4.5 Plate Coefficient vs. Aspect Ratio (d/b)[32]

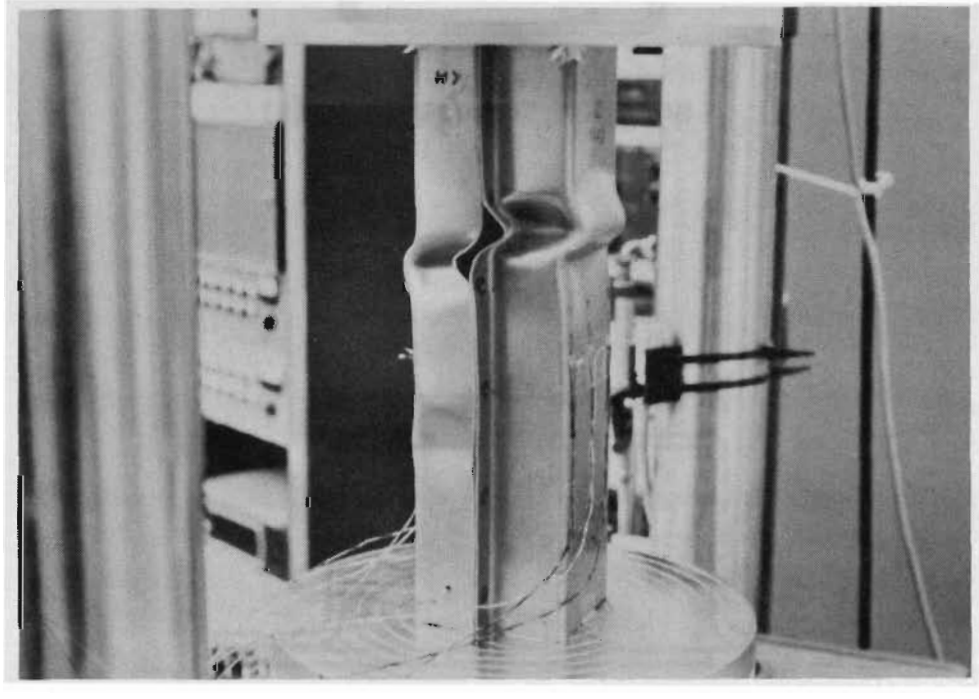

Figure 4.6 Photograph of a Stub Column with Large w/t Ratio (Spec. 1B0A2)

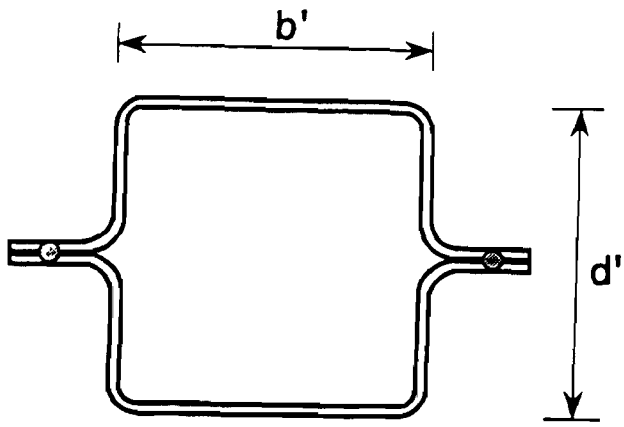

(a) Box-Shaped Stub Column

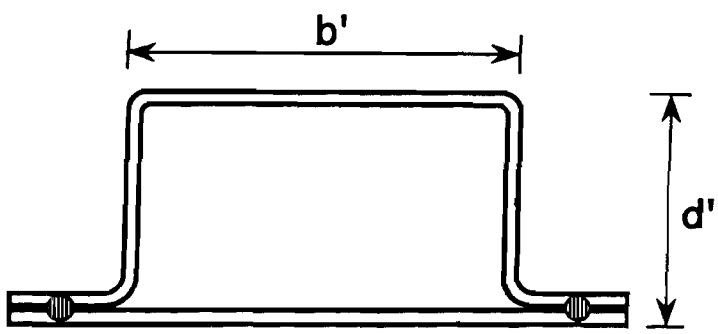

(b) Hat-Shaped Stub Column

Figure 4.7 Definition of Symbols b' and d' Used in This Study

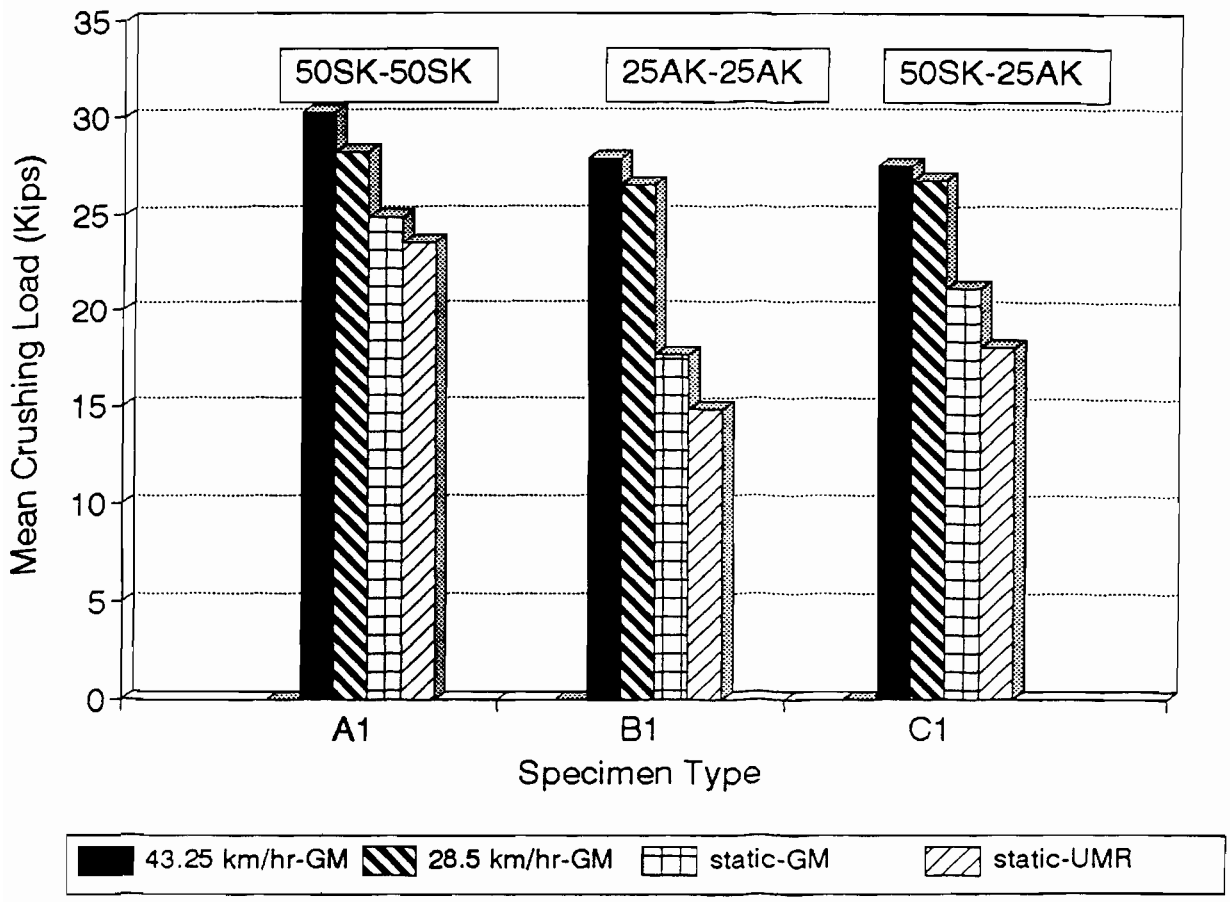

Figure 4.7 Comparisons of Mean Crushing Loads of Box-Shaped Stub Columns (Case 1 of Groups A, B, and C)

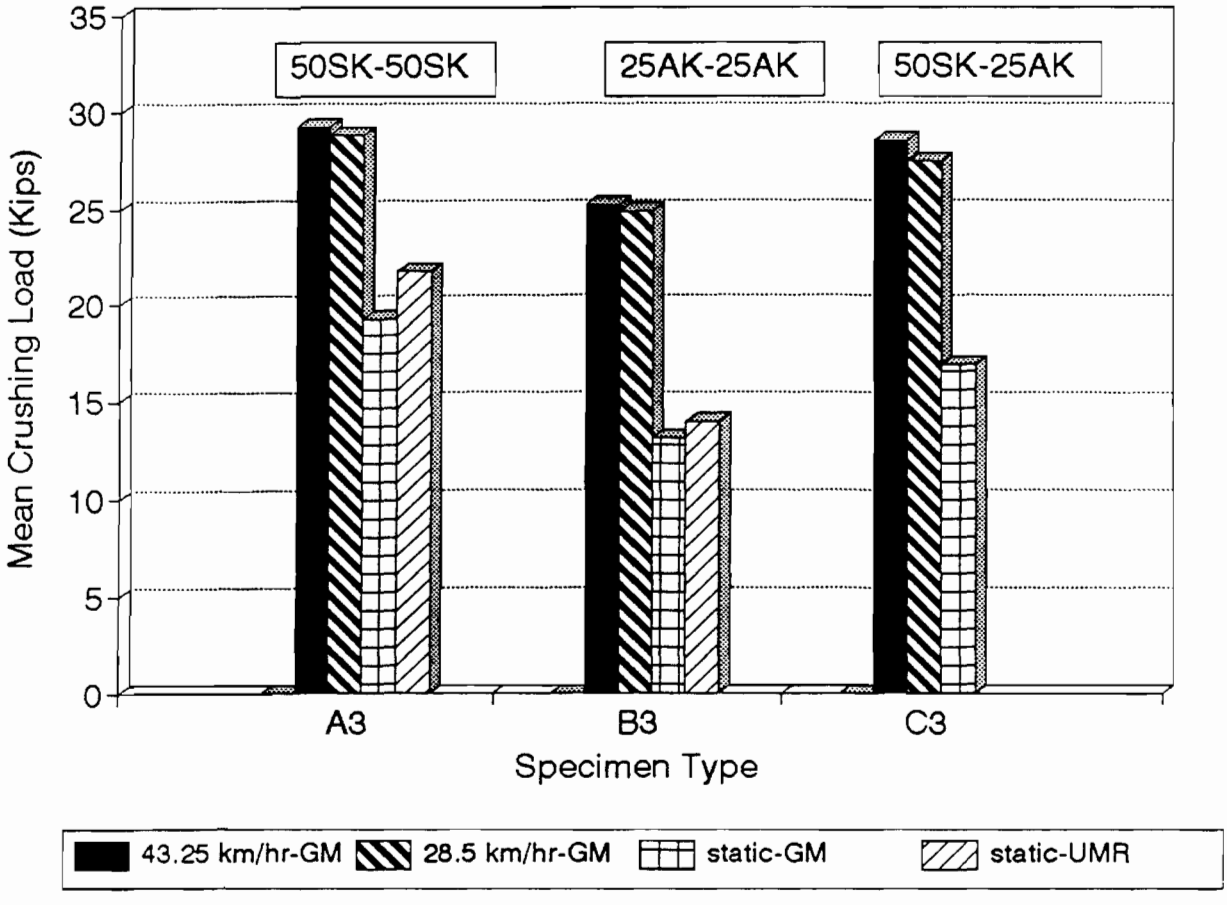

Figure 4.9 Comparisons of Mean Crushing Loads of Box-Shaped Stub Columns (Case 3 of Groups A, B, and C)

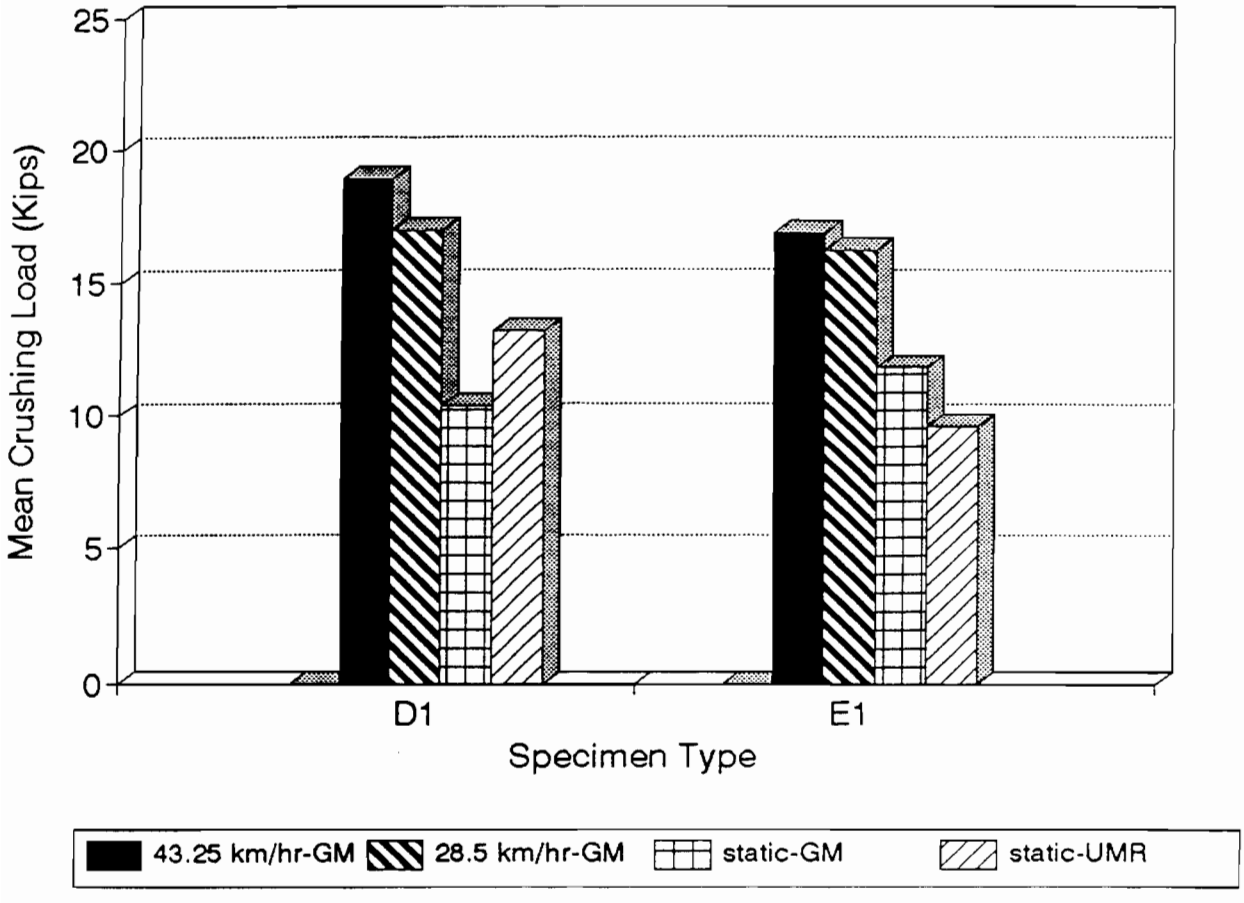

Figure 4.10 Comparisons of Mean Crushing Loads of Hat-Shaped Stub Columns (Case 1 of Groups D and E)

NOTATION

The following symbols are used in this report:

A_e	Effective cross-sectional area of stub columns
A_g	Cross-sctional area of stub columns
b	Effective width of a compression element
b'	Overall width of stiffened flange of box-shaped and hat-shaped stub columns
C	Ratio of the total corner cross-sectional area to the total cross-sectional area of the full section
D	Flexural rigidity of plate
d'	Overall depth of box-shaped and hat-shaped stub columns
E	Modulus of elasticity of steel, 29,500 ksi
f	Edge stress in the compression element
f_{cr}	Critical local buckling stress
$(f_{cr})_E$	Elastic critical local buckling stress
$(f_{cr})_I$	Inelastic critical local buckling stress
f_x	Stress component normal to the edges of the plate
F_{pr}	Proportional limit
F_y	Yield stress
F_{ya}	Average tensile yield stress of steel
F_{yc}	Corner yield stress
F_{yf}	Weighted average tensile stress point of flat portions
F_{yv}	Tensile yield stress of virgin steel
$(F_y)_c$	Compressive yield stress
$(F_y)_t$	Tensile yield stress
F_u	Ultimate tensile strength
F_{uv}	Ultimate tensile strength of virgin steel
k	Buckling coefficient

k_p	Crippling plate coefficient
k_2	Plate coefficient
P_{cr}	Critical local buckling load
$(P_{cr})_{comp}$	Computed critical local buckling load
$(P_{cr})_{test}$	Tested critical local buckling load
P_{mean}	Mean crushing load
P_u	Ultimate load
$(P_u)_{comp}$	Computed ultimate load
$(P_u)_{test}$	Tested ultimate load
R	Inside bend radius
t	Thickness of element
w	Flat width of a compression element
λ	Slenderness factor
ω	Lateral deflection of the plate
μ	Poisson's ratio
ρ	Reduction factor
α	Aspect ratio